

Copyright is owned by the Author of the thesis. Permission is given for a copy to be downloaded by an individual for the purpose of research and private study only. The thesis may not be reproduced elsewhere without the permission of the Author.

---

# LUMBER MOISTURE MEASUREMENT USING A SIX-PORT REFLECTOMETER AND WAVEGUIDE APERTURE ARRAY

---

*Wayne S. Holmes*

*School of Engineering and Advanced Technology  
Massey University*

*Supervisor: Professor SC Mukhopadhyay,*

January 2013



**MASSEY UNIVERSITY**  
**ENGINEERING**

A thesis submitted in fulfilment of the requirements for  
the degree of Master of Engineering, Massey  
University, 2013

---

## ABSTRACT

*This Thesis covers the development of a six-port and slotted waveguide based measurement system for the determination of the variation of moisture content (mc) of stacked lumber. A Six-port reflectometer was developed and used throughout the trials incorporating an automatic calibration system. This was implemented using switched coaxial standards, producing improvement in the long term stability of the six-port.*

*In addition the measurement of the dielectric properties of the typical lumber types of Heartwood, Sapwood and internal Branches is examined. Measurements were made using the waveguide cell technique covering the frequency range of 2.3 to 6.5GHz. Additional work was undertaken to establish a method to correct these measurements for variations in basic density and Earlywood \Latewood banding, giving rise to a potential moisture content estimation error of 0.63%.*

*Both an explicit first order model and multivariate regression analysis of the sensor was proposed and experimental results presented for lumber mc spanning the range of 10 to 180% by dry basis. From these trials a mc measurement error of 3% for the explicit model and 2% for regression of individual boards covering the sensor was determined without incorporating density effects.*

**Keywords:** six-port, moisture content, lumber, permittivity

---

## TABLE OF CONTENTS

ABSTRACT .....	i
TABLE OF CONTENTS .....	ii
TABLE OF FIGURES .....	iv
1.0 INTRODUCTION.....	1
1.1 Overview .....	1
1.2 Microwave Averaging Sensor (MKS version 1.0).....	4
1.3 Hypothesis .....	7
1.4 Contributions .....	8
2.0 PERMITTIVITY MEASUREMENT .....	9
2.1 Dielectric Measurement System.....	11
3.0 PHYSICAL PROPERTIES OF WOOD AND PERMITTIVITY .....	15
3.1 Dielectric Models .....	15
3.2 Density Independent Function .....	16
3.3 Experimental Results.....	17
3.4 Early Wood /Late Wood layer Orientation .....	20
3.5 Experimental Results.....	21
3.6 Discussion .....	22
4.0 MKS Measurement System.....	24
4.1 Six-port Reflectometer .....	24
4.2 Six-port Implementation .....	26
4.3 Switched standard calibration: .....	28
4.4 MKS Measurement Instrument .....	29
5.0 TRANSMISSION LINE MODEL OF WAVEGUIDE SENSOR .....	32
5.1 Reflection Coefficient of an Individual Waveguide Slot:.....	34
5.2 Power Sharing .....	39
5.3 Determining Permittivity from the Individual Slot Reflection Coefficients:.....	40
5.4 Permittivity Mixture Models to Determine Wood Moisture content:.....	42
5.5 Explicit Algorithm Trial.....	42

5.7 Potential sources of error in model .....	45
6.0 REGRESSION MODELLING OF WAVEGUIDE SENSOR.....	48
6.1 Modelling the moisture content of samples under Microwave technique .....	48
6.2 Potential sources of error.....	54
6.3 Using Temp Set Points in Regression .....	55
7.0 CONCLUSION .....	58
7.1 Future Work .....	59
ACKNOWLEDGMENTS.....	60
Bibliography.....	61
Appendix A: Permittivity results 2-3GHz.....	65
Appendix B: Permittivity results 4.5 -6.5 GHz.....	69
Appendix C: Regression Results for individual Sample Boards.....	76
Appendix D: Regression coefficients for various samples .....	80
Appendix E: MKS source code .....	81

---

## TABLE OF FIGURES

Figure 1 Typical commercial high temperature kiln .....	2
Figure 2 FEM model of Moisture distribution during kiln drying .....	3
Figure 3, modeled aperture array vs measured for 26 slot array .....	5
Figure 4 Microwave stack average sensor .....	5
Figure 5 Typical response gradient vs average moisture content for 130/80 schedule.....	7
Figure 6 Sample orientations w.r.t. grain direction .....	12
Figure 7 Waveguide calibration cells .....	13
Figure 8 Dielectric constant and loss factor for 3 types of wood taken from log 1. ....	14
Figure 9 Dielectric constant versus frequency for 6 samples both Parallel and Tangential to direction of grain .....	16
Figure 10 Independent function versus moisture content for published data .....	17
Figure 11 moisture content versus dielectric constant with no density correction. ....	18
Figure 12 Dielectric Constant versus Basic Density .....	19
Figure 13 Density corrected dielectric constant versus moisture content. ....	19
Figure 14 EW/LW layering.....	20
Figure 15 EWLW variation across wood sample.....	21
Figure 16 Density corrected measurements for flat and quarter sawn samples .....	22
Figure 17 Conceptual Sixport .....	24
Figure 18 Graphical solution of six-port equations.....	25
Figure 19 Hybrid based broadband sixport .....	26
Figure 20 Six-port Implementation .....	26
Figure 21 Photograph of Six-port.....	27
Figure 22 Sixport long term stabilityTerm.....	28
Figure 23 MKS Software User Interface.....	30
Figure 24 MKS measurement system block diagram .....	31

Figure 25 Photograph of MKS Measurement system .....	31
Figure 26 Propagation in a rectangular waveguide .....	32
Figure 27 Rectangular waveguide .....	33
Figure 28 Waveguide Aperture array .....	34
Figure 29 Conceptual view of single slot.....	35
Figure 30 Waveguide slot in broadwall .....	36
Figure 31 Reflection coefficient of an air covered slot in waveguide.....	38
Figure 32 Slot reflection versus permittivity at 6GHz .....	39
Figure 33 MKS probe layout.....	40
Figure 34 transmission line model .....	41
Figure 35 Explicit Measurement Trial .....	43
Figure 36 Explicit trial below FSP .....	44
Figure 38 Mutual coupling between slots .....	46
Figure 39 Calc mc of sample 5C as a function of time Run 1311. ....	49
Figure 40 Variation of Moisture content of all samples Run1311. ....	50
Figure 41 Comparison of measured and calculated of mc for Sample 25C in Run S1428.....	50
Figure 42 Reflection coefficient for air covered probe for 50/40 and 90/60 kiln schedules....	54

---

## 1.0 INTRODUCTION

### 1.1 Overview

This work is a continuation of the development of a microwave waveguide based sensing system developed by Holmes [1] for the measurement of moisture content of sawn lumber during kiln drying. The lumber drying kiln, as shown in Figure 1, environment is not suitable for many forms of electronic sensing with temperatures reaching 200°C and high humidity. Microwave waveguides offer one potential sensing approach that can withstand such environments. The sensor is based on a waveguide aperture array in which each aperture in the array is covered by an individual board within the timber drying stack

Work performed by King [2] [3], Torgovnikov [4], James [5] and others have shown that the permittivity of wood can be related to the physical properties of wood and in particular moisture content. Therefore by relating the amount of energy reflected or absorbed by each aperture the permittivity and hence the moisture content of individual boards can be assessed.

The ability to assess the moisture content of individual boards within a layer of the stack gives the kiln operator the ability to manipulate environmental factors within the kiln. These factors such as fan airspeed and direction allow for both increased drying speed and also control of the uniformity of moisture contents within the stack. As discussed by Tronstad [6], this yields economic benefits to the kiln drying process, both in kiln throughput and also reducing the amount of lumber out of the target moisture specification

The need for an accurate means of remotely determining kiln stack moisture content in situ is well known in the wood drying industry. Drying plantation grown softwood at accelerated temperatures leads to high production, high throughput dryers whose efficiency is dependent on accurately determining end point of drying. With schedules that use equalizing steps, a steaming period to minimize final moisture content distribution, there is a need to know the highest moisture contents within the stack to determine when this process should begin. With hardwood drying there is often the need to know the current moisture contents of the lumber to allow for

kiln temperature changes, this allows for accelerated drying whilst minimising the danger of surface checking. Overall, with the trend towards quality assurance, moisture content uniformity is increasingly an issue and ideally information on moisture content distribution should be available to the operator or control system to enhance decision making.

The only available systems that measure moisture content distribution are those using electrical resistance pins. These systems work over a restricted moisture content range (6 -25 %), are highly species and schedule dependant, awkward to use and usually have insufficient sampling points to allow accurate distribution assessment. Other available in-kiln systems, like those studied by Flotaker [6], based on resistance (Dryline) or capacitance (Dryzone, Wagner Kiln alert etc) only measure average, over a restricted range and require extensive individual kiln, size, grade and species calibration. This is primarily due to the distribution of water within the boards which tends to concentrate the moisture in the middle of the volume as it dries, as shown in the Finite Element Model (FEM) model of moisture distribution during drying as presented in Figure 2.



Figure 1 Typical commercial high temperature kiln

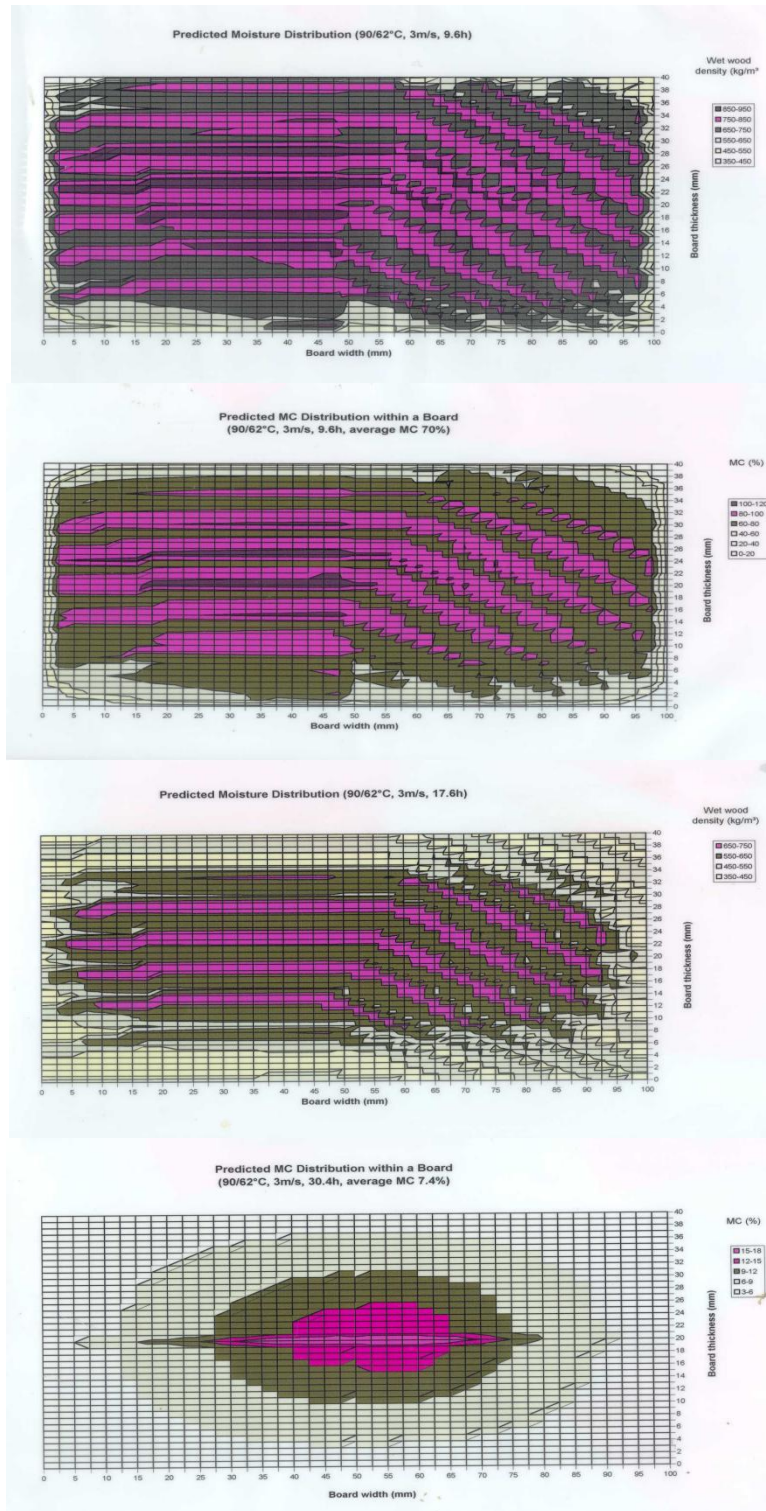


Figure 2 FEM model of Moisture distribution during kiln drying

The concentration of the moisture in the middle requires a sensing structure that interacts with the entire volume of the timber and is not dependent on contact or localised effects such as the impedance pin, or capacitive approaches. Hence a microwave approach is desirable as it will interact with the entire volume of the wood.

Industrial Research Limited and NZ Forest Research Institute Limited commenced an investigation into the application of microwave techniques for endpoint determination in 1993, from which the successful development of a microwave sensor for determining the bulk average moisture content of the timber stack has been developed. This sensor, described by Holmes et al [7] [8] [9] [10], is based on a waveguide aperture array. It offers an accurate measurement in-situ of average moisture content. The sensor consists of a length of rectangular waveguide with slots cut periodically along its length. Each slot is then covered by the lumber being dried and microwave energy inside the waveguide is allowed to interact with the volume of wood above the slot. By measuring the microwave energy reflected back down the waveguide by the slots a sensitive measurement of average moisture content can be made.

### **1.2 Microwave Averaging Sensor (MKS version 1.0)**

The fundamental concept embodied in the construction of this sensor structure is that microwave energy propagating along the interior of a waveguide will radiate when presented with a resonant length aperture in the broadwall. The microwave energy will partially radiate from the aperture and due to the presence of the covering material, partially undergo reflection back into the waveguide and hence the energy will propagate back to the measurement plane where these reflections can be measured directly. For the current design the slot was chosen to be a resonant length in air at 5.3 GHz. The slot is centred in the broadwall and for minimum reflection in the air covered case a slot angle was determined. A slot in this configuration is analogous to a series of lumped admittances at intervals along the waveguide.

In order to sample the average moisture content across the stack a linear array of slots was constructed in the waveguide using the slot design described in the previous section. Since the slots may be considered as lumped parallel admittance elements we can assume that if we have a linear array of admittance elements the overall input admittance measured at the measurement plane will be the algebraic sum of these admittance elements. This is subject to the condition that the admittance's are spaced at multiples of half wavelengths so that negative reinforcement does

not occur at the slots. Figure 3 below was presented by Holmes [8], shows the magnitude of reflection coefficient for both measured data and modelled for a 26 slot array in 35mm x 20mm waveguide with slots spaced at half wavelength spacings (in air) at 5.2 GHz.

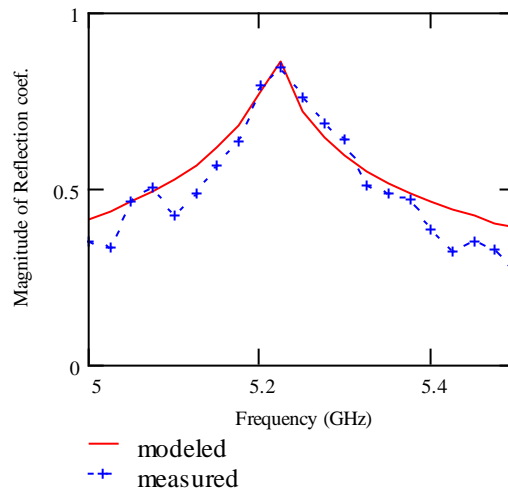


Figure 3, modeled aperture array vs measured for 26 slot array

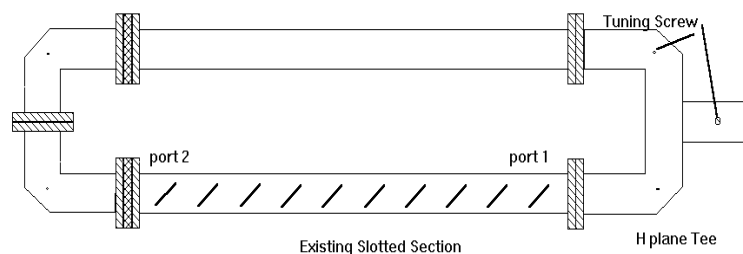


Figure 4 Microwave stack average sensor

To improve the performance of the array and to compensate for mechanical tolerances the linear aperture array was driven from travelling wave's incident from both ends. This has the effect of setting up a standing wave inside the waveguide which excited the slots, which at certain frequencies forces all the slots to be in phase and add constructively. Figure 4 shows one possible implementation of the sensor structure.

A series of experimental trials were performed in a wood drying tunnel with the waveguide sensor orientated with the sensor beneath the sample boards with the slots facing upwards. In each series 600mm long Radiata pine sample boards were stacked in 1.5 m wide layers suspended

on a load cell, and then dried using a range of commercial schedules. Air flow could be directed from either direction or inlet dry bulb and wet bulb temperatures were controlled as in a commercial drier. The waveguide sensor was inverted and attached to the load cell frame. This removed taring problems and since all samples rested on the array, there was no air gap. In some kiln charges weighing's were conducted during the run to allow more accurate average moisture content assessment and as well assess uniformity.

The microwave reflection coefficient measurements were performed using a Hewlett Packard 8720B vector network analyser. The HP8720B was configured to measure frequency points from 5 to 5.8 GHz. The system was calibrated using the standard Agilent [11] Thru-Reflect-Line (TRL) algorithm which placed the measurement reference plane in the waveguide, hence the reflection coefficients measured were within the waveguide structure and reflections due to the input coax and waveguide to coax transitions were removed. A simple software programme was written to control the HP8720B remotely and allowed for measurements to be performed and data stored at predetermined intervals during the drying runs.

For each of the kiln drying charges the magnitude of the reflection coefficient was calculated for all frequency points covering the range of 5.3 to 5.55 GHz which were then summed to produce a measure of the frequency response gradient. From the work of Holmes [7], It can be shown that this measured response gradient is related to the power spectral density. This had the additional effect of reducing measurement noise.

In addition to this the average moisture content of the stack at the time of measurement was calculated using the final oven dried weight and the kiln load cell measurements. Figure 5 shows a graph of response gradient as a function of the average moisture content across the stack for a 130°C drybulb /80°C wetbulb schedule charge determined using the procedure described above. The shape of this response gradient is typical of all the charges measured.

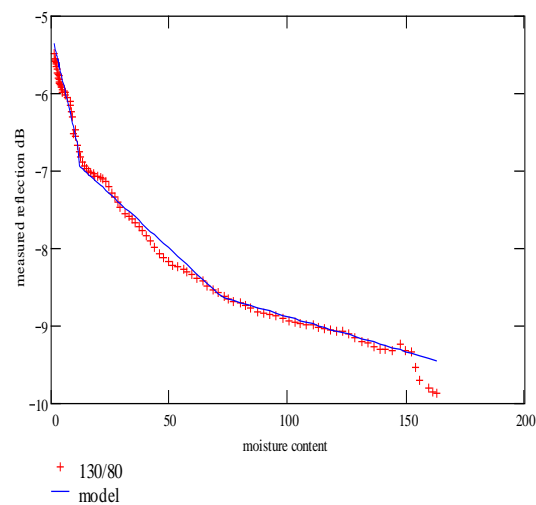


**Figure 5 Typical response gradient vs average moisture content for 130/80 schedule**

The drying charges used in this study and report by Holmes [9] showed that for moisture contents in the three regions the error between the model and actual are typically; <3% for 99% confidence levels for moisture content less than 15%, and <10% for 99% confidence levels for moisture content less than 40%.

The use of a waveguide aperture array as presented by Holmes [1] [8] [9] [10] has shown to be an accurate method of measuring the average moisture content of a timber stack in the harsh kiln drying environment. Accuracies of better than 1% rms are achievable at moisture contents below 15% and hence the technique has shown to be useful for determining the endpoint of drying, whilst still providing useful moisture content estimates throughout the drying process.

### 1.3 Hypothesis

The fundamental hypothesis behind this paper is that microwave energy propagating along the interior of a waveguide, or transmission line, will radiate when presented with a resonant length aperture (slot) in the waveguide broadwall. If we consider that each slot is covered by a dielectric then the microwave energy will partially radiate from the aperture and due to the presence of the covering material, partially undergo reflection back into the waveguide and hence the energy will propagate back to the measurement plane where these reflections can be measured directly. Previous studies have shown that the permittivity of timber is directly related to the moisture content (mc) and basic density thus as the timber is dried the permittivity change will influence the amount of microwave energy reflected by the slot. If the measurement is made over a

significant frequency range the individual slot reflections can be extracted from the total reflection coefficient measured at the measurement plane.

To test this hypothesis, a theoretical and practical analysis of a slotted waveguide array covered by timber has been performed. Both an explicit and regression based approach have been employed for the measurement analysis, along with the construction of sensor and measurement system for trials.

### **1.4 Contributions**

This thesis reports two main contributions:

- The proof of the hypothesis that individual measurements can be made from slots within a linear waveguide array.
- Development of a waveguide sensor and reflection coefficient measurement system based on six-port technologies for the measurement in-situ of lumber whilst being kiln dried

Publications to date on the research covered in this thesis are:

- W. S. Holmes, S. C. Mukhopadhyay, and S. G. Riley, "Lumber Moisture Measurement using a Six-port reflectometer and Waveguide Aperture array," in *46th Microwave Power Symposium, Institute of Microwave Power International, Las Vegas, 2012*.

---

## 2.0 PERMITTIVITY MEASUREMENT

In order to redesign the MKS averaging sensor to allow for measurement of individual board moisture contents, we first need to examine the dielectric properties of wood itself. To achieve this, a series of measurements were undertaken, and reported in this chapter, to not only investigate the contribution of moisture to permittivity but also the impact of typical types of wood structures and basic density variation. This knowledge will not only assist in the design of the sensor but also have impacts in the analysis and modelling of the system.

Wood has two basic important physical characteristics when using the propagation of electromagnetic energy through it as a means of the determination of permittivity. Firstly wood is a hygroscopic material in that it is able to absorb water from the atmosphere and tends to remain at equilibrium with the water vapour content in the air. The second factor of interest is that wood has an anisotropic structure. This arises from the cell pattern laid down while the tree is growing always in a defined direction. Added to this, the growth rate is dependent on seasonal and climatic variations, so during slow growing periods such as winter the cells are laid down more densely than those created during the summer months. This leads to the grain, Earlywood/ Late wood (EWLW), structure in the timber.

Microwave sensors essentially measure either the energy transmitted or reflected back from a material. The composition and structure of the material give rise to a measurable signature that then can be related to other physical properties such as moisture content or density. This defined microwave signature of a material arises from a physical constant known as permittivity, (dielectric constant) which relates the electric flux density ( $\mathbf{D}$ ) illuminating the material to the electric field strength ( $\mathbf{E}$ ), intensity, inside the material. Often the permittivity of a material is expressed as a multiplier of the permittivity of free space ( $\epsilon_0$ ) and is then known as relative permittivity ( $\epsilon_r$ ).  $\mathbf{D}$  and  $\mathbf{E}$  are both vector quantities and contain both phase and magnitude information.

$$\bar{D} = \varepsilon_o \cdot \varepsilon_r \cdot \bar{E}$$

The magnetic field component of the microwave energy similarly has a physical constant of permeability but only Ferrous materials have a relative permeability of greater than one and in the context of the types of measurements undertaken in this work it will always be assumed to be one.

Waveguide cell measurements were selected as the best means to provide the bulk permittivity of the various types of wood, this was due to the fact that both transmission and reflection data and the microwave energy interacts with the entire volume of the sample. Waveguide cell measurements involve inserting a sample inside a waveguide and measuring the microwave reflection from and transmission through the sample. Then using the Nicolson Ross Weir (NRW) method presented by Nicolson [12] and Weir [13] these two measured coefficients yield the complex permittivity of the sample material.

There are many techniques for determining the dielectric constant of a material filling a waveguide, however the NRW method is universally seen as the most accurate and also accommodates imperfections in sample preparation such as sample faces and wall air gaps. The NRW method works well for all frequencies away from the TEM mode resonances that occur when the sample is a multiple of half wavelengths in the waveguide, and also for high to medium loss materials. The permittivity of the material is determined by the equation;

$$\varepsilon = \frac{c^2}{\omega^2} \left[ \frac{2\pi}{\lambda_c} \right]^2 - \frac{1}{L^2} \ln Z + j2\pi n^2 / u_r$$

Where

for non-ferrous materials the relative permeability  $u_r = 1$

$c$  is the speed of light

$\omega$  is the angular frequency

$\lambda_c$  is the cut-off wavelength of the waveguide

$L$  is the waveguide cell electrical length

and

$$Z = \frac{x+1}{2y} \pm \sqrt{\left(\frac{x+1}{2y}\right)^2 - 1}$$

And

$$x = S_{21}S_{12} - S_{11}S_{22} e^{2\gamma_0 L_{air}-L}$$

And

$$y = S_{21} + S_{12} e^{\gamma_0 L_{air}-L}$$

Where  $\gamma_0$  is the free space propagation constant and  $S_{11}, S_{12}, S_{22}, S_{21}$  are the measured S parameters from the network analyser. In essence the permittivity is determined by the measurement of the group delay through the measurement cell and the correct value of n is determined using this.

The samples used in this experiment came from the samples used to determine density from the previous trial [14] and had been stored in a sealed plastic bag for over 12 months. Their moisture contents were 10.3 +/- 0.1 and their density values had previously been determined by ENSIS (a joint venture arrangement between Scion Ltd and CSIRO in Australia).

The samples were cut to as best as possible to give the two extremes of Earlywood \Latewood orientation (flat and quarter sawn) however several would be better described as intermediate. Most samples density's chosen lay in the around 350 kg/m<sup>3</sup> +/- 10Kg/m<sup>3</sup> however 2 samples were chosen around 450. From each of three sources, samples of heart, Sap and Branch wood were taken and dimensioned so as to fit into waveguide cells.

A simple three character naming convention was adopted for each sample. Firstly a number denotes which of the three sample logs the cube was taken from. A letter SH or K was used to denote if the sample was Sapwood, Heartwood or Knot material. Finally a number defines the replicate number, where possible usually three replicates were taken from each site.

For example a sample labelled 2H3 would denote the sample as log 2, Heartwood, replicate 2.

## 2.1 Dielectric Measurement System

As Wood is anisotropic in nature the waveguide cells were designed in a square cross-section allowing the samples to be cut as cubes. The cubic samples could then be rotated and measured to allow us to see this anisotropic effect in the measured results. The figure below shows the naming convention selected for the measurement files, which would be appended after the sample name.

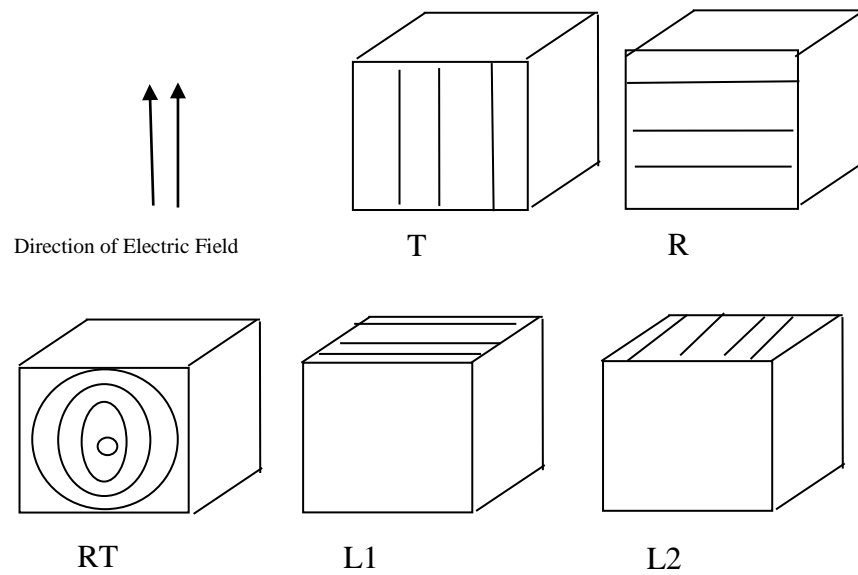


Figure 6 Sample orientations w.r.t. grain direction

Waveguide cells were fabricated using stainless steel using a 70.2mm Aluminium box section which would cover the 2.3 to 4.2GHz band, and a 35.6mm Aluminium box section to cover the frequency range 4.5 to 9 GHz. As the waveguide cells are square in cross section, the possibility of more than one mode of wave propagation exists. Within our measured data this effect did occur once the cell length exceeded a half wavelength within the material, and hence the presented results in appendix A and B show only the single moded region from 2.3 to 3GHz for cell 1 and 4.5 to 6.5GHz for cell 2.

For measurement of the samples a set of calibration standards was fabricated (Table 1 ) so as to allow for a Thru-Reflect-Line calibration to be performed. The TRL procedure [11] [15] allows for the measurement plane to be set at the interface between the measurement cell and the waveguide to coax transitions, hence removing all connector effects. For each chosen dimension of box section, a measurement cell (allowing for cubic samples) was made.

Table 1 TRL Calibration cell lengths

cutoff freq	freq range	Box dim	cell 1	cell2	cell3	cell4	<b>D</b>
4.2	4.5-9	35.6	25.4	15.3	9.2	4.1	12.2
2.1	2.3-4.2	70.2	50.1	30.1	18.1	8	24.1
Ghz	Ghz	mm	mm	mm	mm	mm	Mm

In addition to each cell a shorting plate was required. The dimensions given are those calculated so a tolerance of  $\pm 0.5\text{mm}$  was acceptable in manufacture. The cells, shown in Figure 7, were measured to  $\pm 0.1$  after they were constructed and the actual lengths were used in the calibration.



Figure 7 Waveguide calibration cells

The measurements were undertaken using an Agilent PNA vector network analyser and each sample was weighed after measurement. The PNA is a 2port device which allowed for the measurement of microwave reflection and transmission coefficients to be obtained. Using these measured microwave parameters the permittivity was calculated using the standard Nicholson-Ross-Wier algorithm [12]. This gave us the permittivity data shown for each sample in appendices A and B.

### Observations

Initial observations from the data across the range 2.3 to 6.5 GHz both branch and Heartwood permittivities remain constant. The Dielectric constants (real part of permittivity) of both Branch and Heart wood at the frequencies measured are similar. The Loss Factor (imaginary part of permittivity) of both Branch and Heart wood whilst similar showed some small frequency dependence in the Branch wood which is not apparent in the Heart wood. As the reflection from the boundary of two media comprises both dielectric constant and loss factor there should be a small but measurable reflection between Branch and Heartwood. The Sapwood measurements

showed that at the lower band 2.3-3GHz region, the measured dielectric constant and loss factor to be exceptionally low, so as to make the sapwood almost transparent in a image, as shown in Figure 8. Both the dielectric constant and loss factor showed, as expected, a frequency dependence increasing rapidly as we approach 10GHz due to the large water component within the sapwood structure.

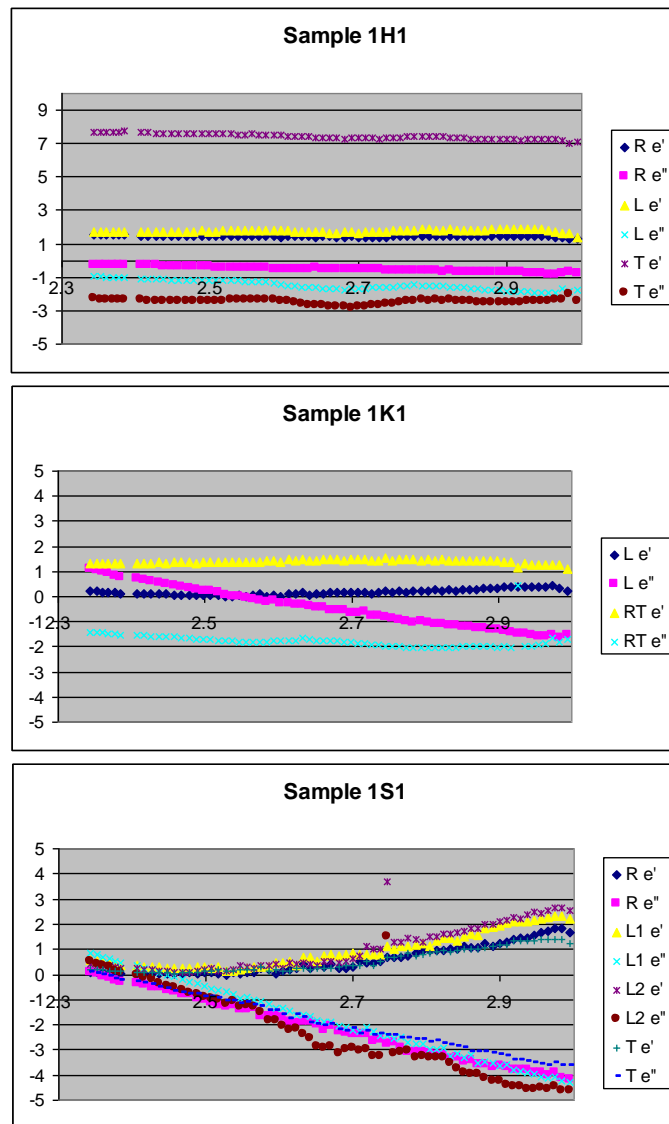


Figure 8 Dielectric constant and loss factor for 3 types of wood taken from log 1.

---

## **3.0 PHYSICAL PROPERTIES OF WOOD AND PERMITTIVITY**

This chapter looks at the effect of basic density on the accuracy of the MKS and examines potential methods to remove this effect.

### **3.1 Dielectric Models**

The initial approach to accounting for density variations was to develop a model that describes the dielectric behaviour of a material by using the permittivity of the individual constituents. The most commonly used model would be a volumetric one, which simply sums the permittivity of each part, multiplied by its fraction of the volume. Hence a simple model would be the permittivity's of dry wood plus water plus air. Then using the frequency dependence of the sum (usually the water component as the permittivity of air and solids change slowly with frequency) the individual volume fractions of each constituent can be determined.

In the case of this study both the published data and the experimental permittivity data measured, Figure 9 below, show that the permittivity of wood below the Fibre Saturation Point (FSP) (which is approximately 33% moisture content and the point where all free water has been removed), is essentially constant over the 4 to 8 GHz range. In essence the water remaining within the wood structure is so tightly bound that it no longer contributes significantly to the dielectric losses. This gives wood below FSP a very slow variation in dielectric properties with frequency.

Without any change in permittivity the model approach cannot be considered a useful approach for removing the basic density effect.

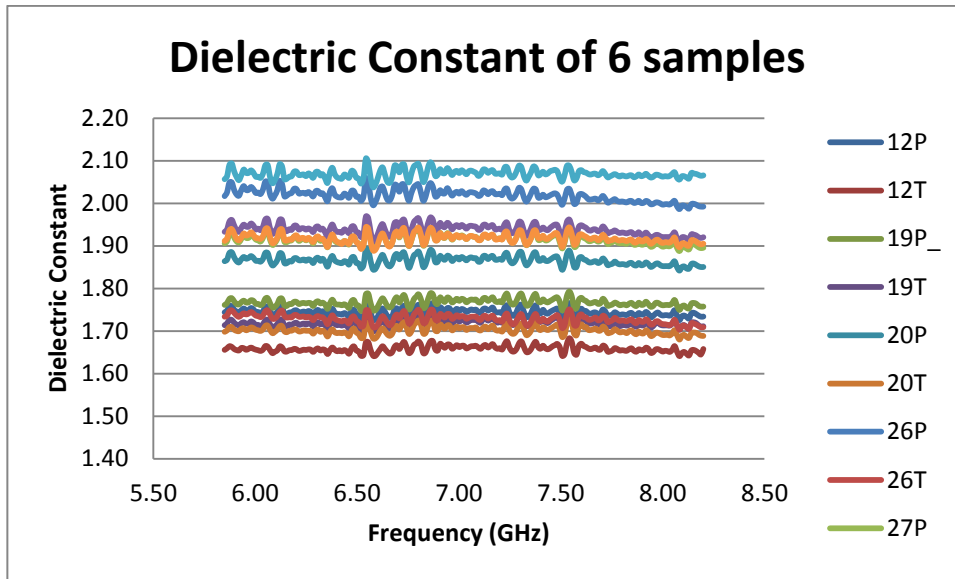


Figure 9 Dielectric constant versus frequency for 6 samples both Parallel and Tangential to direction of grain

### 3.2 Density Independent Function

An alternative approach is to use the density independent function developed at the USDA by Trabelsi [16]. This is a commonly used method for microwave sensors to remove the effect of density from their measurements.

The universal permittivity based method for determining moisture content independent of density was reported and has the form

$$\Psi = \sqrt{\frac{\epsilon''}{\epsilon' - \epsilon'' - a_f}}$$

Where  $a_f$  is a constant that is a function of frequency only, and is determined by a least squares minimisation so that the resulting function  $\Psi$  varies linearly with moisture content.

Figure 10 shows the density independent function versus moisture content for a range of wood densities spanning 300 to 700 KG/m<sup>3</sup> using data from Torgovnikov [4]. It can be easily seen that as the moisture content drops below the FSP the function no longer accounts for the density variation.

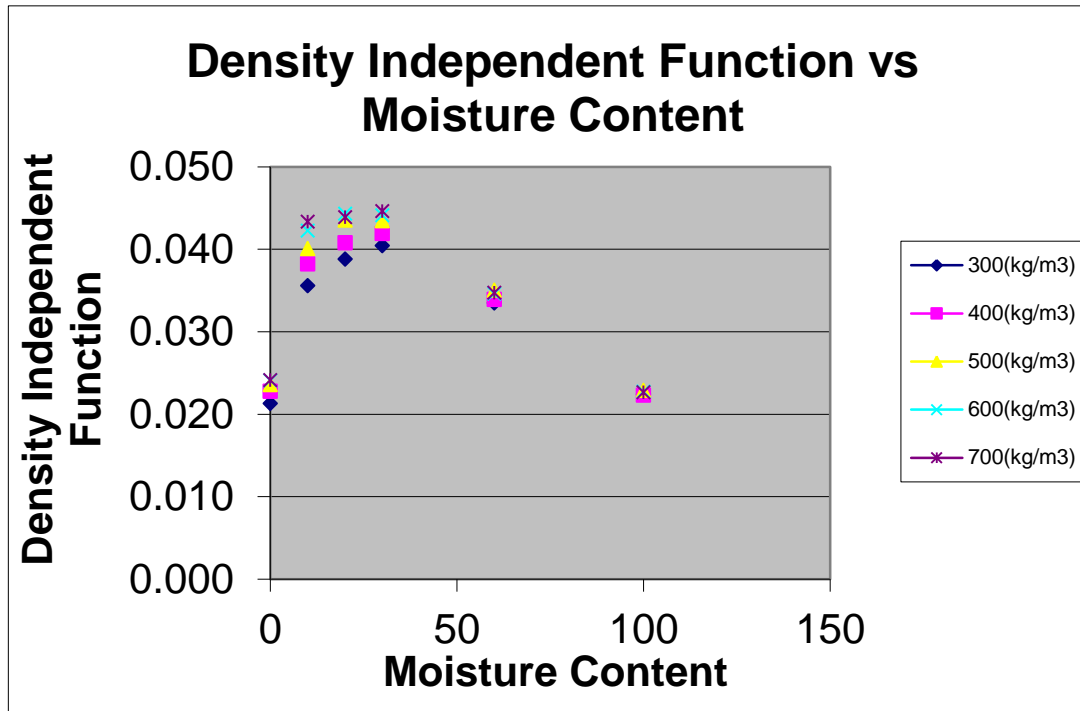


Figure 10 Independent function versus moisture content for published data

The explanation for the failing of the density independent function is in the nature of the water binding below the fibre saturation point. The water in this region is heavily bound in the structure of the wood and the dielectric properties of the water approach that of ice. This means that the remaining water no longer contributes significantly to the dielectric losses, and the loss factor ( $\epsilon''$ ) becomes small.

However what this figure does show us is that above the FSP we can easily negate the effects of density and accurately extract the moisture content. This in turn would also let us accurately determine the density so that it can be used later as a correction in measurements below the FSP.

### 3.3 Experimental Results

Using the fact that we can use the density independent function in the earlier phases of drying to determine the basic density, we can apply this as a correction to the measurements made below the FSP.

The plot below (Figure 11) shows the experimental measurements made on 12 samples at 10% moisture content. The purple and blue lines represent best fits to Torgovikov's [4]

published data for 400 and 300 kg/m<sup>3</sup> respectively, the measurement data (shown in red) has density ranging from 340 to 440 Kg.m<sup>3</sup>.

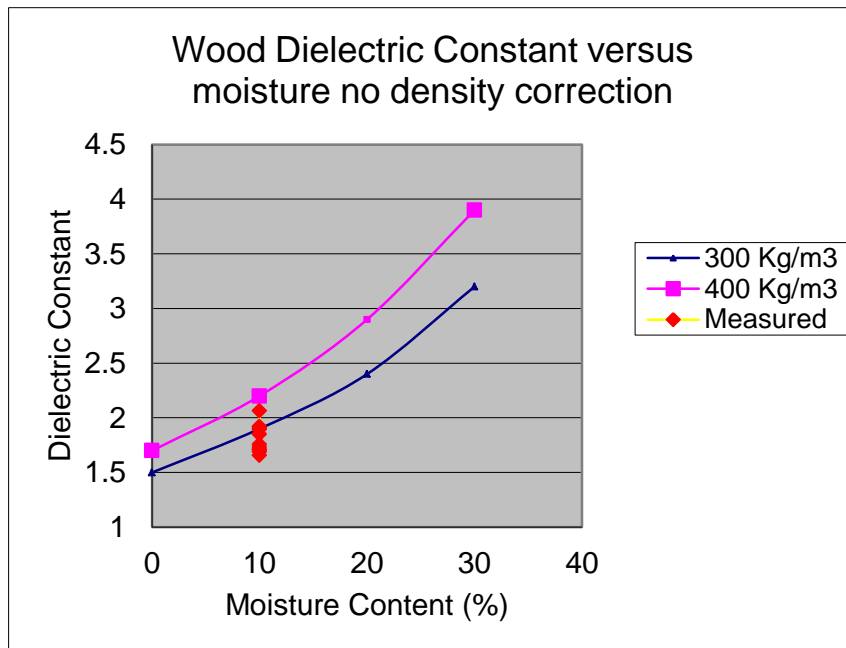


Figure 11 moisture content versus dielectric constant with no density correction.

This degree in spread of the data, if density was not known, would yield an RMS error in moisture content estimation of 3.59% with a mean of 0.2%, which is consistent with those reported in the earlier study.

If we now correct the data using the density previously determined, in this case normalize to 300KG/m<sup>3</sup>, the resulting figure 6 is found. This yields an rms error of 1.38% with a mean of 0.012%. The normalization process is simple as the variation due to density is simple linear function, as shown in Figure 12. In this Figure series 2 data is from all measurements made and the series 1 data comes from those published by Torgovnikov [4] for moisture contents of 10%.

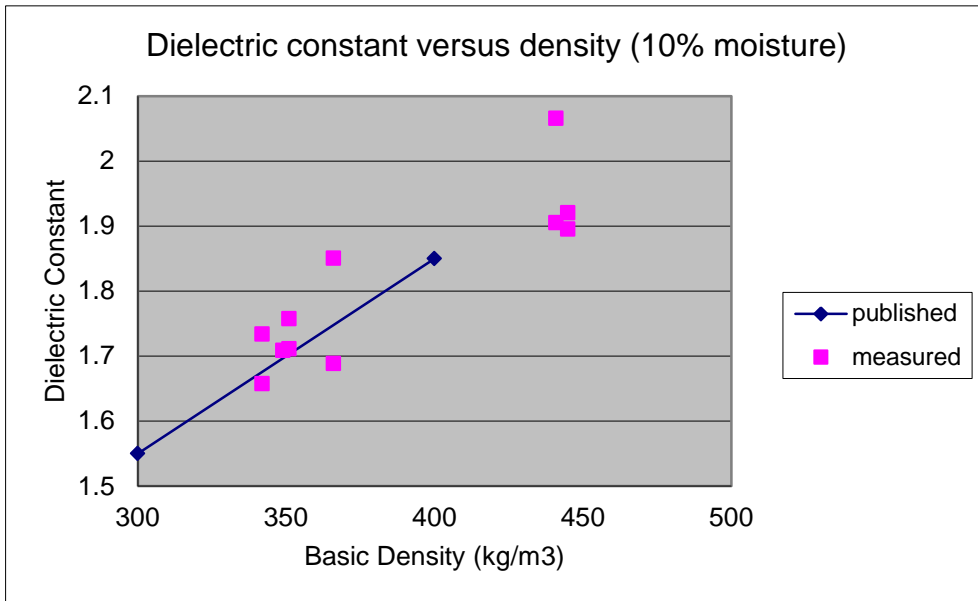


Figure 12 Dielectric Constant versus Basic Density

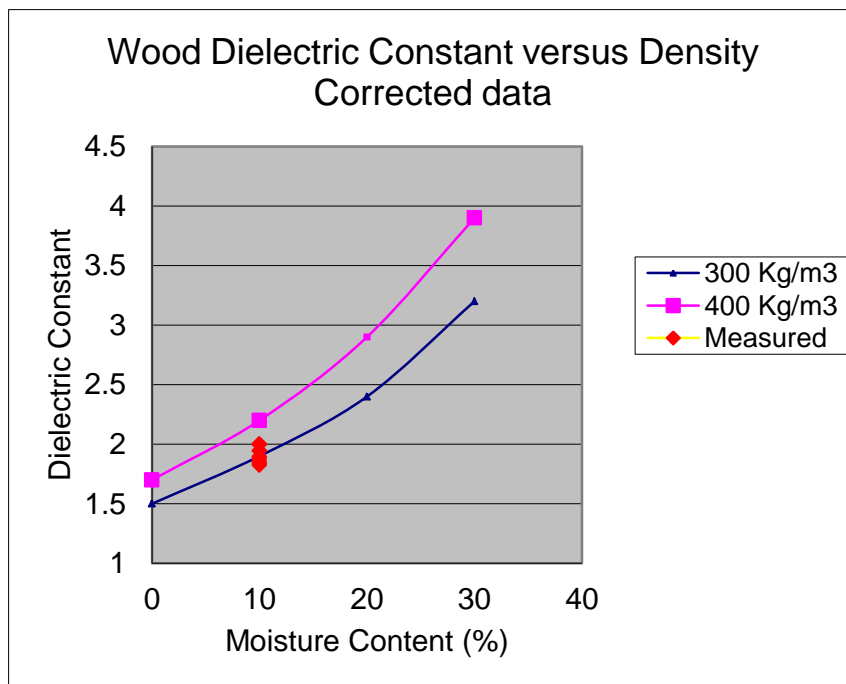


Figure 13 Density corrected dielectric constant versus moisture content.

The above Figure 13 shows the density corrected data in red for 10% moisture content samples, which does show a reduction in spread, however there still exists a very significant error (> 1%) by comparison to those gained by the earlier regression models used in the MKS.

In his book, although he does not directly mention the effect of the early wood late wood layer orientations, Torgovinikov [4] does present measurements on polarization of the applied field and also the ratio of Early wood to Late wood. The following section looks at the effect of this EW/LW layer orientation on the permittivity of wood.

In summary the Permittivity of wood below FSP is constant across the operation frequency of the MKS for moisture contents below FSP. This makes the determination of moisture content using a dielectric model unworkable. If density is not accounted for then RMS errors of 3.59% in moisture content were measured which is consistent with earlier MKS explicit model measurements.

For Moisture contents above FSP density can be determined using the standard density independent function. From this using density correction RMS errors of 1.38% in moisture content were achieved.

### 3.4 Early Wood /Late Wood layer Orientation

The following looks at the effect of early wood /latewood layer orientation on inferring moisture content of using permittivity measurements.

Wood has an anisotropic structure that arises from the cell pattern laid down in a defined direction by seasonal changes while the tree is growing. This Earlywood Latewood layering has the effect of ducting the microwave energy in a preferred direction (polarisation of the fields)

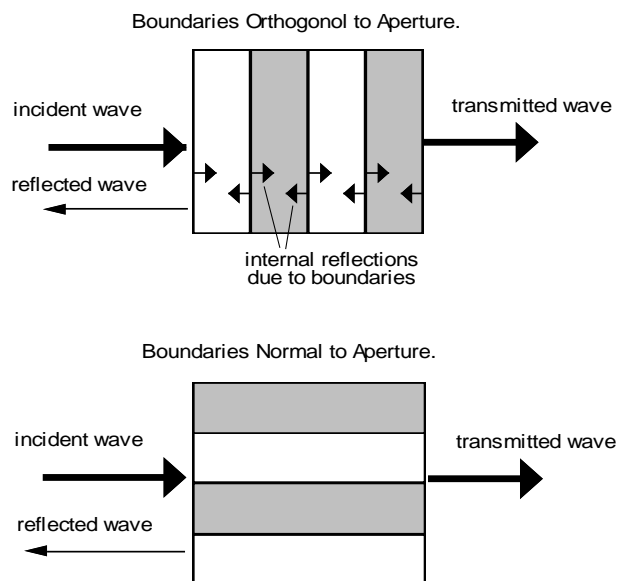


Figure 14 EW/LW layering

The change in polarisation of the microwave fields due to EW/LW layering has given rise to many systems proposed for the measurement of grain angle. One such system was developed by [2] which involved a rotating antenna that used the angle of the antenna and a maximum in the received signal to determine the grain angle of lumber.

In 1993 [17] coaxial probe permittivity measurements were made on a number of sawn lumber samples. The measurements were made every 5mm and the permittivity for two samples was plotted versus distance across the sample to produce Figure 15 from [17] shown below.

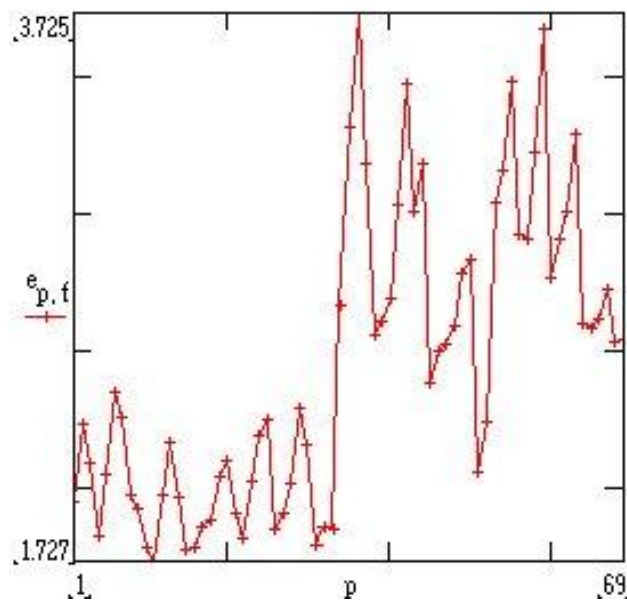


Figure 15 EWLW variation across wood sample

This EWLW experiment showed the cyclic variation in permittivity due to the EW/LW regions. The step change is due to the second sample having a significantly higher basic density due to a mix of heartwood and sapwood within the sample. This published graph does clearly demonstrate however the localised differences in permittivity between EW and LW.

### 3.5 Experimental Results

The measurements undertaken in Chapter 2 purposefully covered the full range of EW/LW layer orientations so as to reflect flat, intermediate and quarter sawn lumber.

Hence to examine the effect of this, the data covering flat and intermediate sawn were chosen to repeat the error analysis. Figure 16 below using only this data shows that the RMS error in moisture content using density correction is now reduced to 0.63%. Hence we can

see that much of the residual error in the previous section can be demonstrated to be due to the effect of EW/LW layer orientation.

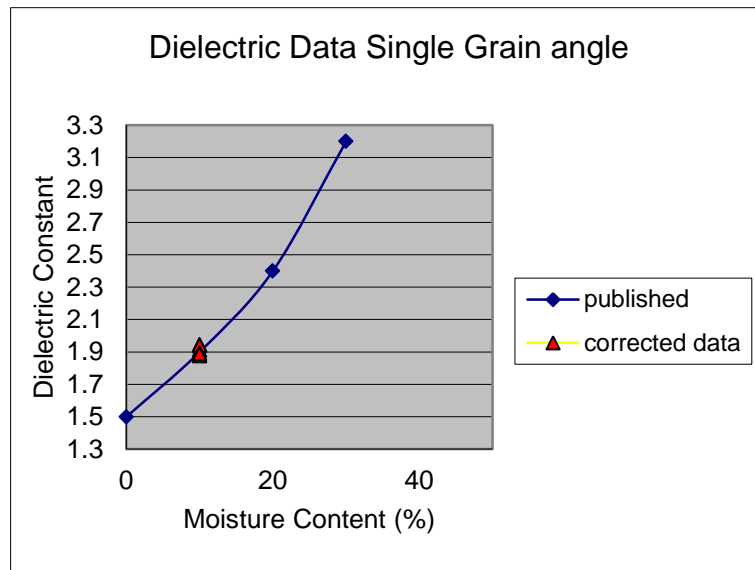


Figure 16 Density corrected measurements for flat and quarter sawn samples

### 3.6 Discussion

This work was aimed at determining the potential accuracy in moisture content measurement that the explicit MKS approach could achieve for lumber dried below the FSP. Previous work had shown an RMS residual error of 3%. In order for further development of the explicit approach to continue, a reduction in this error was required and also density independence of the measurement was critical.

This study has shown the weakness in the previous approach of using the universal permittivity based density independent function for wood below the FSP. This experiment demonstrated and confirmed the 3% error previously found.

This work also showed that if we determine the density using this function earlier in the drying cycle ( $mc's > 30\%$ ) it can be easily used to correct the measurement and result in residual RMS errors of 1.4% for all lumber flat through to quarter sawn.

Finally if we restrict the measurement to flat and intermediate sawn lumber we see that the residual error reduces again to 0.6%.

This positive result demonstrates that an explicit algorithm approach to inferring moisture content of lumber based on the measurement of permittivity at microwave frequencies is in fact feasible.

## 4.0 MKS Measurement System

The measurement of reflection coefficient from the sensor was accomplished using the well-known six-port reflectometer proposed by Engen [18]. This was selected as the most cost effective means of producing a broad band measurement which was robust enough for industrial trialling.

### 4.1 Six-port Reflectometer

The six-port is essentially a tapped transmission line with 4 ports equally spaced at  $\lambda/4$  as below in Figure 17. As the power measured at each port varies by the reflection coefficient, they in fact create the radius ( $r_i$ ) of a circle in the reflection coefficient plane of possible solutions. If placed in the four quadrants of the complex plane the intersection of these circles gives a unique solution.

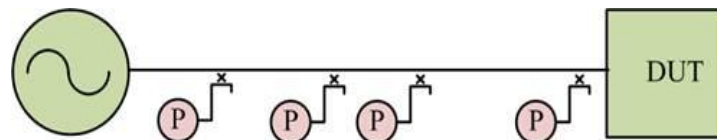


Figure 17 Conceptual Sixport

A refinement to this technique is by using the ratio of power measurements made by detector diodes at the measurement ports to the source power. This has the effect of reducing the problem to the intersection of three circles in the reflection coefficient plane, as shown in Figure 18, allowing the reflection coefficient at the measurement port can be determined.

If we normalize the powers to port4 such that

$$p_i = \frac{P_i}{P_4}$$

We can write the expression

$$p_i = \frac{P_i}{P_4} = C_i \frac{\Gamma - q_i}{d\Gamma + 1} \quad \text{for } i = 1 \dots 3$$

Graphically the six-port equations can be represented as circles, as shown in Figure 18, in the reflection coefficient domain ( $\Gamma$  circles). Each circle represents a range of possible solutions which satisfy the six-port equation and hence the unique intersection of the three yields the true solution.

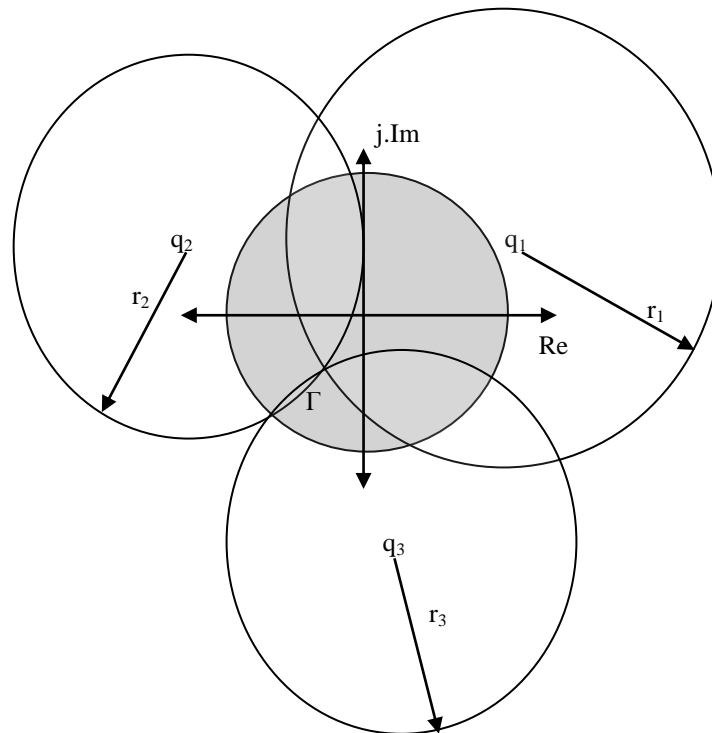


Figure 18 Graphical solution of six-port equations

In reality to achieve this and to allow for the centres  $q_i$  to be fixed with respect to frequency the six-port is implemented using  $90^\circ$  hybrids and directional couplers, as shown in Figure 19. As these are broadband devices whose properties are known we can insure that across the desired operating frequencies that the electrical lengths between the measurement ports remain at  $\lambda/4$ . This effectively fixes the centres of the circles in the reflection coefficient plane across the operating range.

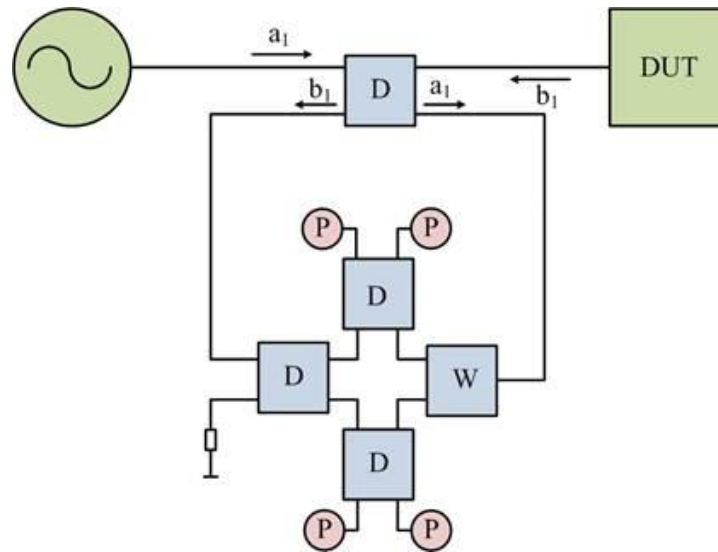


Figure 19 Hybrid based broadband sixport

#### 4.2 Six-port Implementation

The actual six-port used in this study was a variant of the standard design proposed by Judah [19] as shown in Figure 20. In this design a directional coupler is used to control the power sharing between the six-port and the load and hence forces the detector diodes into their linear operating regions, hence removing the need for a separate diode linearization.

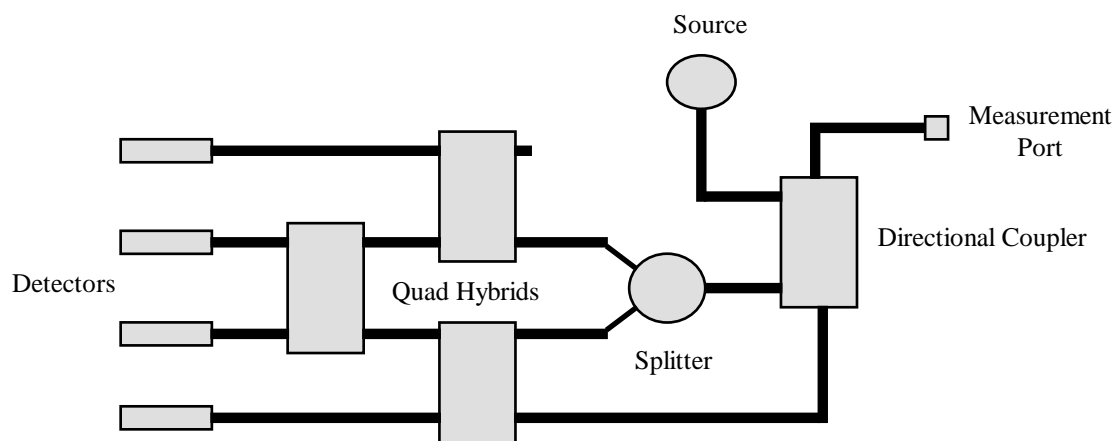


Figure 20 Six-port Implementation

In this basic configuration the measurement of reflection coefficient has a residual error of around 2%. This is primarily caused by two main factors; reflections within the six-port due to the diode detectors and harmonics from the source.

Although the diode detectors used in this design are a good match to the 50 ohm system within the six-port, they will still however give rise to small reflections. This issue is resolved by the inclusion of isolators before the detectors. This means any reflection back from the diodes is absorbed in the isolator and not propagated back through the six-port to interact with the other measurement ports.

The second issue of harmonics from the source is by far the dominant contributor towards measurement errors. As the diode detectors are not frequency selective they will also measure any harmonic component on the measured signal. To mitigate this, a low pass filter was designed and constructed to remove any harmonics or signals present above the maximum operating frequency. The filter itself was constructed using shorted stubs on a microstrip substrate. By incorporating the filter and isolator's into the final six-port (Figure 21) the achievable accuracy of measurement was improved by an order of magnitude to better than 0.2%.

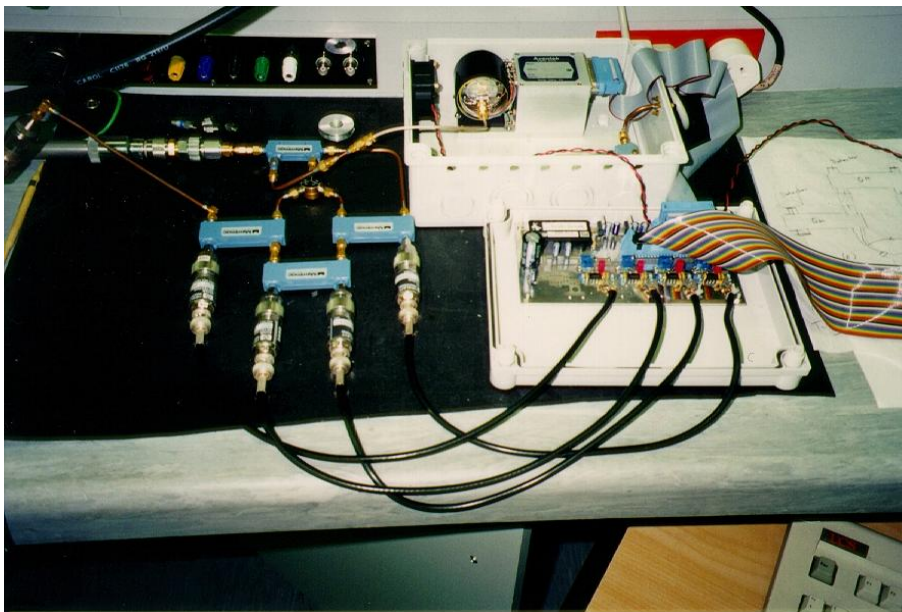


Figure 21 Photograph of Six-port

Calibration of the six-port is achieved by the measurement of a short circuit and an additional five offset shorts. These offset shorts are chosen such that they occupy each quadrant of the complex reflection coefficient plane. Using this calibration technique, the measurement error of the six-port was better than  $\pm 0.1\%$  in magnitude and  $5^\circ$  in measurement of phase.

As the kiln measurements can span several days in duration, the long term stability of the system was assessed. Measurements of a short circuit, after the successful calibration of the six-port, continuously for three days are presented in Figure 22 showing the port ratios along with the ambient room temperature. This showed that despite the six-port being held at a constant 31°C, there was still substantial temperature effects on the external measurement port itself.

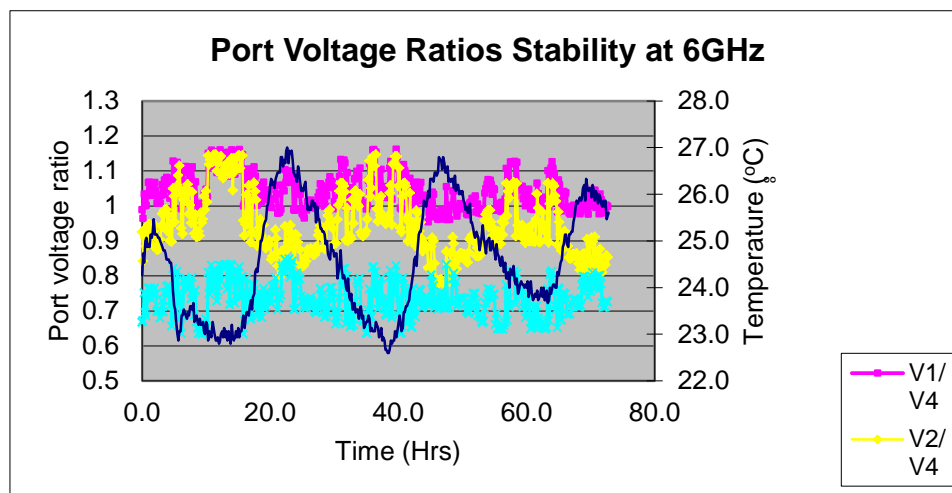


Figure 22 Sixport long term stabilityTerm

#### 4.3 Switched standard calibration:

As there is no control of the external temperature of the system the solution proposed was to routinely calibrate the six-port during the kiln measurement cycle. To achieve this standards were fabricated and using a 6 position electromechanical switch the five measurement standards could be measured on demand, with the sixth position as a through to the sensor, and hence calibrate the six-port.

The standards themselves required characterisation prior to fitting to the switch. Once fabricated the standards were measured using an Agilent PNA vector network analyser and adjusted so as to produce the best possible spread across the four quadrants of the complex reflection coefficient plane. During the course of the measurement and adjustment of the standards for the calibration system, it was noted that the accuracy of standard lengths is largely determined by the initial cutting, with a 0.5mm error completely renders the standard unusable. The semi rigid coax used suffers from dispersion over the 2 GHz range due to the changing dielectric properties of the coax. This means that the phase change produced by the standard is a function of frequency as well as the length of line used. Due to these

dispersive effects we cannot specify a single electrical length in the calibration routine, instead a simple polynomial function was used to specify the phase of the standard at each frequency; as usual the magnitude is equal to 1. Table 2 shows the polynomial expressions used to calculate the phase of each standard and their associated  $R^2$  value, where  $f$  is the frequency in GHz.

**Table 2**  
**Table of Fitted Standard Definition**

<b>Standard</b>	<b>Polynomial</b>	<b><math>R^2</math> value</b>
STD 0:	$ph0 = -2.5429f^3 + 49.899f^2 - 315.71f + 826.75$	0.9984
STD1:	$ph1 = 2.4789f^4 - 69.389f^3 + 720.3f^2 - 3288.6f + 5714.8$	0.9982
STD2:	$ph2 = 4.9928f^3 - 101.81f^2 + 660.57f - 1336.4$	0.9997
STD3:	$ph3 = 29.603x^2 - 462x + 2033.2$	0.9984
STD4:	$ph4 = -10.873x^3 + 238.33x^2 - 1784.4x + 4689.8$	1

Due to the dispersive nature of the semi rigid coax used it is difficult to maintain the desired spread of standards around the complex plane. This means that accuracy of the six-port at the high end of the measurement plane may be reduced.

#### 4.4 MKS Measurement Instrument

Whilst the sixport forms the basis of the MKS it requires a substantial infrastructure to enable the measurements to be made, as shown in Figure 24 the system block diagram. A standard personal computer was used to control and process all data from the reflectometer. This was achieved by a C++ program, source code listed in Appendix E, which undertook process control and conversions from the raw port voltages into reflection coefficients. The main user interface, as shown in Figure 1 allows for full configuration of the sixport and measurement cycle.

The software was configured so that the user could select the time period between measurements, which is necessary when varying kiln temperature settings can result in drying times ranging from 8 hours to several days. The user also had the ability to vary the start, stop frequency and number of measurement points within the frequency range. In addition it controlled the auto calibration function which was timed to occur every three hours.

The frequency would be set by the PC using a USB connection to a National Instruments NI6501 DIO board. This was used to drive the synthesiser and set the desired frequency for the measurement. A time delay of 0.5 seconds was then used to allow for the source to stabilise prior to any data acquisition from the measurement ports. The NI6501 was also used to set the mechanical switch positions in the auto calibrator section of the instrument

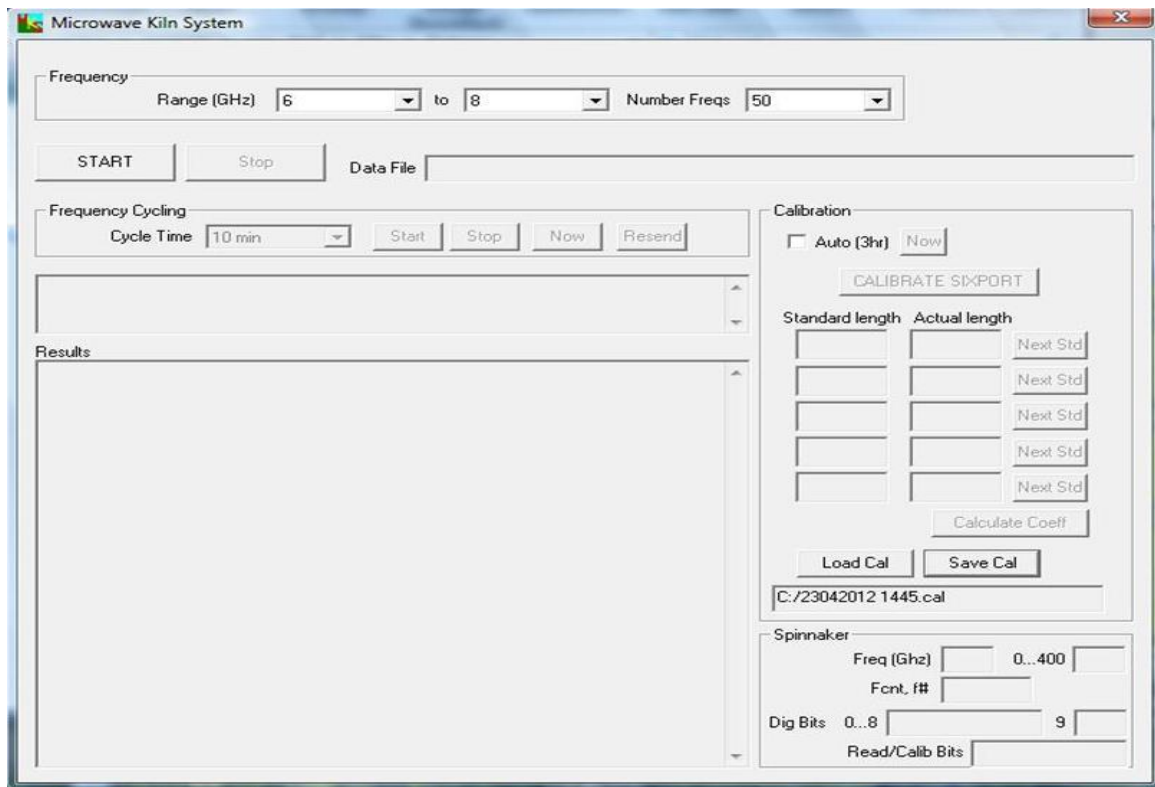


Figure 23 MKS Software User Interface

.Within the Instrument itself the data acquisition was achieved using a standalone microprocessor that communicated with the computer via a serial connection. The microprocessor would receive a request for a measurement and commence the measurement of the port voltages. For each of the four measurement port the average of 100 separate analogue to digital conversions would be made and then transmitted back to the PC.

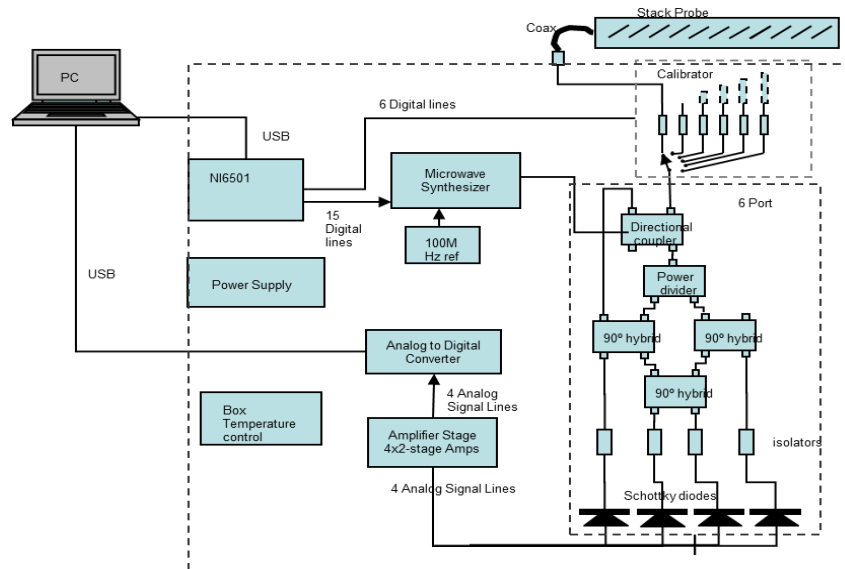


Figure 24 MKS measurement system block diagram

Perhaps the most critical section of the whole measurement system is the amplifiers which take the small voltages from the diode detectors and amplify them prior to analogue to digital conversion. This was accomplished by a separate amplifier board using Texas Instruments TLC2652A high precision chopper stabilised operational amplifiers. These were used primarily for their low input offset voltage which would otherwise have introduced unwanted errors into the measurement. A circuit diagram of the amplifier board is presented in Appendix F. Finally to improve the stability of the measurement system temperature control of the instrument case was also incorporated this was done using a PID temperature controller along with a heater to maintain the internal temperature at a constant set temperature. The final instrument is shown below in Figure 25.

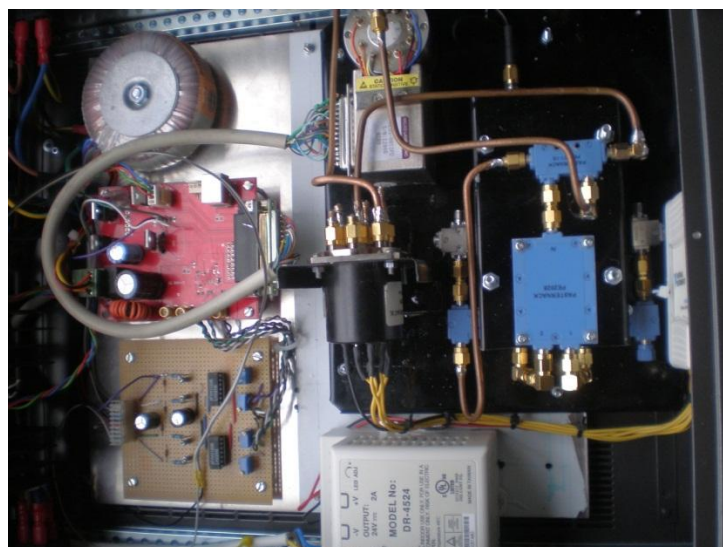


Figure 25 Photograph of MKS Measurement system

---

## 5.0 TRANSMISSION LINE MODEL OF WAVEGUIDE SENSOR

The kiln environment exhibits high temperature and humidity and potential for physical damage when the stack is placed in and out of the kiln, makes many forms of modern electronic componentry unsuitable. The sensor and associated apparatus are required to withstand these environmental factors. The simplest one of the microwave structures that meets these requirements is a hollow rectangular tube commonly termed as rectangular waveguide. As the name suggests a waveguide is a structure which will guide electromagnetic waves in a specified direction.

A full description of the mechanism of propagation down a uniform waveguide involves the solution of the Laplace wave equation. For the purposes of this paper a simplified explanation for a wave propagating down a hollow rectangular tube, ray bouncing as shown in Figure 26 Propagation in a rectangular waveguide, will be used. The wavefront maybe considered to be reflected off a perfectly conducting wall at oblique angles. When a second parallel wall is considered the wave is again reflected causing the wave to propagate in the desired direction down the tube.

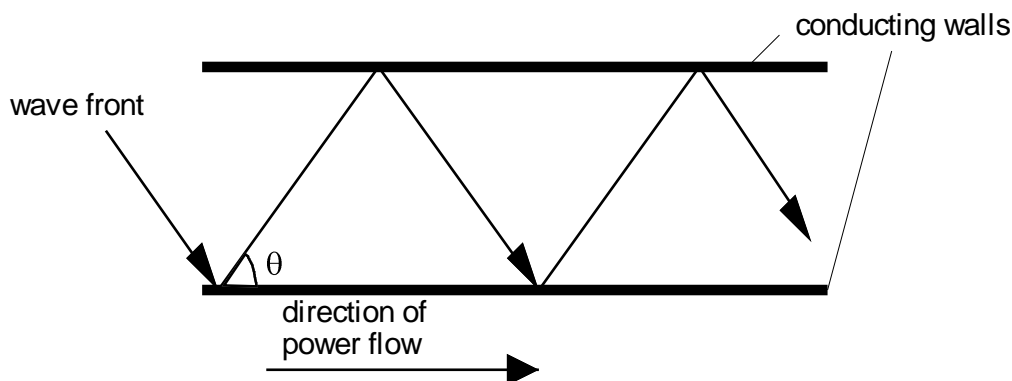


Figure 26 Propagation in a rectangular waveguide

The distance between successive intersections (along the waveguide) of the wave propagating in the guide is a function of  $\theta$  so it can be seen that as the applied wavelength is increased then  $\theta$  becomes larger up to a point where the wavefront is normal to the walls and at this wavelength no power can propagate down the guide. This is defined to be the cut-off wavelength and is a function of the waveguide broadwall dimension  $a$  (Figure 27). The wavefronts propagating in this waveguide can be represented as a combination of a time varying electric (E field) and magnetic field (H field) however knowledge of the electric field only is sufficient to characterise the problem considered here.

As well as propagating along the length of the waveguide the E field inside the guide has a defined spatial distribution (mode) in the transverse direction. The form of the electric field must obey the boundary conditions that the tangential component of the electric field is zero on a conducting surface. This boundary condition forces the E field modes to be sinusoidal in shape across the broad dimension of the waveguide and the existence of these modes is determined by the wavelength of the applied fields. The work presented in this report has been performed so that only one mode can be propagated along the waveguide. This mode is known as the  $TE_{10}$  mode expressed as;

$$E_x = E_o \sin\left(\frac{\pi x}{a}\right)$$

In this mode the E field is a constant value in the  $y$  direction and varies in a half sine wave in the  $x$  direction as shown in Figure 27. This fact allows us to across the single moded operating band of the waveguide reduce the height of the waveguide ( $b$ ) without changing the performance of the waveguide.

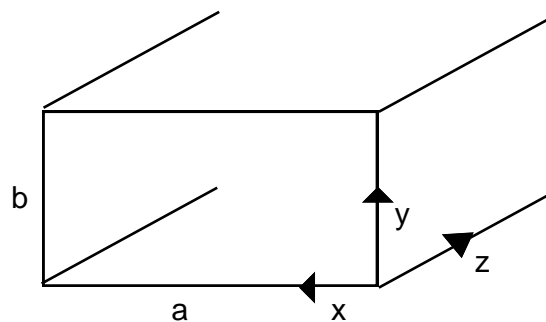
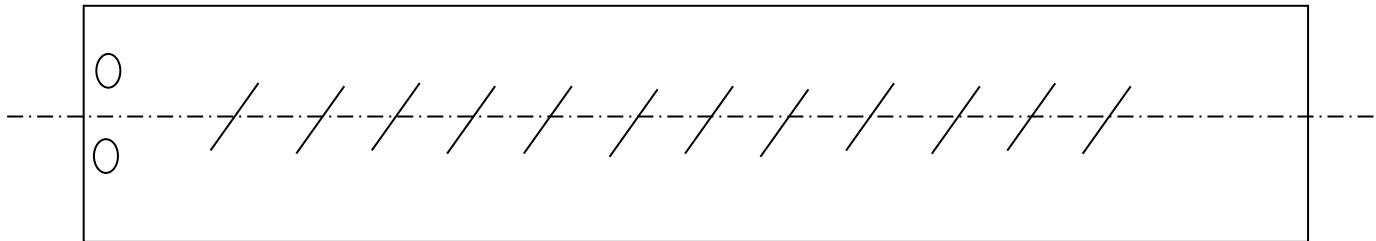


Figure 27 Rectangular waveguide

As the rectangular waveguide is a closed structure sensor provision is made for the E field to interact with a volume of timber in the stack by cutting slots in the broad wall.

For the current design shown in Figure 28, the slot was chosen to be a resonant length in air at 6.0 GHz and to be excited by the dominant TE<sub>10</sub> mode in the waveguide. The slot is centred in the broad wall and for minimum reflection in the air covered case a slot angle was determined. A slot in this configuration is analogous to a series of lumped admittances at intervals along the waveguide.

The aim of this new design iteration of the Kiln sensor was to reduce the domination of the early slots in the array. The original design by Holmes [1] suffered from poor power sharing and hence reduced sensitivity as a large proportion of the available energy in the guide is used in the initial slots. In order to improve the power sharing along the waveguide we have manipulated the coupling of the slots along the waveguide. Increasing the coupling as the energy passes down the waveguide by varying the slot angle from 15° to 30°



**Figure 28 Waveguide Aperture array**

Rather than varying the slot angle of each slot, which would be difficult to fabricate, the array was broken into four distinct slot angles. This means that the array has now four distinct sections comprising six slots.

### **5.1 Reflection Coefficient of an Individual Waveguide Slot:**

In order to determine the permittivity of the covering media we first need to determine the effect of permittivity on the reflection coefficient of the slot itself.

The fundamental concept embodied in the construction of this sensor structure is that microwave energy propagating along the interior of a waveguide will “leak out ” when presented with a resonant length aperture in the broadwall (Figure 29). The microwave energy will partially radiate from the aperture and partially undergo reflection back into the waveguide due to the presence of the covering material, and hence will propagate back to the measurement plane where these reflections can be measured directly. The proportion of the energy reflected back or transmitted through a material is governed by the permittivity of timber which is directly related to the moisture content (mc) and thus as the timber is dried the permittivity change will influence the amount of microwave energy reflected by the slot.

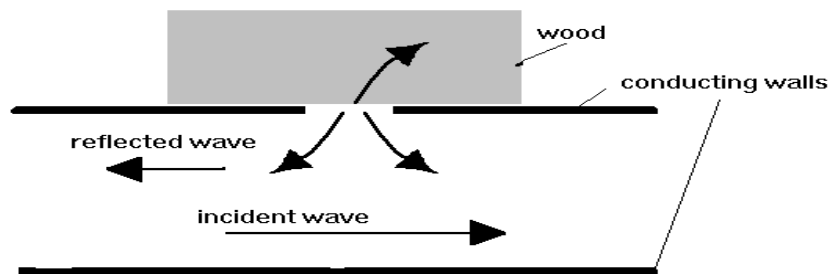


Figure 29 Conceptual view of single slot

In order to realise the design concept described above it was required that a design of an efficient radiating slot in the broadwall of the waveguide be produced. The radiating characteristics of the slot are governed by factors such as the position, angle and width of the slot along with the excitation voltages established by the propagating modes within the waveguide and characteristics of the materials both inside and outside the waveguide (figure 4). In this case the material inside the waveguide is air ( $\epsilon = 1$ ) and outside it is the wood being dried. Thus the electrical properties of the slot will be influenced by the moisture content of the wood ( $\epsilon = f(\text{mc})$ ). This is the fundamental component of this measurement technique

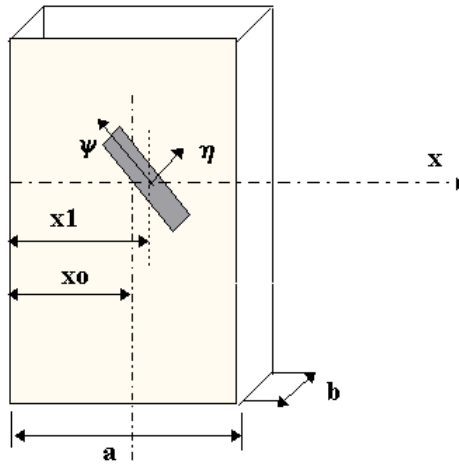


Figure 30 Waveguide slot in broadwall

The reflection coefficient ( $\Gamma$ ) (which is the quantitative ratio of reflected electric field to the incident electric field) from a resonant slot in the centre of the broad wall can be determined analytically from the expression below if the excitation voltage along the slot is assumed to have a cosine form yielding;

$$\Gamma = \sqrt{\epsilon} \frac{73\pi k \beta ab}{60|F(\Psi)|}$$

Where

$$F(\Psi) = \frac{j\pi}{k} \left( \beta \sin(\Psi I(\Psi)) + \frac{\pi}{a} \cos(\Psi J(\Psi)) \right)$$

and

$$I(\Psi) = \frac{\cos\left(\frac{p(\Psi)\pi}{2}\right)}{1 - p(\Psi)^2} + \frac{\cos\left(\frac{q(\Psi)\pi}{2}\right)}{1 - q(\Psi)^2}$$

$$J(\Psi) = \frac{\cos\left(\frac{p(\Psi)\pi}{2}\right)}{1 - p(\Psi)^2} - \frac{\cos\left(\frac{q(\Psi)\pi}{2}\right)}{1 - q(\Psi)^2}$$

And

$$p(\Psi) = \frac{\beta \cos(\Psi)}{k} - \frac{\pi \sin(\Psi)}{ka}$$

$$q(\Psi) = \frac{\beta \cos(\Psi)}{k} + \frac{\pi \sin(\Psi)}{ka}$$

and

$$k = \frac{2 * \pi}{\lambda}$$

and

$$\lambda = c/f$$

and

$$\beta = k \sqrt{1 - \frac{f_c^2}{f^2}}$$

where

$\lambda$  = free space wave length

$c$ = speed of light

$a$ = broadwall dimension

$b$ = sidewall dimension

$\Psi$ = angle of slot w.r.t longitudinal axis

$\epsilon$  = permittivity of the covering wood

$f_c$ = waveguide cutoff frequency

where  $a$  and  $b$  are the waveguide dimensions,  $k$  is the free space wave number and  $F(\Psi)$  is a function of the angle of the slot with respect to the centreline of the waveguide. A full derivation of the above is given by [20] and by [21] for the general case of thin slots in both shunt and series configurations. In order to examine the effects on the reflection coefficient, within the waveguide of a slot due to changes in frequency, the following expression for reflection coefficient of a slot, covered by air, can be found;

$$\rho = \frac{0.131 \cdot \lambda_{air}^3}{a \cdot b \cdot \lambda_g} \cdot \left( I_{\Psi} \sin \Psi + \frac{\lambda_g}{\lambda_c} \cdot J_{\Psi} \cos \Psi \right)^2$$

where  $\lambda_{air}$ ,  $\lambda_g$ ,  $\lambda_c$  are the wavelength in air, wavelength within the waveguide and the cutoff wave length respectively.

For use in this application, it is desirable that the slot admittance, for a given permittivity value of the covering media, should remain constant over a reasonable bandwidth. With this in mind the reflection

coefficient for an air covered slot was calculated from 6 GHz to 8 GHz, and is presented in Figure 31 for both the standard 20mm height waveguide previously used in the original MKS and the proposed reduced height guide (5mm) used in this new sensor design.

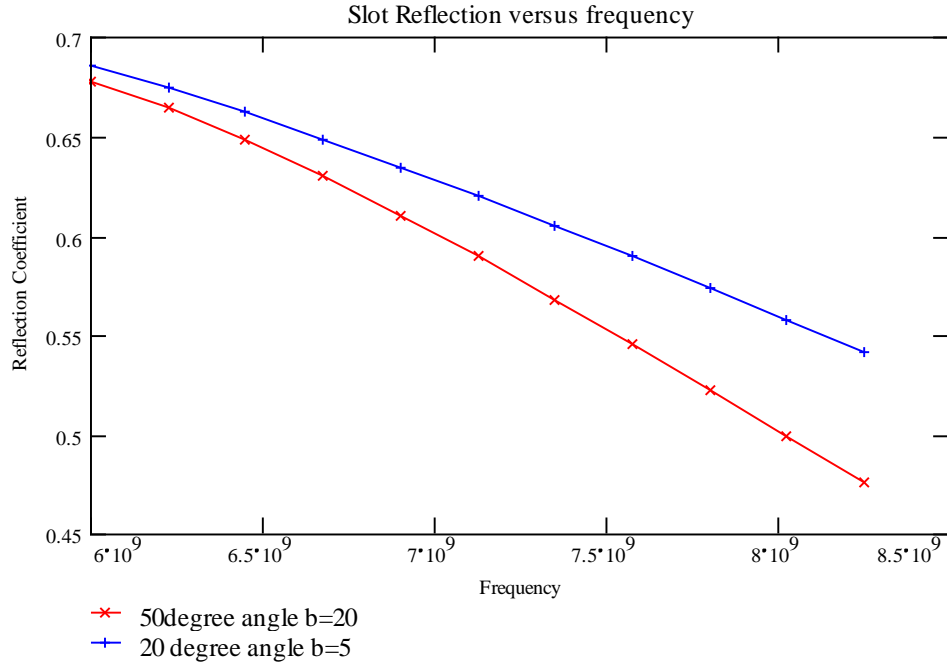


Figure 31 Reflection coefficient of an air covered slot in waveguide

As can be seen from Figure 31 above the reflection coefficient of the slot does not change rapidly with frequency, across the range of 6GHz to 8GHz for both the original MKS and new waveguide dimensions. This factor should allow an objective function to solve for the admittances of a particular slot in the waveguide as long as the number of frequencies within the range is greater than the number of slots. As the propagation of this energy within the waveguide is not affected by the covering material on the slot, a simple air measurement could be used as the calibrating standard for this system.

By replacing  $\lambda_{air}$  with  $\lambda\varepsilon$  it is a simple process to determine the permittivity of the covering wood layer.

$$\varepsilon = \left( \frac{1}{\Gamma} \cdot \frac{73\pi k \beta ab}{60|F(\Psi)|} \right)^{-2} \quad (\text{Eqn 2})$$

A plot of the change of slot reflection coefficient versus change in permittivity of the covering media is show below in Figure 32

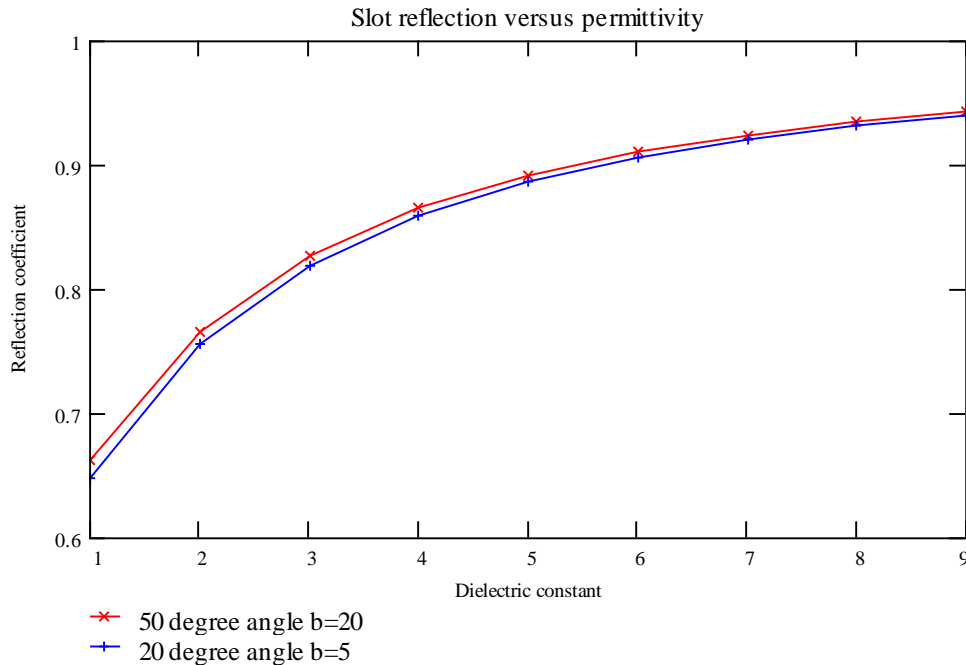


Figure 32 Slot reflection versus permittivity at 6GHz

## 5.2 Power Sharing.

The current design of the MKS comprises of an array of equi-spaced centre inclined slots operating as a standing wave array. The characteristics of the centre inclined slots are ideal for this application as they have excellent, and predictable, off resonance performance.

In order to improve the power sharing along the length of the sensor we need to reduce the effect of the first slots and increase the contribution of the latter slots in the array. This is achieved by altering the reflection coefficient of slots to either reduce or increase the energy that the slot contributes to the reflection from the array as a whole. This essentially means that as we move along the array the reflection coefficient of the slots will increase. In order to increase or decrease the reflection coefficient of the slot we adjust the angle of the slot with respect to the longitudinal direction of the waveguide.

The current sensor has 24 slots along its length. A typical piece of 100 x 50 mm lumber will cover 2 slots. In order to use the current probe, with only a new top plate to be fabricated, so we can maintain this design.

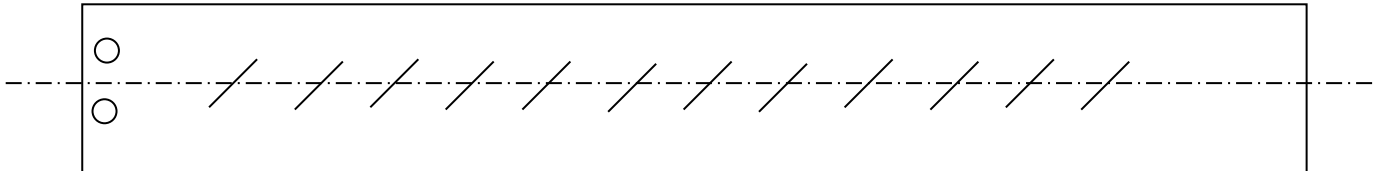


Figure 33 MKS probe layout

In addition to this rather than varying the slot angle of each slot, which would be difficult to fabricate, I have broken the array into four distinct slot angles. This means that the array has now four distinct sections comprising six slots. The following table outlines the required slot angles for the new MKS top plate.

Angle	Slots	Reflection Coefficient
15°	1-6	0.01
20°	7-12	0.16
25°	13-18	0.23
30°	19-24	0.3

### 5.3 Determining Permittivity from the Individual Slot Reflection Coefficients:

The current waveguide sensor can be modelled as a simple transmission line structure terminated in a short circuit, with periodic reflections from the slots, as shown below in Figure 34 transmission line model.

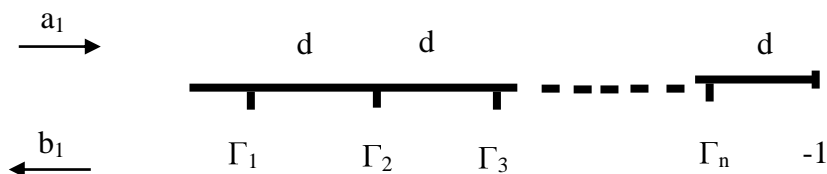


Figure 34 transmission line model

Using the above and defining the measured reflection coefficient as

$$\Gamma_{meas} = \frac{b_1}{a_1} - 1 = a_1 e^{-j2\vartheta} \Gamma_1 + a_2 e^{-j4\vartheta} \Gamma_2 + a_3 e^{-j6\vartheta} \Gamma_3 + \dots + a_n e^{-j2n\vartheta} \Gamma_n$$

Where n is the number of slots and the phase change is expressed as

$$\vartheta = \frac{2\pi}{\lambda} * d$$

When expressed for multiple frequencies we can write the above as a matrix

$$\begin{bmatrix} \Gamma m_1 \\ \Gamma m_2 \\ \dots \\ \Gamma m_i \end{bmatrix} = \begin{bmatrix} A_{1,1} & A_{1,2} & \dots & A_{1,n} \\ A_{2,1} & A_{2,2} & \dots & A_{2,n} \\ \dots & \dots & \dots & \dots \\ A_{i,1} & A_{i,2} & \dots & A_{i,n} \end{bmatrix} \begin{bmatrix} \Gamma_1 \\ \Gamma_2 \\ \dots \\ \Gamma_n \end{bmatrix}$$

Where

$$A_{i,n} = a_{i,n} e^{-j2n\theta_i}$$

Where n is the number of slots and  $\theta$  is the phase change between slots at the  $i$ th frequency. And  $a$  is a constant for that slot. Now that we have a way of relating the individual reflection coefficients from the slots to the measured reflection coefficients at the measurement plane, we now need to relate these to the permittivity of the covering timber. So if we express the matrices as

$$\Gamma m = A \Gamma$$

We can determine the individual slot reflection coefficients by inverting the A matrix.

$$A^{-1} \Gamma m = \Gamma$$

Hence we can now use the measured reflection coefficient at multiple frequencies to determine the reflection coefficient of an individual slot. The next step is to relate this to the permittivity of the covering material.

#### 5.4 Permittivity Mixture Models to Determine Wood Moisture content:

Once we have obtained the permittivity of the covering lumber from the individual slots we still have relate these to moisture content. There are many models which relate the permittivity of a mixture of materials to the individual permittivity of the component materials. For this study we have used the most commonly used volumetric model. This simply multiplies the individual permittivity values by the volume fraction of the mixture. It assumes a simple two component mixture of wood and water then

$$\varepsilon = \varepsilon_{water} \cdot V + \varepsilon_{wood} \cdot (1 - V)$$

Where  $V$  is the volume fraction of water in the mixture. This simplistic model is then used to determine the moisture content from the measured

$$V = \frac{\varepsilon - \varepsilon_{wood}}{\varepsilon_{water} - \varepsilon_{wood}}$$

Hence the moisture content by percentage dry basis can be found as

$$mc = \frac{V}{1 - V} \cdot 100 \quad (\%)$$

The calibration process is simply the inverse of this procedure, using boards of known moisture content we can work backwards to determine the elements in the A matrix.

#### 5.5 Explicit Algorithm Trial

In order to test the algorithm described three trials were undertaken in the experimental kiln at Scion in Rotorua using the new sensor and sixport system. The three charges labelled 050909, 240809 and 110909 were performed using a 15 hour 140°C kiln schedule. During the course of each kiln charge the process was routinely interrupted and the sample boards weighed, so as to assess the moisture content of each board via the oven dry method at the completion of each charge.

Using the measured data from the sixport and also the known sample moisture contents the coefficients of the A matrix were calculated for each charge, hence allowing for the mc of the individual boards to be determined. In order for this approach to be successful the calibration coefficients determined (A matrix) must be transferable from one like charge to another.

The following graphs (Figure 35) show the results for the second board from the coax end on the sensor (sample 43A) in charge 110909 using A matrix coefficients from trials 240809 and 050909 respectively along with a prediction of moisture content based on the actual sample weighing (solid line). As can be seen from the plots below a step change in the measurements occurred around the 9 hour mark which coincided with a sample weighing. After this point calibration coefficients from run 240809 no longer give accurate results and run 050909 coefficients are now correct.

Because of this change it can be seen that there is another reflection which has been introduced into the measurement system. This is most likely a connection to the probe or cabling issue. This problem will need to be located and mitigated by both removing connectors in favour of fixed permanent connections and reducing cabling lengths.

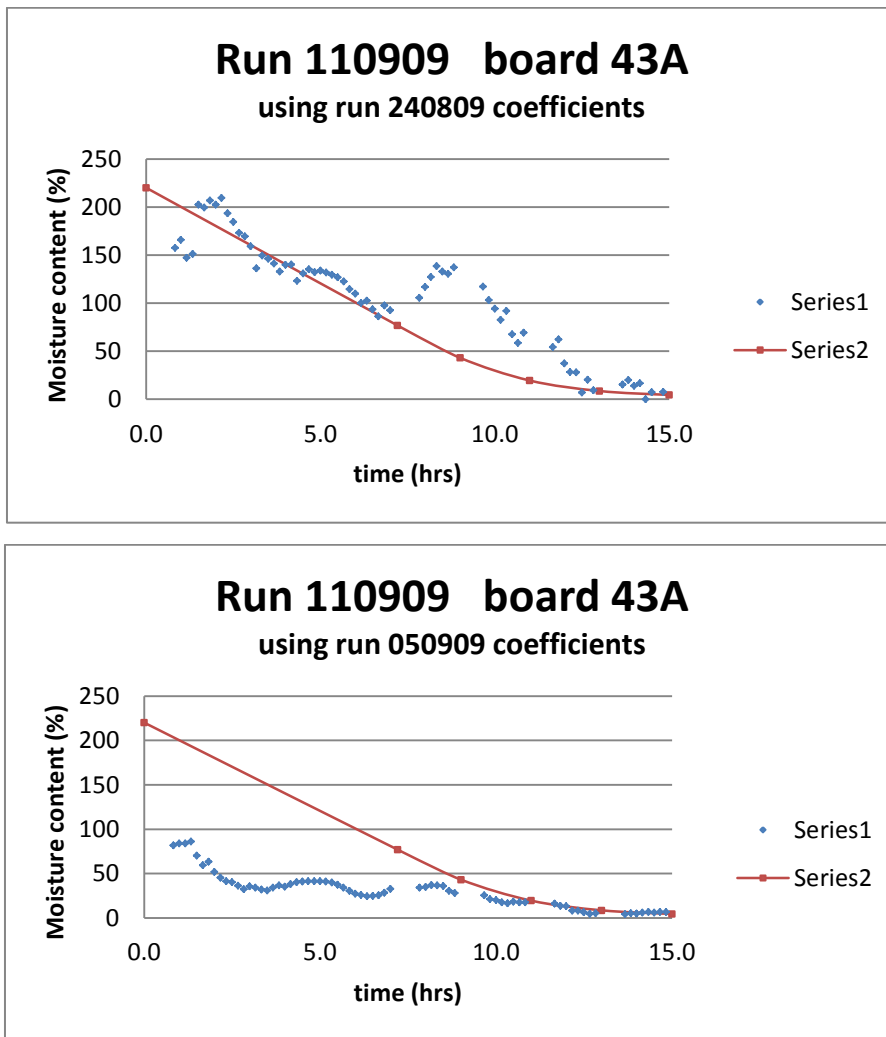


Figure 35 Explicit Measurement Trial

The two following plots (Figure 36) show the results above and below the event at the 9 hour point using the best calibration coefficients. The results are pleasing in that they show that the probe is functioning and once the unknown reflection source is remedied the system is functioning as expected.

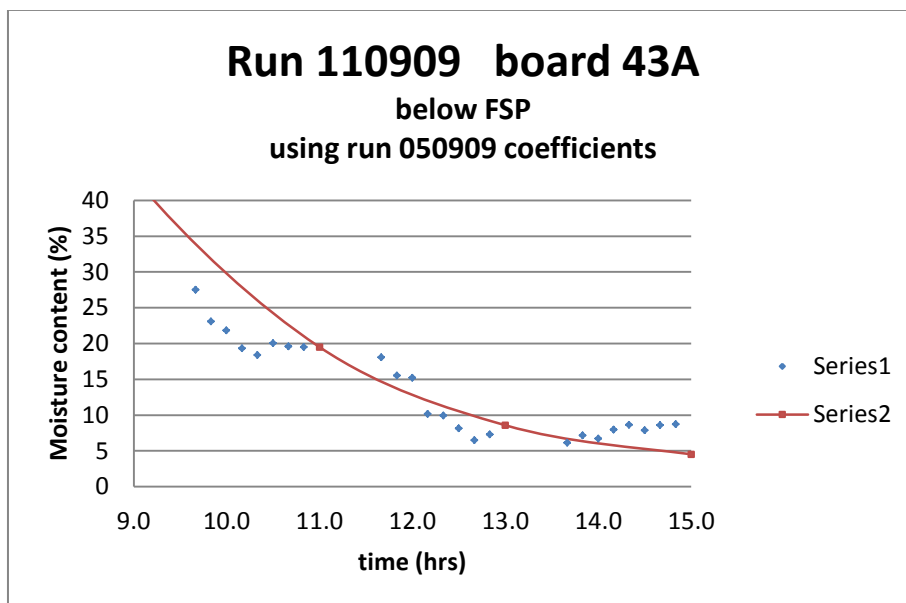
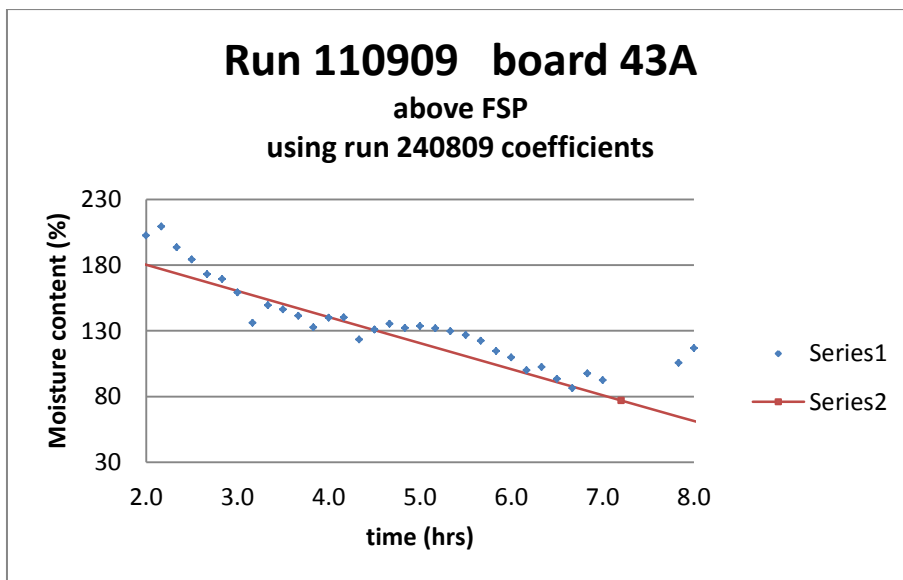


Figure 36 Explicit trial below FSP

Presented below in Table 3 is the error analysis for each sample board on the probe. The table is laid out sequentially with row one corresponding to the sample closest to the coaxial end and the final row being the shorted end of the waveguide. These results are for the measurements below the Fibre Saturation point of 33% and use the probe calibration coefficients developed from run 050909. As can be seen an rms error of approximately 3% is typical for each board on the probe across the range 33% to 1% moisture content.

Sample No.	Mean Error	Error RMS
42A	0.053	2.893
43A	0.176	3.076
44A	0.132	3.056
45A	0.052	2.897
46A	0.086	2.416
47A	0.183	3.052
48A	0.098	2.773
49A	0.066	2.761
50A	0.032	2.893
51A	0.109	3.002
52A	0.099	3.091
18AB	0.043	2.913
	%	%

Table 3 Error for all sample boards in Run 110909 below FSP using Run 050909 calibration coefficients

The measurement above makes no effort to correct for the basic density of the samples. Although the concept and algorithm to perform this has been developed it has yet to be tested on the MKS system. It is considered however that the correction for density will reduce this measurement error considerably.

### 5.7 Potential sources of error in model

The first order approach proposed in this section has three potential sources of measurement error that have not been accounted for and will contribute greatly to the overall measurement accuracy.

The first and greatest source of error is the dielectric model used to determine the moisture content from the measured permittivity. The model used is a simple bi-phase mixture model which assumes that the timber contains only wood and free water. Whilst this is a common approximation used it does not cater for the fact that there is at least three states of water contained within the sample, namely free water and intra cellular and extracellular bound water. The nature of the water binding as discussed by Kraszewki [22] greatly influence's the dielectric constant and loss factor. Also grain angle as shown

by Torgovnikov [4] will also greatly influence the permittivity and hence the moisture content calculated.

A second potential source of error unaccounted for by this model is mutual coupling by the slots both outside and within the guide as described in [23] [24]. This shows that via the mutual coupling each slot will influence those adjacent to it. In the context of this sensor the external mutual coupling is somewhat mitigated by the covering timber samples as shown in Figure 37, as the internal reflection due to the air gap between the samples suppress this. However mutual coupling within the waveguide itself between slots will still occur.

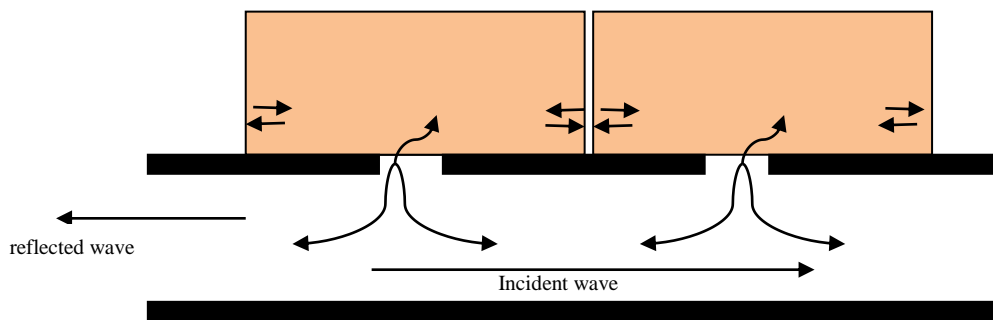


Figure 37 Mutual coupling between slots

Board thickness is also another source of errors in both the explicit and regression approaches. We cannot use a free space approach to modelling the interactions between the covering dielectric and the energy propagating within the waveguide. In other words the bulk of the measured reflection is not from the interface between the dielectric covering and the slot. As described in [25] [26] when a wave propagating in a waveguide encounters an aperture, this discontinuity establishes an infinite number of modes in this region. The effect of this is to establish an evanescent field which, can be modelled as a localised capacitance within the transmission line. This evanescent field essentially establishes the voltages and currents required for the slot to act as an antenna. Effectively this allows us to consider the slot as a radiating structure within a space field with the covering dielectric medium.

Now that we have radiation, we must consider that the antenna is radiating into a medium that is not infinitely thick. In actuality the dielectric covering only occupies the near field region Hence an evanescent field exists within the volume of the timber covering the slot. This mismatch, as shown by [27], between the air and dielectric at the boundary constrains the field within the dielectric. Hence as

wood has dielectric loss, along with half wavelength effects, the thickness of the covering timber layer will have an influence on the effective capacitance of the slot.

The final source of errors not considered by this first order model is the reflections from imperfect components such as waveguide to coax transitions and other connectors. These connections will have small but measureable reflections and also generate other modes of propagation within the sensor and measurement system. Although these are mostly accounted for during calibration, any minor disturbance during operation such as a cable moved will result in a measurement error being introduced.

---

## 6.0 REGRESSION MODELLING OF WAVEGUIDE SENSOR

A series of experimental trials were performed in the Scion wood drying tunnel with the waveguide sensor orientated with the sensor beneath the sample boards with the slots facing upwards. In each series 600mm long radiata pine sample boards were stacked in 1.5 m wide layers, dried on a range of commercial schedules. The kiln control software (Dryspeg) gives each individual kiln charge run a unique number so as to allow for later investigation of actual kiln conditions during the run. This unique number (eg 1428,1414,1419 etc) was also used as the identifier for these trials. Air flow could be directed from either direction and inlet dry bulb and wet bulb temperatures were controlled as in a commercial drier. Each sample board was weighed initially and periodically during each run. This allowed for actual moisture contents of each sample board to be determined at periodic points throughout the kiln run. A line of best fit was used on these periodic moisture measurements to give us our dependent variable of moisture content for later off-line regression analysis.

The microwave reflection coefficient measurements were performed using a sixport analyser, configured to measure 16 frequency points from 6.0 to 8.0 GHz. A simple software programme was written to control the sixport remotely and allowed for measurements to be performed and stored at predetermined intervals during the drying runs. This interval was chosen based on the anticipated length of the drying run such that a total of approximately 150 measurements would be performed.

### 6.1 Modelling the moisture content of samples under Microwave technique

For each of the kiln drying charges the magnitude of the reflection coefficient was calculated for all frequency points covering the range of 6.0 to 8.0 GHz. The multivariate regression analysis was carried out in Microsoft Excel using the following equation

$$mc = B_0 + B_1 \cdot A_1 + B_2 \cdot A_2 + \dots + B_{16} \cdot A_{16} \quad (1)$$

where mc is the dependent variable of actual moisture content,  $B_i$  ( $i = 0, 1, \dots, 16$ ) are regression coefficients and the independent variables  $A_i$  ( $i = 0, 1, \dots, 16$ ) which are the measured magnitudes of the reflection coefficients at each equi-spaced frequency. Figure 38 and Figure 39 present the variation of calculated moisture content for timber samples and the actual during the course of heating

in the kiln for Run 1311. It must be remarked here that the samples in the kiln are all different ranging from sap wood to heart wood having different values of initial moisture content and density.

The results of this regression are presented, sequentially from the first board by the measurement plane through to the last sample board by the shorted end of the guide, as shown in Figures 1 to 9 for various samples in Appendix C with the values of regression Appendix D. These figures show the variation of moisture content as a function of time. The points in these figures show the values of Moisture content computed from the regression equation (1) using measured reflection coefficient values and curves are the measured ones. Figure 38 presents the measured values of Moisture content as a function of time in reduced unit for a single sample board.

There is a very good agreement between the computed values of Moisture content and the measured values of Moisture content for all 9 samples in the entire range of Moisture content ranging from about 200% to 4% with a value of  $R^2$  for 9 samples is  $R^2 = 0.96$ . More accurate measurements of Moisture content over smaller time intervals, accurate account of timing and averaging of the S-parameters can further improve the accuracy.

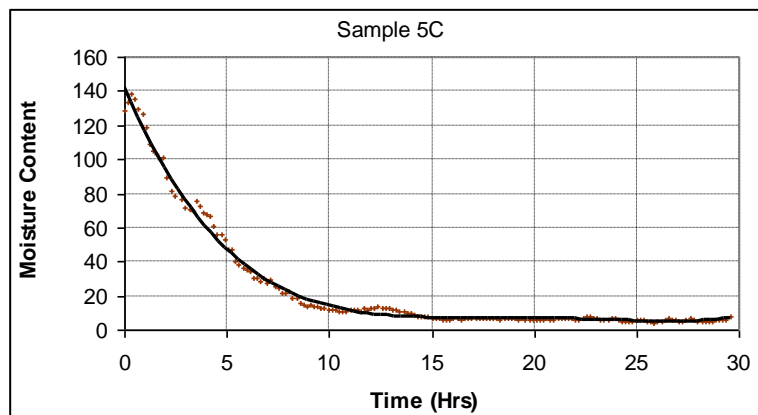


Figure 38 Calc mc of sample 5C as a function of time Run 1311.

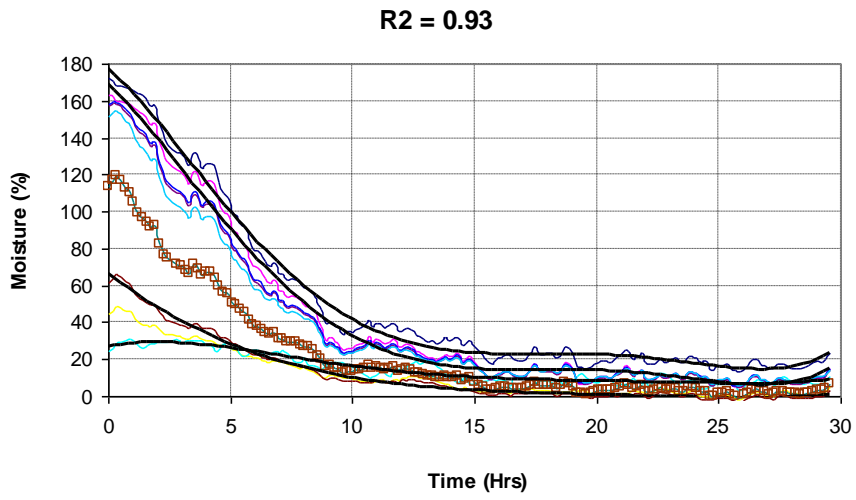


Figure 39 Variation of Moisture content of all samples Run1311.

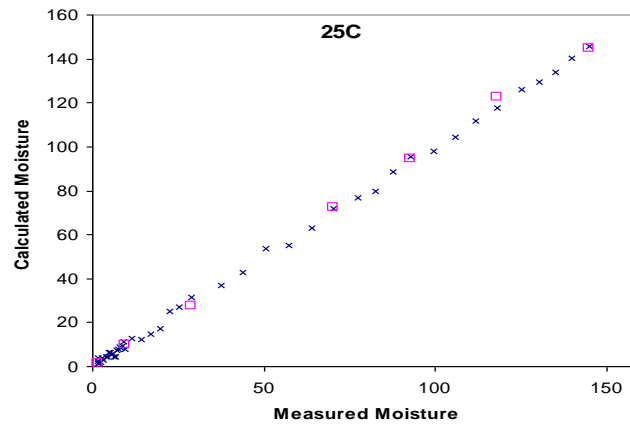


Figure 40 Comparison of measured and calculated of mc for Sample 25C in Run S1428.

charge 1428 90/60 (26 training 25 validate 12 sample boards)								
	all				less 30			
Samlpe No.	mean	Stdev	rms	mean abs	mean	stdev	rms	mean abs
25C	-0.72	2.62	2.67	1.97	-0.94	2.73	2.82	2.04
31I	-0.59	1.67	1.74	1.27	-0.92	1.74	1.92	1.38
26D	-1.45	4.55	4.69	3.44	-2.11	4.07	4.48	3.24
16F	-0.97	3.06	3.15	2.33	-1.51	3.02	3.30	2.37
31B	-0.78	2.35	2.43	1.85	-1.25	2.34	2.59	1.98
17D	-0.76	2.90	2.94	2.10	-1.32	2.95	3.16	2.33
20D	-0.42	1.81	1.82	1.31	-0.75	1.90	1.99	1.47
34A	-0.58	2.46	2.48	1.80	-1.03	2.53	2.66	1.97
24F	-0.55	2.32	2.34	1.73	-0.96	2.45	2.56	1.90
26B	-0.54	3.48	3.45	2.50	-1.00	3.38	3.43	2.62
14A	-0.33	2.86	2.82	2.07	-0.73	2.91	2.92	2.31
23A	-0.23	2.75	2.62	2.17	-1.62	2.07	2.18	1.62
all slot	<b>-0.66</b>	<b>2.74</b>	<b>2.76</b>	<b>2.04</b>	<b>-1.18</b>	<b>2.68</b>	<b>2.83</b>	<b>2.10</b>
charge 1414 90/60 (98 training 146 validate 12 sample boards)								
1A	5.15	6.78	8.50	6.67	6.19	6.49	8.95	7.07
1H	4.07	5.43	6.77	5.49	4.74	5.24	7.05	5.73
3A	3.39	5.13	6.13	4.98	3.83	5.07	6.34	5.18
1F	5.08	6.56	8.27	6.63	5.99	6.33	8.70	7.01
11C	2.53	4.87	5.48	4.43	2.76	4.95	5.65	4.64
1B	5.41	7.08	8.89	6.99	6.42	6.86	9.38	7.43
1G	5.50	6.67	8.63	6.81	6.56	6.36	9.14	7.27
12B	5.59	6.59	8.65	6.81	6.59	6.35	9.17	7.30
1E	4.52	6.10	7.57	6.00	5.39	5.92	7.99	6.37
5C	5.66	6.51	8.68	6.82	6.67	6.30	9.25	7.40
1C	5.68	6.51	8.70	6.83	6.72	6.28	9.29	7.46
1D	5.67	6.51	8.72	6.85	6.74	6.27	9.33	7.51
ave	<b>4.85</b>	<b>6.23</b>	<b>7.92</b>	<b>6.28</b>	<b>5.72</b>	<b>6.04</b>	<b>8.35</b>	<b>6.70</b>
charge 1419 140/90 (67 training 52 validate 12 sample boards)								
25a	2.41	16.06	16.08	13.04	11.17	11.45	15.83	11.79
29E	2.48	15.46	15.51	12.56	10.79	11.06	15.29	11.35
30C	3.41	16.68	16.86	13.49	11.53	12.71	16.96	12.26
24E	2.29	12.13	12.23	9.80	8.17	9.24	12.19	8.78
17A	2.21	16.89	16.87	13.63	11.28	12.19	16.42	12.02
32B	2.00	14.48	14.48	11.72	9.89	10.50	14.26	10.52
15C	1.93	17.54	17.48	14.20	11.96	12.39	17.03	12.80
34B	5.90	4.12	2.58	5.24	8.31	4.01	3.10	7.68
21B	1.20	11.77	11.71	9.48	7.81	8.45	11.38	8.42
33A	0.84	13.22	13.12	10.61	8.61	9.19	12.45	9.36
29D	0.83	16.07	15.93	12.86	10.45	11.04	15.03	11.39
14B	-0.06	19.62	19.43	15.54	12.41	13.10	17.85	13.81
all	<b>2.12</b>	<b>14.50</b>	<b>14.36</b>	<b>11.85</b>	<b>10.20</b>	<b>10.44</b>	<b>13.98</b>	<b>10.85</b>
	<b>%</b>							

Table 4 calculated errors for charges 1414, 1419,1428.

Table 4 presents the measurement error from the validation data for each sample board measured during the kiln charge. The data has been separated into two sections presenting the results for the complete range of moisture contents (ALL) and those measurements below the FSP (less 30). The boards closest to the measurement port is listed first, then sequentially with the last sample being closest to the shorted end of the sensor. In each case the sensor is covered by nine sample boards. The data set was set up so as to use some of the measurements to determine the regression coefficients (training) whilst other points were reserved for the final validation of the model. These results are better than anticipated and show that the system has extremely good accuracy across the full operating range of moisture contents. Whilst this does show that the sensor is sensitive to the moisture of individual boards it does not show how the system will perform between charges. To show this the regression coefficients from 1428 which is a 90/60 charge were applied to another 90/60 charge (1414) and the error results for the full range of moisture contents are shown below in Table 5.

<b>charge 1414 90/60 coefficients used from 1428</b>				
<b>Board position</b>	<b>mean</b>	<b>stdev</b>	<b>rms</b>	<b>mean abs</b>
<b>1</b>	-459.02	180.01	492.92	459.02
<b>2</b>	-237.33	91.95	254.45	237.33
<b>3</b>	-252.89	201.90	323.34	275.11
<b>4</b>	-313.79	168.78	356.14	320.03
<b>5</b>	-196.52	124.03	232.26	206.11
<b>6</b>	-311.14	195.36	367.18	325.24
<b>7</b>	-238.62	129.28	271.27	243.69
<b>8</b>	-261.98	165.28	309.59	273.68
<b>9</b>	-314.68	158.47	352.19	318.98
<b>10</b>	-388.43	262.51	468.53	409.70
<b>11</b>	-408.56	234.51	470.85	420.88
<b>12</b>	-416.81	212.35	467.60	423.79
<b>allslot</b>	-316.65	177.04	363.86	326.13

**Table 5 errors for charge 1414 using coefficients from 1428**

As can be seen from Table 5 the results are extremely poor showing that the coefficients from one charge do not translate to another similar one. This showed that another key input to the model was missing.

Temperature variation, whilst only small, between similar charges was inputted to the model which did not improve the result. Finally board thickness was presented as an inputted as an independent variable using

$$mc = B0 + B1*A1 + B2*A2 + \dots + B16*A16 + B17*Th$$

where Th is the independent variable of sample board thickness (mm) to the model and the error analysis results for all moisture contents measured are given below in Table 6.

<b>charges 1414 + 1428 90/60 board thickness included</b>				
<b>125 training 172 validate 12 sample boards</b>				
	<b>mean</b>	<b>stdev</b>	<b>rms</b>	<b>mean abs</b>
<b>1.0</b>	4.52	7.67	8.88	7.30
<b>2.0</b>	4.52	7.67	8.88	7.30
<b>3.0</b>	3.75	8.04	8.85	6.92
<b>4.0</b>	6.20	9.42	11.26	9.10
<b>5.0</b>	3.07	7.91	8.46	7.02
<b>6.0</b>	5.04	8.47	9.83	7.88
<b>7.0</b>	5.34	8.63	10.13	8.05
<b>8.0</b>	4.26	9.09	10.01	8.00
<b>9.0</b>	5.01	7.94	9.37	7.49
<b>10.0</b>	4.14	8.69	9.60	7.60
<b>11</b>	5.40	8.68	10.20	8.08
<b>12</b>	5.57	9.18	10.72	8.44
<b>all slot</b>	4.73	8.45	9.68	7.76
<b>charges 1414 + 1428 90/60 board thickness included steaming removed</b>				
<b>110 training 130 validate 12 sample boards</b>				
	<b>mean</b>	<b>stdev</b>	<b>rms</b>	<b>mean abs</b>
<b>1.0</b>	2.35	7.19	7.54	5.85
<b>2.0</b>	1.70	6.38	6.58	5.43
<b>3.0</b>	2.17	8.37	8.62	6.41
<b>4.0</b>	2.57	7.58	7.98	6.45
<b>5.0</b>	1.01	7.56	7.60	6.23
<b>6.0</b>	2.06	7.42	7.67	5.86
<b>7.0</b>	1.91	6.57	6.82	5.55
<b>8.0</b>	1.37	8.04	8.12	6.38
<b>9.0</b>	1.97	6.47	6.74	5.31
<b>10.0</b>	1.67	8.19	8.32	6.31
<b>11</b>	2.19	7.28	7.58	5.78
<b>12</b>	1.79	6.82	7.02	5.63
<b>all slot</b>	1.90	7.32	7.55	5.93
	<b>%</b>	<b>%</b>	<b>%</b>	<b>%</b>

**Table 6 error analysis of 90/60 charges with board thickness included.**

The inclusion of board thickness into the model has made significant improvement to the error measurement. In addition gains were also made by removing the data obtained during the reconditioning phase (steaming) at the end of each charge.

## 6.2 Potential sources of error

The following discussion outlines areas where potential for errors in this work exist. The first consideration would be the probe itself and the potential for thermal effects to alter its performance. Figure 41 below is a plot for two kiln charges with no wood present over the sensor.

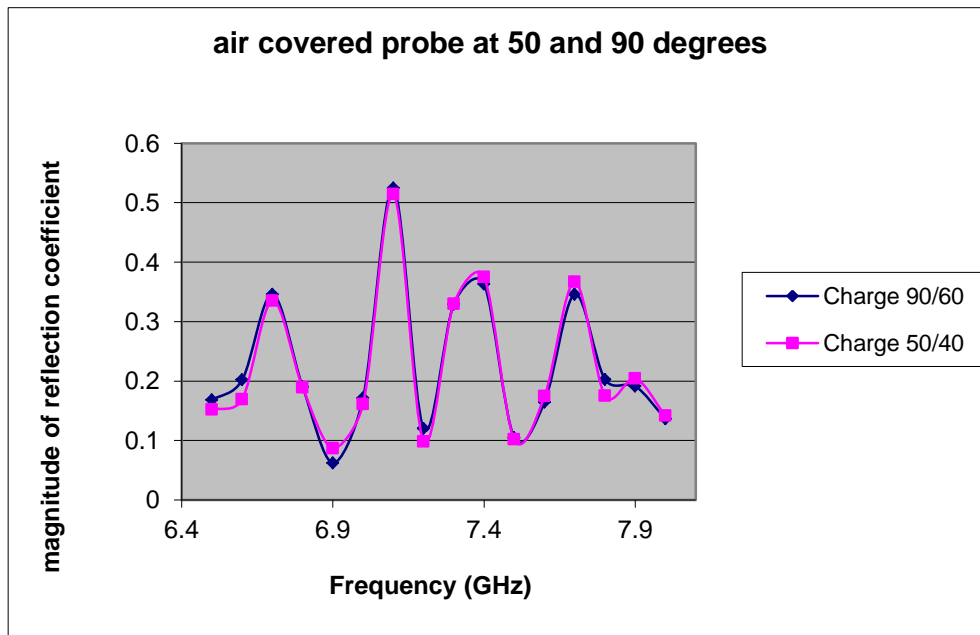


Figure 41 Reflection coefficient for air covered probe for 50/40 and 90/60 kiln schedules

As can be seen from Figure 41 above, the sensor itself does not change significantly due to temperature. The probe itself over this 40 degree range has only altered by a mean of 0.3% with a standard deviation across all frequencies of 1.67%. This shows that for a given kiln schedule where there is variation of a few degrees between charges the probe itself will not attribute any significant error to the measurement.

Perhaps the most significant area where errors are introduced is during the obtaining of the independent moisture content measurements. Although great care was taken during this the removal of the boards for weighing creates an issue over the replacement of the sample in the exact location from where it was taken. This is a concern as the presence of the probe in contact with the wood has created its own micro climate. Even a small translation of the probe would introduce wetter or drier areas into the measurement zone.

Another source of measurement error would be variations due to ambient temperature changes around the sixport. As we have no record of the ambient room temperature during these trials this is

impossible to assess its effect in these data sets. However recent work has shown that an ambient temperature change of greater than three degrees will produce errors in the sixport measurement.

### 6.3 Using Temp Set Points in Regression

Using data from three kiln charges we have undertaken a regression which incorporates the kiln set temperatures for moisture contents in the range of 5 to 50% along with sample board thickness. The charges selected were as follows

Charge number	Dry bulb temp °C	Wet bulb temp °C
1424	160	95
1419	140	90
1428	90	60

The regression was undertaken on all data from these charges and presented below is the results of the regression for a total of 50 observations.

	mean	stdev	rms	mean abs
1	0.0000	1.5602	1.5446	1.1862
2	0.0000	2.2016	2.1795	1.6574
3	0.0000	2.9149	2.8856	2.3335
4	0.0000	1.8144	1.7962	1.4310
5	0.0000	2.8449	2.8163	2.0842
6	0.0000	1.7627	1.7450	1.3593
7	0.0000	1.8560	1.8374	1.3743
8	0.0000	1.4179	1.4037	1.0719
9	0.0000	1.5963	1.5803	1.1972
10	0.0000	1.2845	1.2716	1.0332
11	0.0000	1.5436	1.5280	1.1860
12	0.0000	1.1082	1.0971	0.8188
<b>all slot</b>	<b>0.0000</b>	<b>1.8254</b>	<b>1.8071</b>	<b>1.3944</b>

To validate this we used the coefficients from above and applied them to charge 1422 that is a 120/70 schedule. This yielded the following containing a total of 21 observations

	mean	stdev	rms	mean abs
1	0.971899	1.949582	1.904783	1.449015
2	0.710616	1.968468	1.924522	1.490455
3	0.209136	2.897609	2.831066	2.197167
4	0.922079	1.969923	1.924654	1.553255
5	0.767846	2.5936	2.535132	1.924805
6	0.210224	1.917655	1.873683	1.491331
7	0.483018	1.645637	1.608527	1.247351
8	0.410047	2.112187	2.063629	1.624083
9	0.16778	2.215032	2.16417	1.662934
10	0.266881	2.15981	2.110321	1.727798
11	0.213108	2.704705	2.642606	2.147407
12	0.565751	1.883443	1.841009	1.424891
<b>all slot</b>	<b>0.491532</b>	<b>2.168138</b>	<b>2.118675</b>	<b>1.661708</b>

The above was repeated swapping charge 1419 for 1422

Charge number	Dry bulb temp °C	Wet bulb temp °C
1424	160	95
1422	120	70
1428	90	60

The regression was undertaken on all data from these charges and presented below is the results of the regression for a total of 56 observations.

	mean	stdev	rms	mean abs
	0.00	1.711134	1.695787	1.343311
1	0.00	2.013253	1.995196	1.584065
2	0.00	1.927878	1.910587	1.499964
3	0.00	3.021441	2.994342	2.373456
4	0.00	2.174068	2.15457	1.701881
5	0.00	2.51991	2.497309	1.954986
6	0.00	1.965472	1.947844	1.578088
7	0.00	1.58671	1.572479	1.256304
8	0.00	2.004689	1.986709	1.61555
9	0.00	1.996451	1.978545	1.564439
10	0.00	2.259496	2.239231	1.792954
11	0.00	2.403358	2.381803	1.926254
12	0.00	1.711134	1.695787	1.343311
<b>all</b>	<b>0.00</b>	<b>2.099615</b>	<b>2.080784</b>	<b>1.656505</b>

The following are the results for the validation charge 1419 (140/90) using the coefficients from above

	mean	stdev	rms	mean abs
1	2.144805	5.891813	6.136826	3.72908
2	0.991482	2.574496	2.701008	2.086707
3	1.41331	4.962672	5.039261	4.010456
4	0.918512	3.496684	3.529748	2.814371
5	0.58828	2.257546	2.277666	1.935407
6	0.448037	2.435752	2.415985	1.911145
7	0.45221	1.71333	1.730093	1.47357
8	0.463905	2.237509	2.229649	1.810044
9	0.60691	2.312426	2.334156	1.840735
10	0.60907	3.027141	3.012702	2.400483
11	0.443518	2.185059	2.175423	1.790413
12	0.390251	1.585878	1.594226	1.267444
<b>all slot</b>	<b>0.789191</b>	<b>2.890026</b>	<b>2.931395</b>	<b>2.255821</b>

In conclusion it is found that both board thickness and also kiln setpoint temperatures are required in the multivariate regression in order to achieve an acceptable accuracy.

---

## 7.0 CONCLUSION

This thesis presents a novel waveguide aperture array sensor capable of measuring the moisture content of individual lumber laid upon it during Kiln drying. It also presents the development of a measurement system (MKS) based upon the six-port technique, and dielectric models which attempt to investigate the effects of density and seasonal growth rings on microwave measurements of lumber.

The work has shown that a moisture measurement system based on a single ended slotted waveguide can be used to determine the moisture content of sawn lumber during the kiln drying process. The ability of the sensor to measure to within 3% of the actual moisture content using a six-port reflectometer is pleasing as only first order models were used in the explicit algorithm. This approach can be further enhanced by the incorporation of better permittivity mixture models which can relate the physical properties of the lumber to the measured permittivity.

Regression methods are certainly very useful when some parameter can serve as a benchmark. In this instance it was found that as well as a broadband frequency measurement of the sensor the introduction of both board thickness and kiln temperature set points was required. However the final result showed that this approach could deliver an acceptable measurement of moisture content variation across the stack. In this case there are 17 coefficients that need to be evaluated against a known calibration standard, the regression then proceeds in 17D space. As no benchmark is available in the regression process, there is a likelihood that it may well settle to a local minimum and not to the desired 'correct' value.

A point that needs consideration is that the sensor is a periodically loaded line and the loads are not uniform at each point. Any periodically line will exhibit pass and stop bands and the consequences are that the overall propagation constant is different from the unloaded waveguide. Thus a time domain approach is the only realistic approach. But despite this, if the loads are such that one has a stop band at some frequency, one would measure a reflection coefficient approaching unity or in the pass band nearly zero, in either case the measurement errors can be significant.

An additional finding from this work is the effect of ambient temperature on the external sensor and cabling. This is a substantial source of error for the system and showed that despite careful internal temperature control of the measurement system, frequent calibration was required to overcome this. To enable this to happen an automatic calibration system based on fixed standards was implemented allowing the MKS measurement system to self-calibrate on a three hourly basis.

### **7.1 Future Work**

Based on this work several areas still require either further investigation namely in the areas of dielectric modelling of wood and also the analysis technique employed by the sensor. In the area of dielectric modelling the use of a two phase volumetric model, whilst commonly used, is seriously flawed. A new model must be developed that caters for the various forms of water binding in wood along with the anisotropy effects caused by grain angle. In addition the continued thinking that wood is a homogeneous material should be replaced by the concept of a layered dielectric as the earlywood latewood dielectric properties are significantly differing.

For the analysis of the sensor itself a time domain approach should be adopted. This will enable the use of time gating techniques so that slots can be individually measured and hence remove the effects of mutual coupling between slots in the measurement. As the equivalent circuit model for a slot in the broadwall of a waveguide is a lumped capacitance there also exists the potential to use the Stuchley coaxial probe approach to extract permittivity. This would allow for a simple permittivity measurement calibration based on an open, short circuit and measurement of water.

Finally the use of waveguide as the transmission line structure should also be reconsidered. Chosen because of its mechanical robustness it is by nature band limited. The potential for air filled coaxial lines, or microstrip constructed from temperature stable materials should be investigated as this would greatly increase the available frequency bandwidth.

---

**ACKNOWLEDGMENTS**

The Author would like to thank Steve Riley from Scion and Unitec Institute of Technology for funding this work and their work on sample gathering, preparation and kiln trialing the measurement system. In addition many thanks to my supervisor Professor SC Mukhopadhyay.

---

## Bibliography

- [1] W. S. Holmes and S. G. Riley, "A Microwave Method for the Measurement of Moisture Content Variation in Stacked Lumber," in *Proc. Fifth International conference on electromagnetic wave interaction with water and moist substances*, Rotorua, 2003.
- [2] R. J. King, "A Microwave Method for Measuring Moisture Content, Density and Grain Angle of Wood," USDA Forest Service Research note FPL0250, 1985.
- [3] R. J. King, "Microwave electromagnetic non-destructive testing of wood," in *Proc. 4th non-destructive testing of wood symposium*, Vancouver, 1978.
- [4] G. Torgovnikov, Dielectric properties of wood and wood based materials, Berlin Hiedelberg New York: Springer, 1993.
- [5] W. L. James, "A microwave method for measuring moisture content, density and grain angle of wood," in *USDA Research note FPL-0250*, 1985.
- [6] S. Tronstad and S. Flotaker, "Description and initial test of 8 principles for in-kiln measuring and endpoint control of wood moisture content," The EU Commission SMT4-CT95-2023, Oslo, 2000.
- [7] W. Holmes, S. G. Riley and A. D. Green, "Measurement of Timber using a Waveguide Aperture Array," in *Proc. IMPI Microwave Symposium*, Boston, 1996.
- [8] W. S. Holmes and S. G. Riley, "Microwave Method for In-Kiln Moisture Content Measurement," in *Proc. IUFRO Wood Drying Conference*, Quebec, 1996.
- [9] W. S. Holmes and S. G. Riley, "Method and apparatus for moisture sensing using microwavetechnologies". United States of America Patent US6411106, 25 june 2002.
- [10] W. S. Holmes and S. G. Riley, "Microwave moisture sensing via Waveguide slot array". United States of America Patent US7089047, 7 June 2005.
- [11] Agilent, "Agilent network analysis, applying the 8510 TRL calibration to non-coaxial lines," Product note 8510-8A, USA, 2001.
- [12] A. M. Nicolson and G. F. Ross, "Measurement of the intrinsic properties of materials by time domain techniques," *IEEE trans. I&M Vol. IM-17*, pp. 395-402, 1968.
- [13] W. B. Weir, "Automatic measurement of complex dielectric constant and permeability at microwave frequencies," *Proceedings of the IEEE*, vol. 62, no. No. 1, pp. 33-36, 1974.
- [14] W. S. Holmes and S. G. Riley, "Dielectric measurement of Logs for Improved Internal Imaging," in *ICST 11*, Palmerston North, 2011.
- [15] G. F. Engen and C. A. Hoer, "'Thru-Reflect-Line': An improved technique for calibrating the dual six-port automatic network analyser," *IEEE Transactions on Microwave Theory and Techniques*, Vols. MTT-27, no. 12, pp. 987-993, 1979.

- [16] S. Trabelsi and S. O. Nelson, "Dielectric sensor for multiparameter microwave sensor," Rotorua, 2003.
- [17] W. S. Holmes and J. R. Holdem, "Measurement of Moisture and Preservative Content of Timber using Microwave Sensing Techniques," Industrial Research Limited Report No107, Auckland, New Zealand, 1993.
- [18] G. F. Engen, "The Six-Port Reflectometer: An alternative Network Analyser," *IEEE Transactions on Microwave theory and Techniques*, Vols. MTT-25, no. 12, pp. 1075-1080, 1977.
- [19] S. R. Judah and W. S. Holmes, "A Novel Sixport Calibration incorporating diode detector non-linearity," *IEEE Instrumentation and Measurement Technology Conference vol 1*, pp. 592-595, 1998.
- [20] E. A. Wolf, *Antenna Analysis*, Wiley, 1966.
- [21] S. R. Rengarajan and L. G. Josefsson, "Slotted Waveguide Array Antenna Technology," in *IEEE AP-S / URSI Short Course notes*, Los Angeles, 1995.
- [22] i. A. Kraszewsk, *Microwave aquametry: Electromagnetic Interaction with water containing materials*, IEEE Press, 1996.
- [23] j. Zusheng, G. Montisci, A. Casula, Y. Hu and J. Lu, "Efficient evaluation of the external mutual coupling in Dielectric covered waveguide slot arrays," *International Journal of Antennas and Propagation, Hindawi Publishing*, vol. 2012, no. ID491242, 2012.
- [24] I. A. Esrah, A. A. Kishk, A. B. Yakolev and A. W. Glisson, "Generalised equivalent circuit model for transverse waveguide slots and applications," *Progress in Electromagnetics researarch,PIER 69*, pp. 1-20, 2007.
- [25] R. A. Gilbert, "Waveguide Slot Antenna Arrays," in *Antenna Engineering Handbook*, McGraw-Hill, 2007, pp. 9.1-9.34.
- [26] M. T. Ghasr, D. Simms and R. Zoughi, "Multimodal Solution for a Waveguide radiating into multilayered Structures-Dielectric property and thickness evaluation," *IEEE Trans on Instrumentation and Measurement*, vol. 58, no. 5, pp. 1505-1513, 2009.
- [27] P. S. Neelakantaswamy and D. K. Banerjee, "Radiation Charaacteristics of Waveguide Dielectric Spheres with Matched Spherre-Air Boundary," *Electronics Letters*, vol. 9, no. 2, 1982.
- [28] P. I. Somlo and J. D. Hunter, *Microwave Impedance Measurement*, IEE press, 1985.
- [29] W. S. Holmes, S. C. Mukhopadhyay, K. P. Thakur and S. G. Riley, "Lumber Moisture Measurement using a Six-port reflectometer and Waveguide Aperture array," in *46th Microwave Power Symposium, Institute of Microwave Power*, Las Vegas, 2012.
- [30] A.-H. Boughriet, C. Legrand and A. Chapoton, "Noniterative stable transmission/reflection method for low-loss material complex permittivity determination," *IEEE Transactions on Microwave theory and Techniques*, vol. 45, no. 1, pp. 52-57, 1997.
- [31] Y. Zhang and S. Okamura, "New density independent moisture measurement using microwave phase shifts at two frequencies," *IEEE Transactions on Instrumentation and Measurement*, vol. 48, no. 6, pp. 1208-1211, 1999.
- [32] A. Technologies, "Exploring the Architectures of Network Analysers," Agilent AN 1287-2.
- [33] G. Daian, A. Taube, A. Birnboim, M. Daian and Y. Shamkov, "Modeling the dielectric

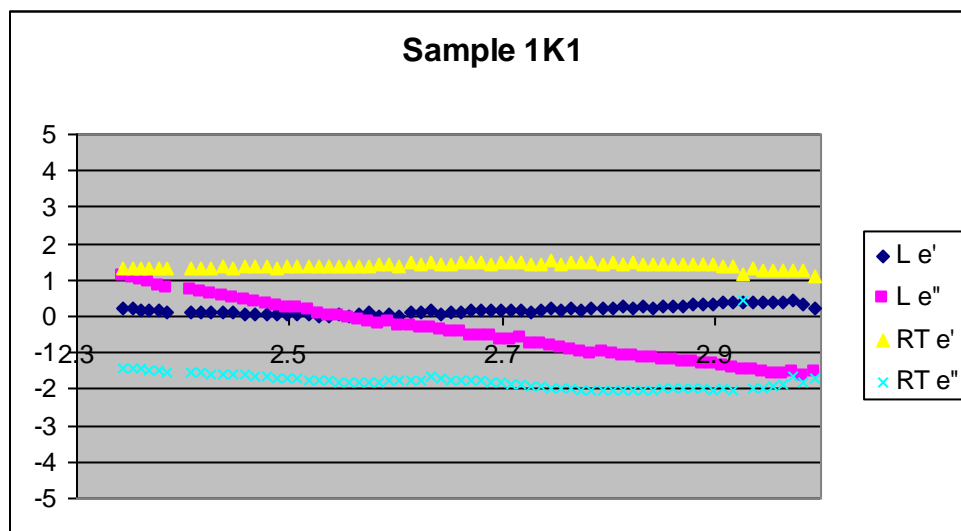
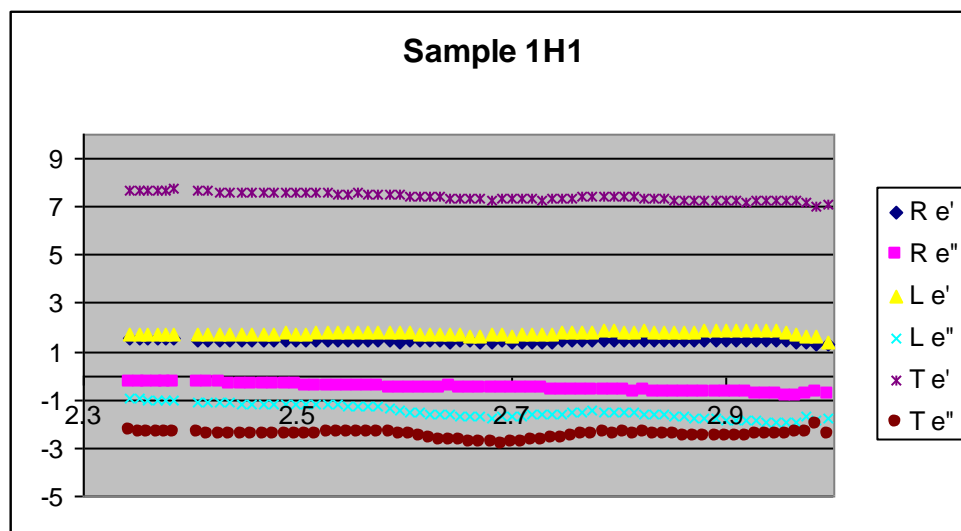
- properties,” *Wood Science Technology*, vol. 40, pp. 237-246, 2006.
- [34] A. vonHippel, *Dielectrics and Waves*, John Wiley & Sons, 1954.
- [35] E. Nyfors, *Industrial Microwave Sensing*, Norwood, MA: Artech House, 1989.
- [36] R. King, “Microwave Sensors for Process control Part I: Transmission Sensors,” *Sensors*, pp. 68-74, 1992.
- [37] K. RJ, “Microwave Sensors for Process Control Part II: Open Resonator Sensors,” *Sensors*, pp. 74-78, 1992.
- [38] A. W. Kraszewski, “Microwave Aquametry-Needs and Perspectives,” *IEEE Transactions on Microwave theory and Techniques*, vol. 39, no. 5, pp. 828-835, 1991.
- [39] S. Okamura, “Microwave Technology for Moisture Measurement,” *Subsurface Sensing Technologies and Applications*, vol. 1, no. 2, pp. 205-227, 2000.
- [40] E. Nyfors and P. Vainikainen, “Industrial microwave sensors,” *Microwave Symposium Digest, IEEE MTT-s International*, pp. 825-835, 1991.
- [41] M. S. Vengatesh and G. S. Raghavan, “An Overview of dielectric properties measuring techniques,” *Canadian Biosystems Engineering*, vol. 47, pp. 7.15-7.30, 2005.
- [42] J. Polivka, “An Overview of Microwave Sensor technology,” *High Frequency Electronics*, pp. 32-42, 2007.
- [43] S. Kharkovsky and R. Zoughi, “Microwave and Millimeter Wave Non-destructive testing and Evaluation; Overview and recent advances,” *IEEE Instrumentation and Measurement Magazine*, pp. 26-38, 2007.
- [44] W. Meyer and W. Schilz, “Feasibility Study of Density independent moisture measurement with microwaves,” *IEEE Transactions on Microwave theory and Techniques*, Vols. MTT-29, no. 7, pp. 732-739, 1981.
- [45] S. Trabelsi, A. Kraszewski and S. Nelson, “A New Density-Independent Function for Microwave Moisture Content Determination in Particulate Materials,” in *IEEE Instrumentation and Measurement technology Conference*, Ottawa, pp.648-652, 1997.
- [46] P. Fratzl and E. Schmid, “Characterising Natural Fibre composites with hierarchical structure,” *Institute of material Science, Loeben, Austria*, pp. 31-39, 2002.
- [47] F. Ulaby and R. P. Jedlicka, “Microwave Dielectric Properties of Plant materials,” *IEEE Transactions on Geoscience and Remote Sensing*, Vols. GE-22, no. 4, pp. 406-415, 1984.
- [48] S. Okamura, “Microwave moisture measurement system for drying lumber,” *Forest Products Journal*, Forest Products Society, Article No 10262, 2007.
- [49] M. T. Afzal, B. Colpitts and K. Galik, “Dielectric Properties of Softwood Species Measured with an Open-ended Coaxial Probe,” in *8th International IUFRO Wood Drying Conference*, 2003.
- [50] A. M. Nicholson and G. F. Ross, “Measurement of the intrinsic properties of materials by time domain techniques,” *IEEE Transactions on Instrumentation and Measurement*, Vols. IM-19, no. 4, pp. 377-382, 1970.

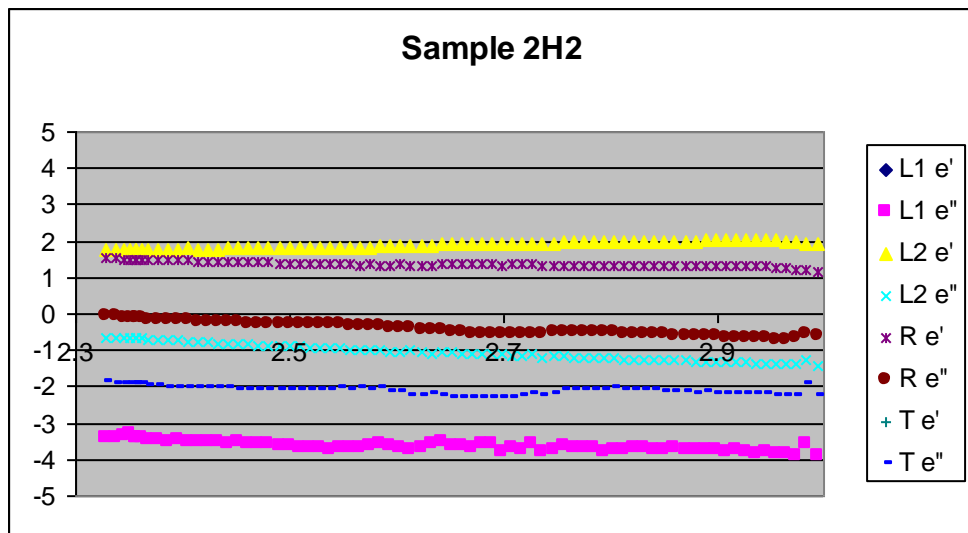
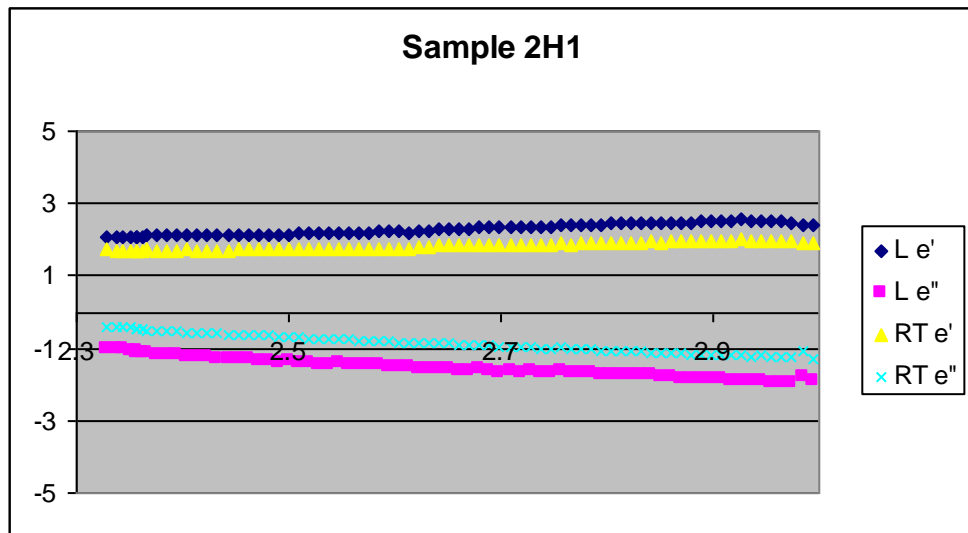
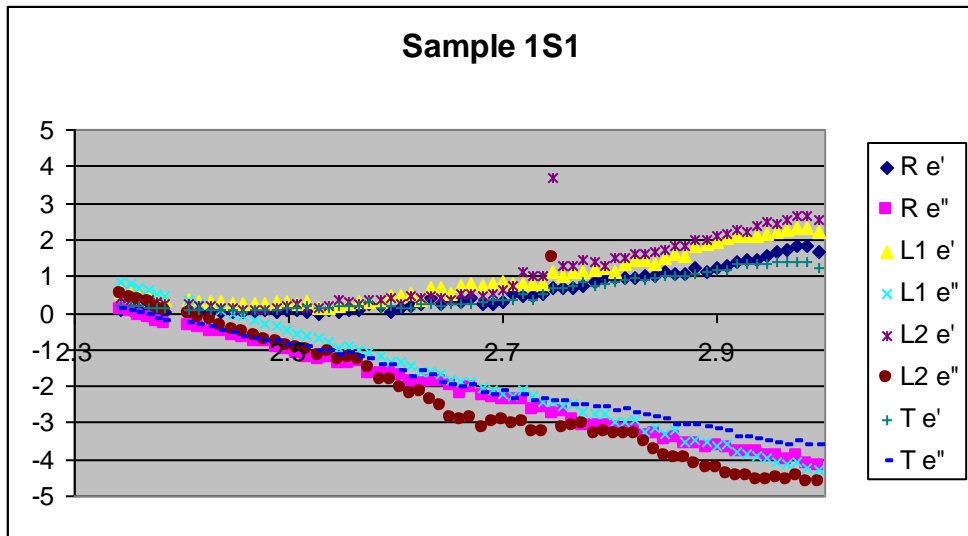


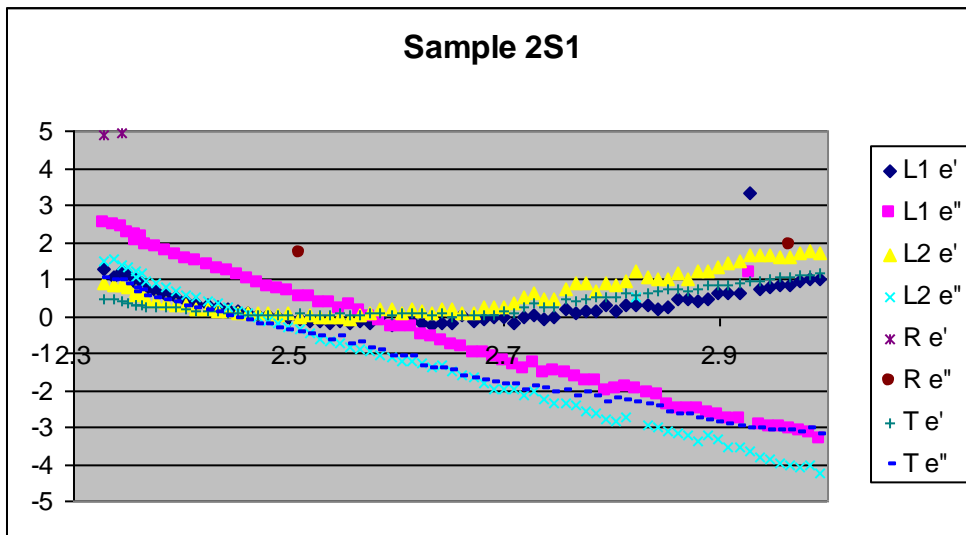
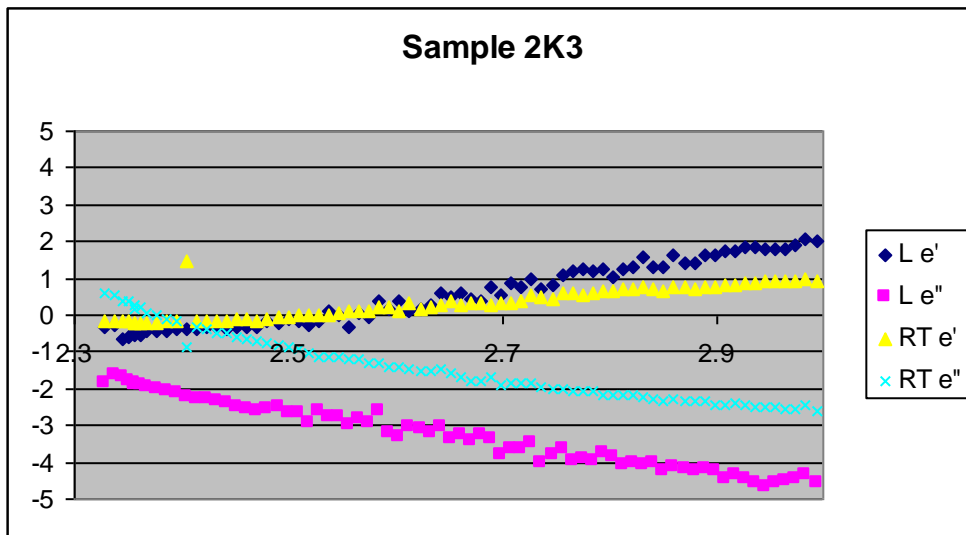
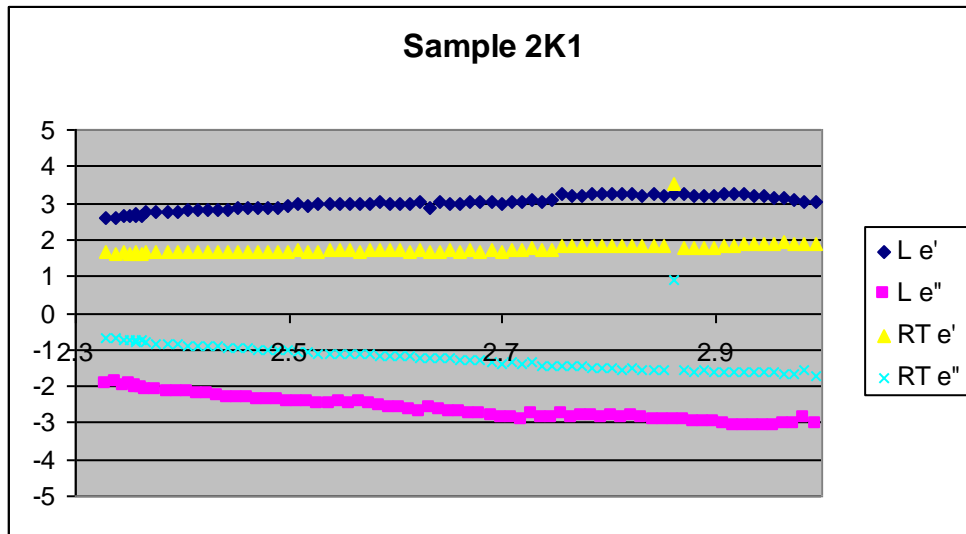
## Appendix A: Permittivity results 2-3GHz

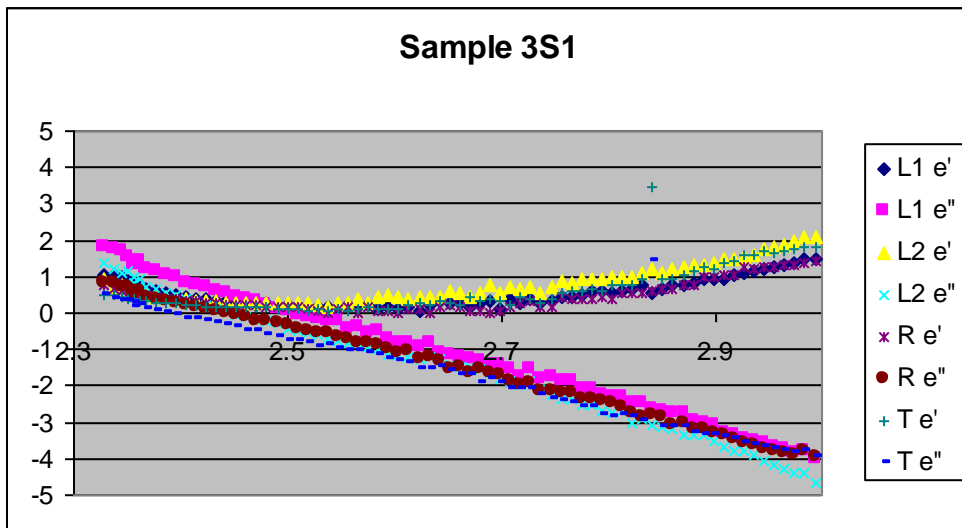
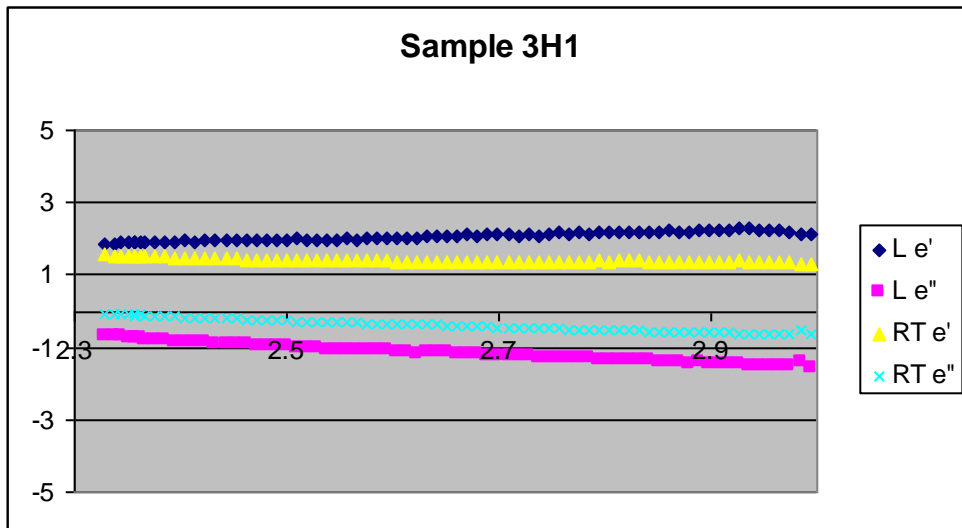
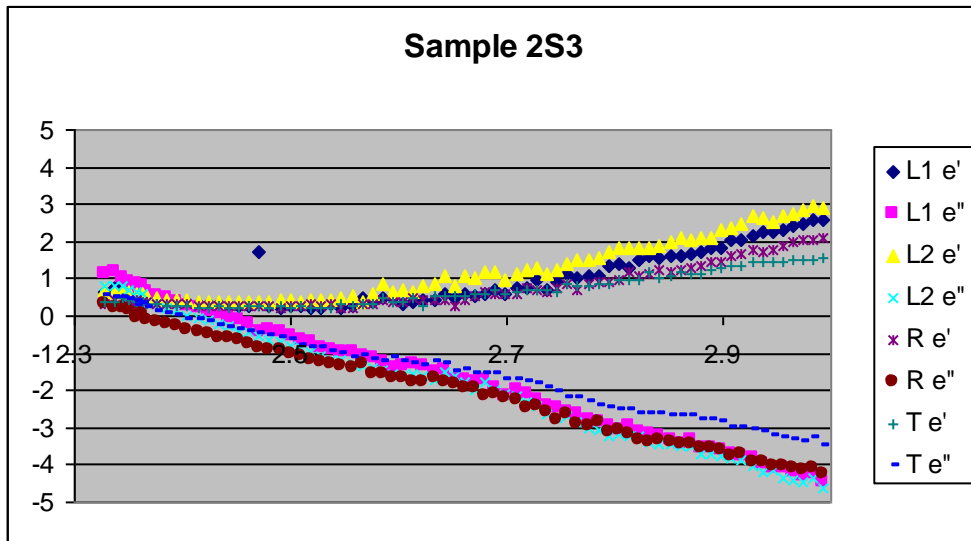
A simple three character naming convention was adopted for each sample. Firstly a number denotes which of the three sample logs the cube was taken from. A letter SH or K was used to denote if the sample was Sapwood, Heartwood or Knot material. Finally a number defines the replicate number, were possible usually three replicates were taken from each site.

For example a sample labelled 2H3 would denote the sample as log 2, Heartwood, replicate 3.







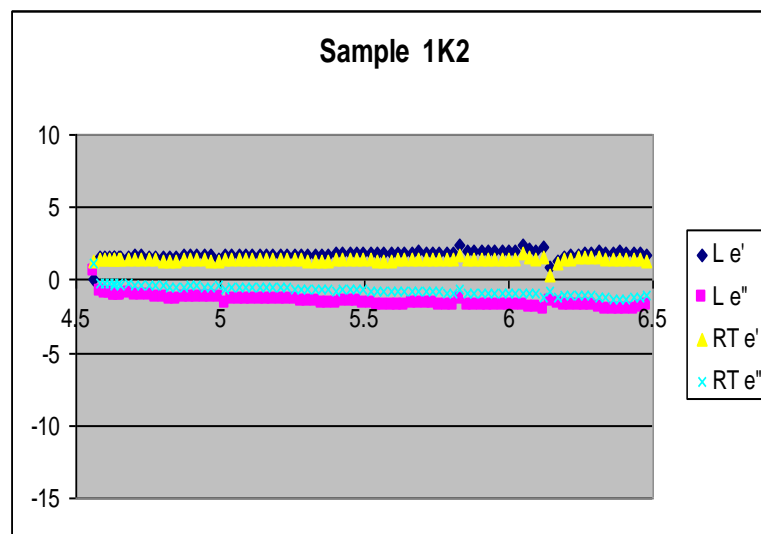


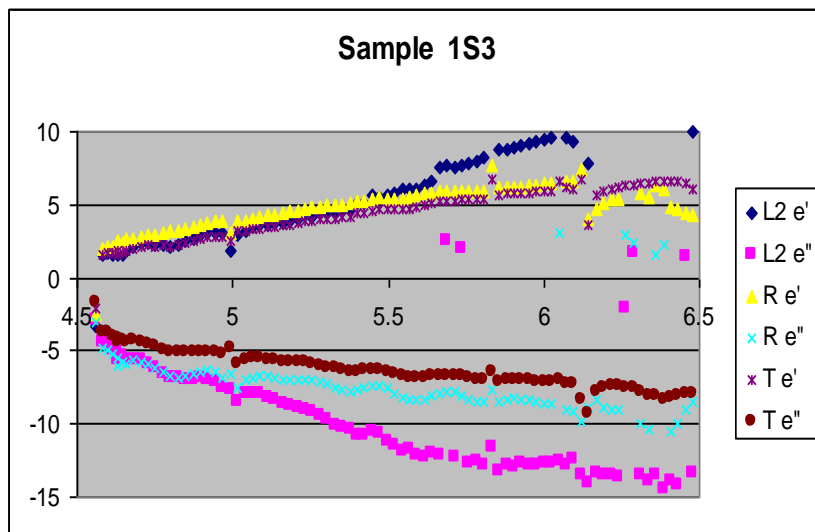
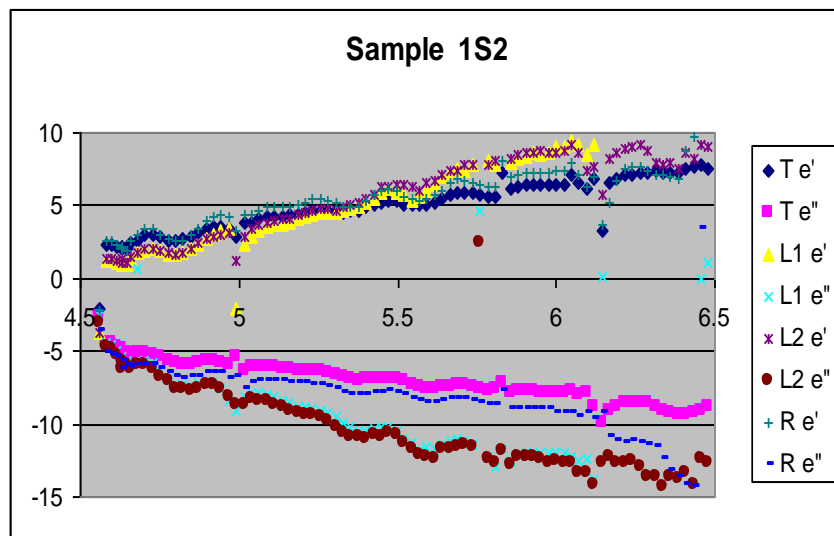
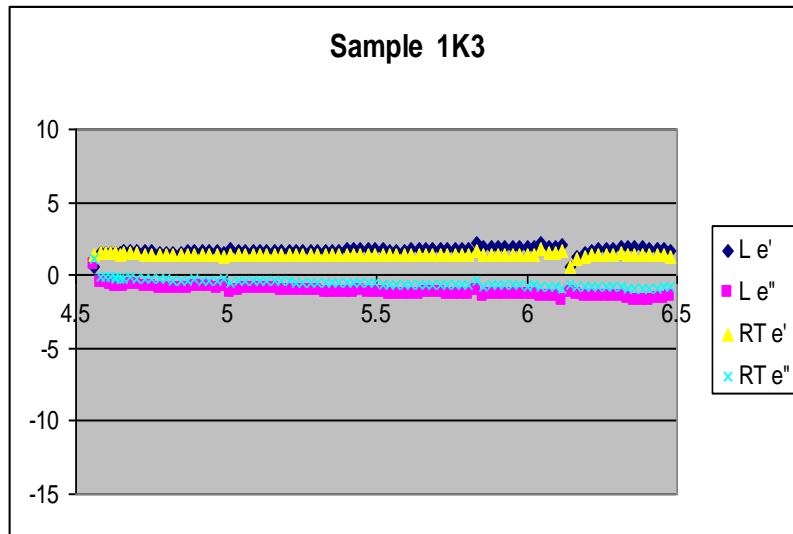
---

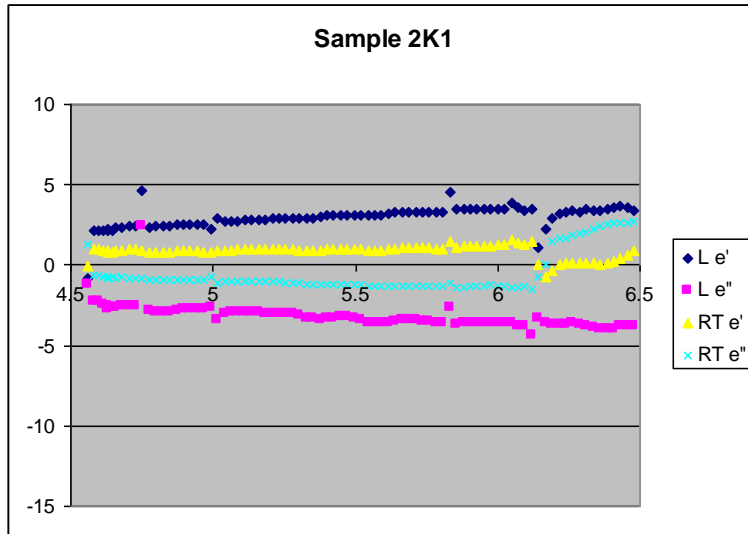
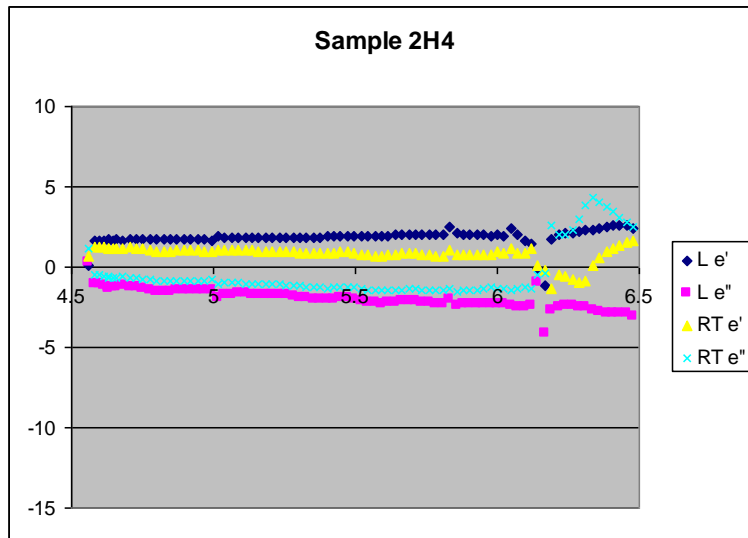
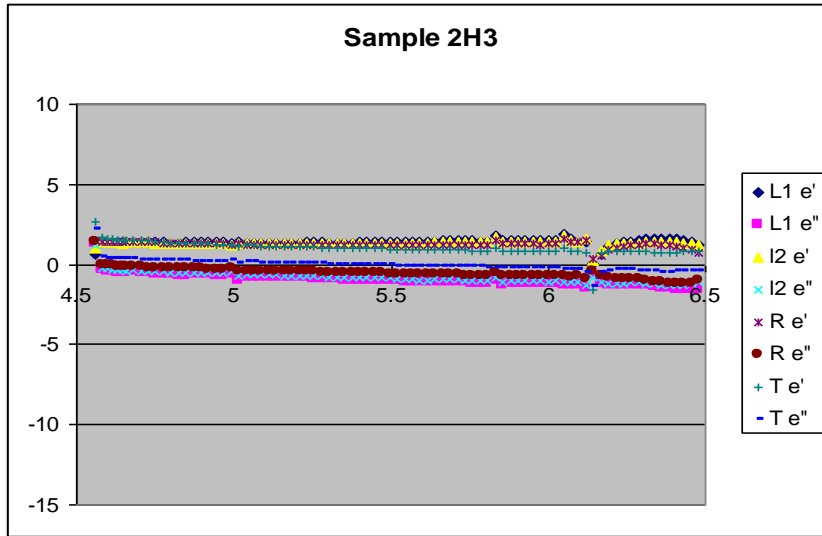
## Appendix B: Permittivity results 4.5 -6.5 GHz

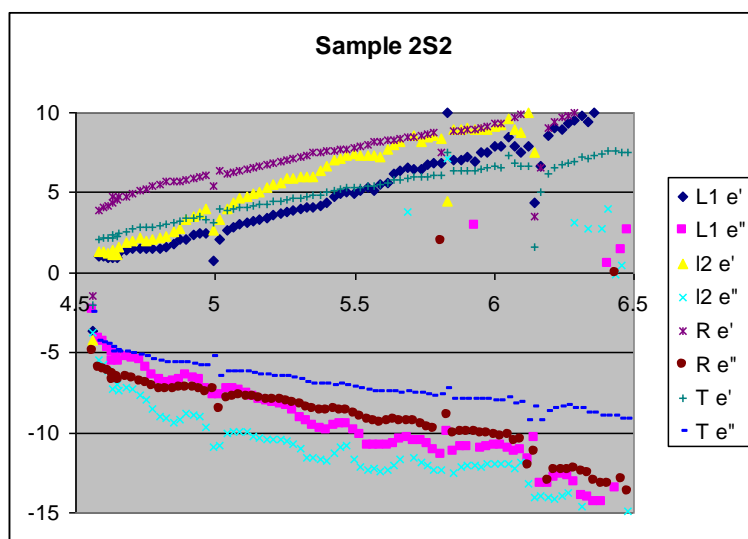
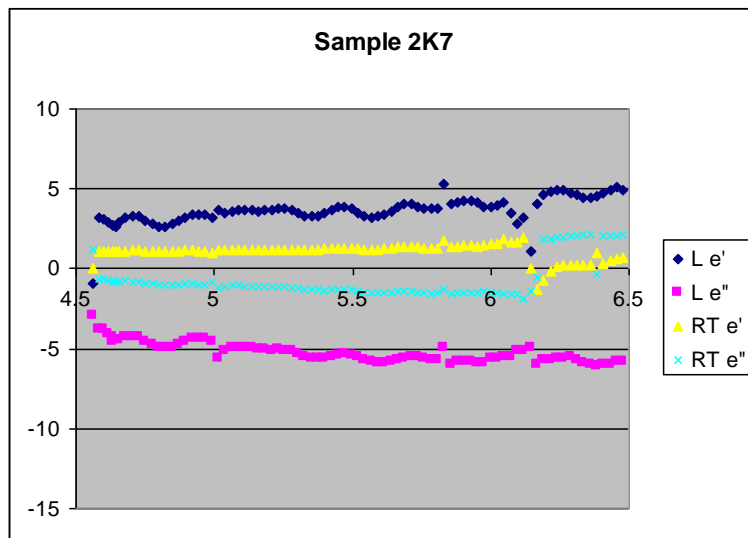
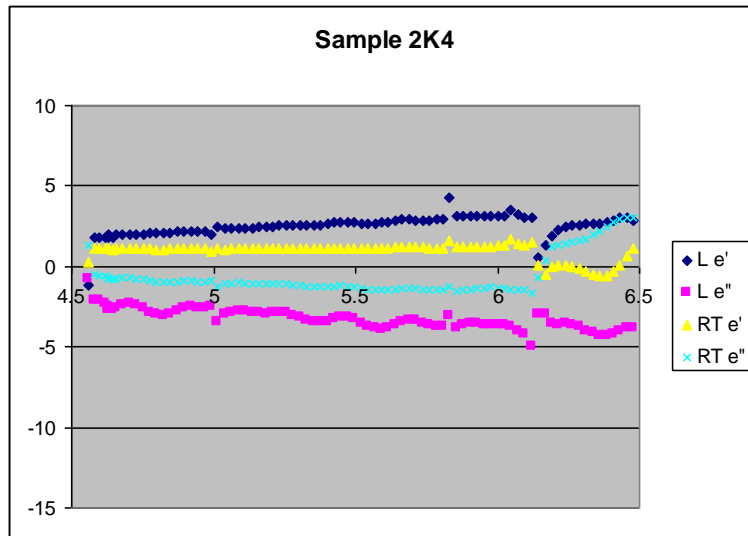
A simple three character naming convention was adopted for each sample. Firstly a number denotes which of the three sample logs the cube was taken from. A letter SH or K was used to denote if the sample was Sapwood, Heartwood or Knot material. Finally a number defines the replicate number, were possible usually three replicates were taken from each site.

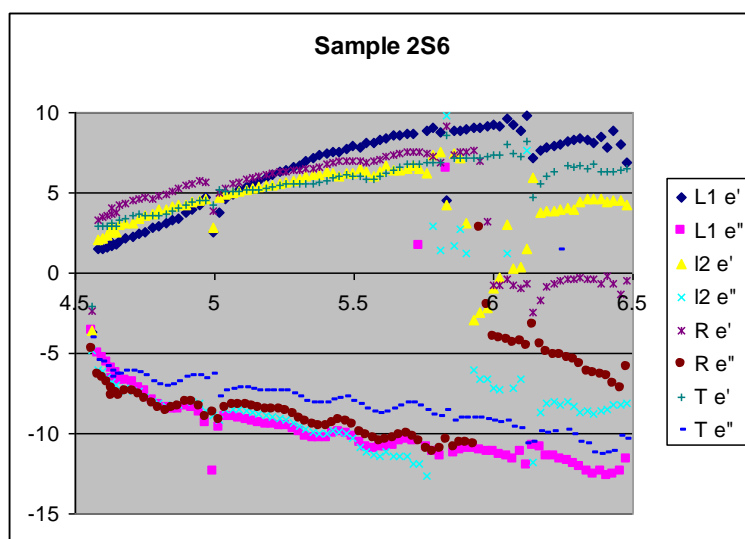
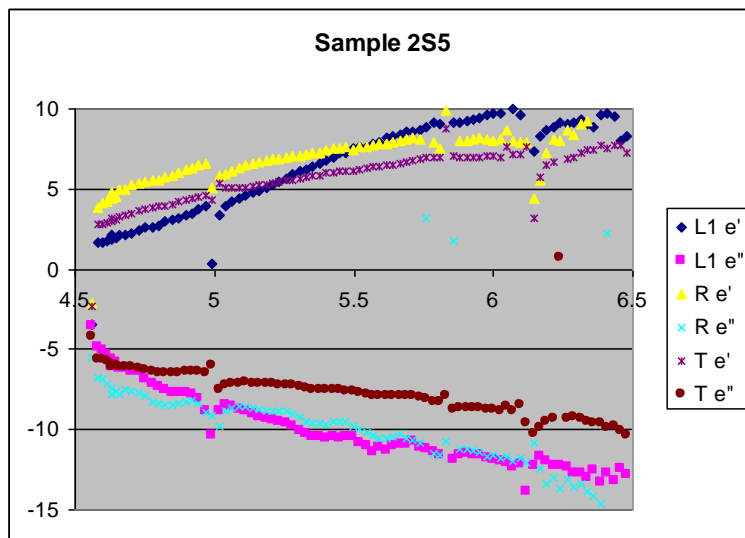
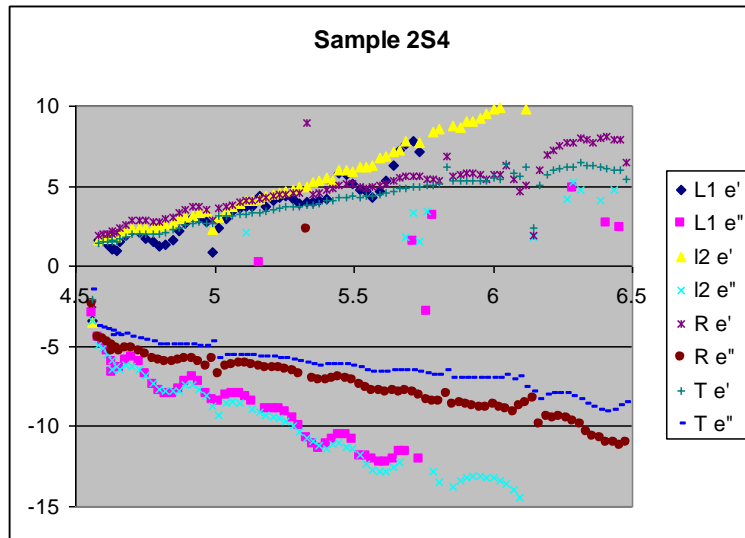
For example a sample labelled 2H3 would denote the sample as log 2, Heartwood, replicate 2.

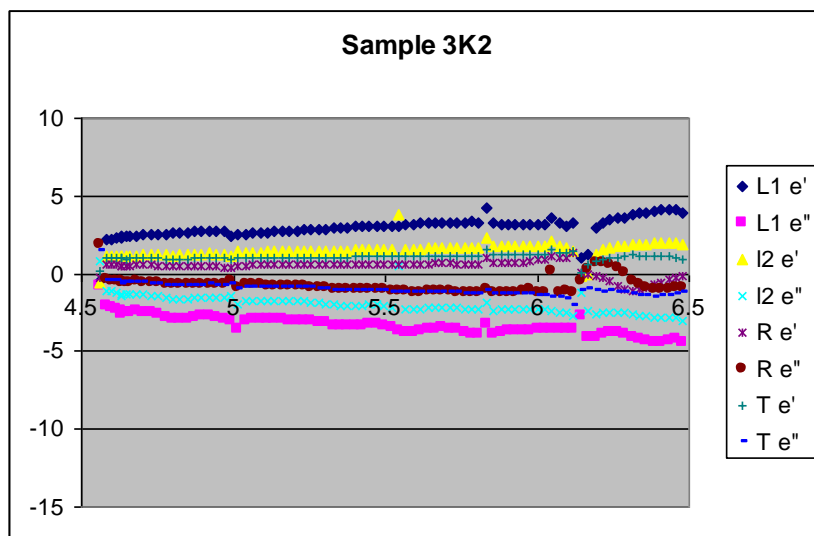
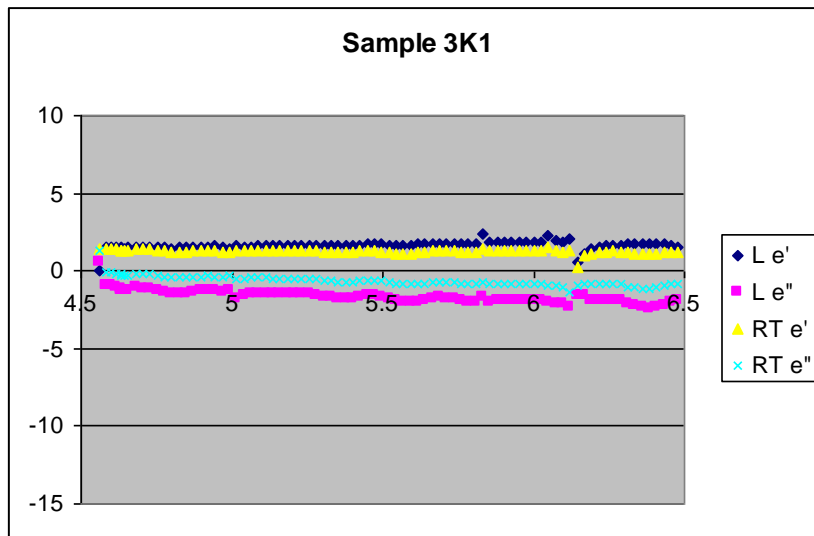
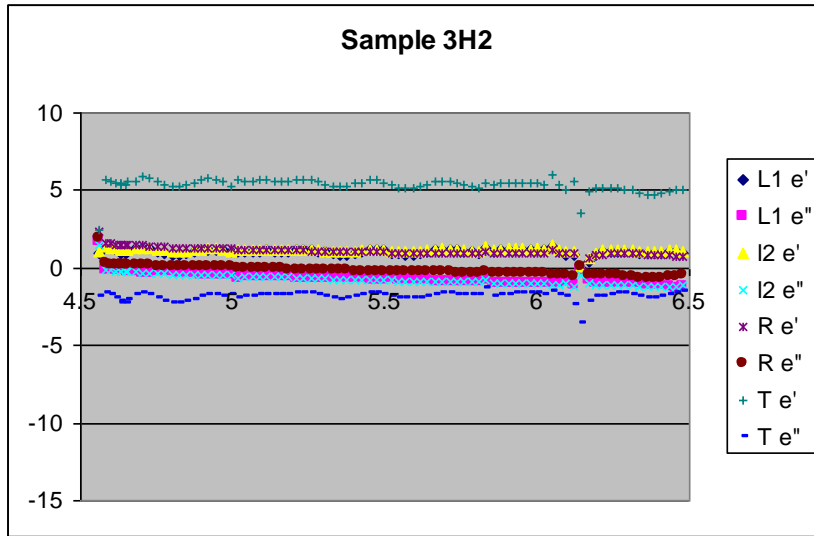


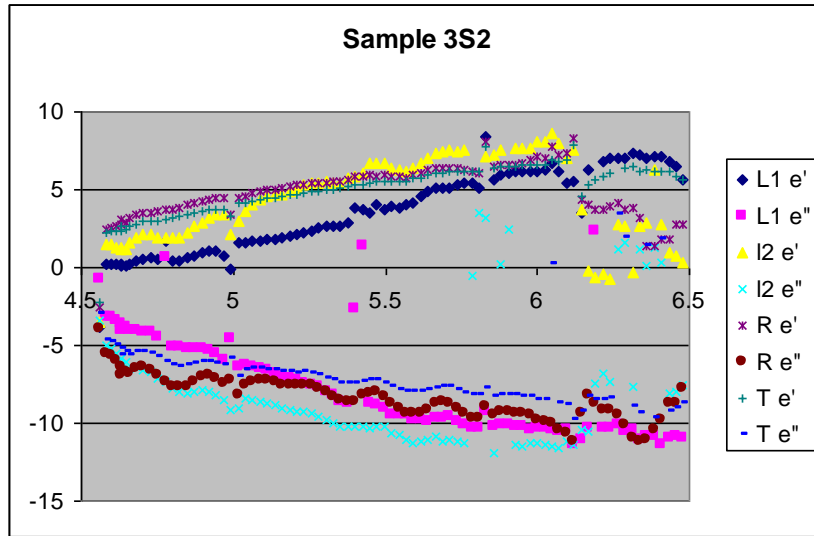












---

## Appendix C: Regression Results for individual Sample Boards

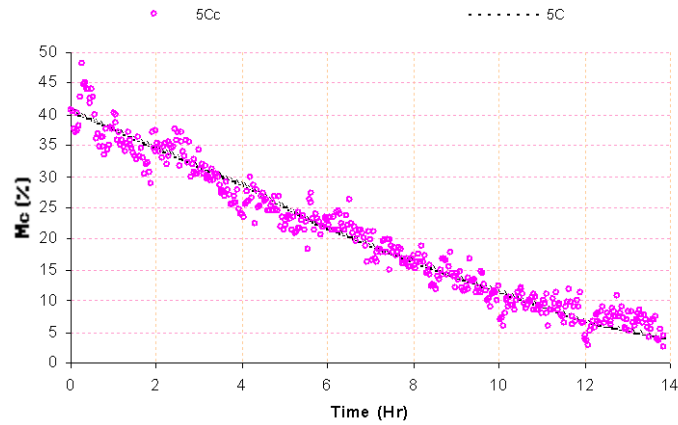


Fig. 1: Plot of computed and experimental Moisture content for sample 5C

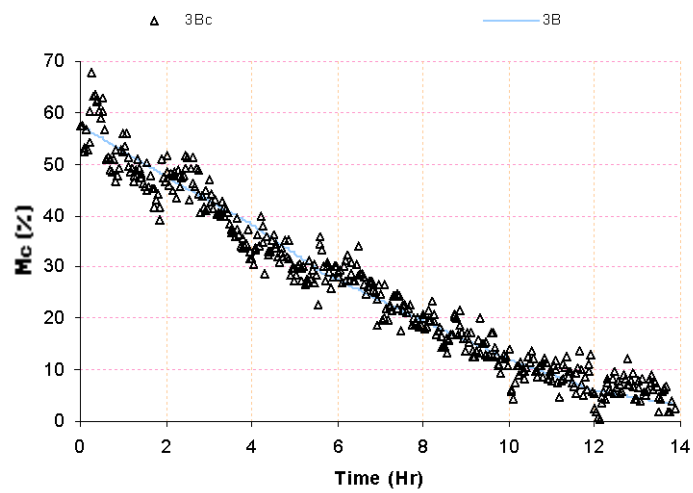


Fig. 2: Plot of computed and experimental Moisture content for sample 3B

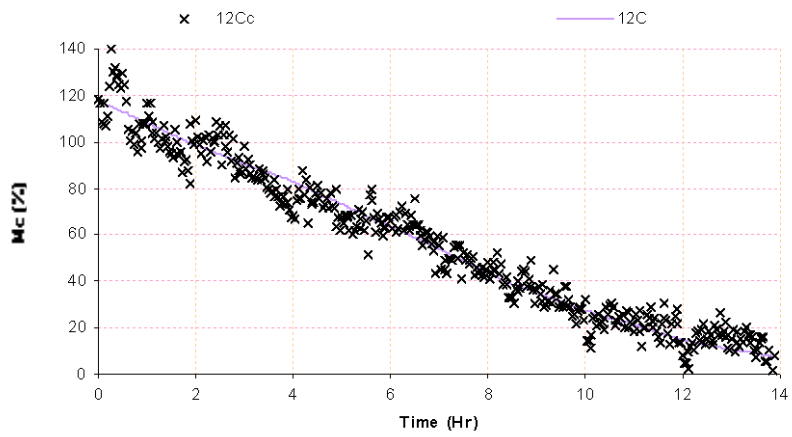


Fig. 3: Plot of computed and experimental Moisture content for sample 12C

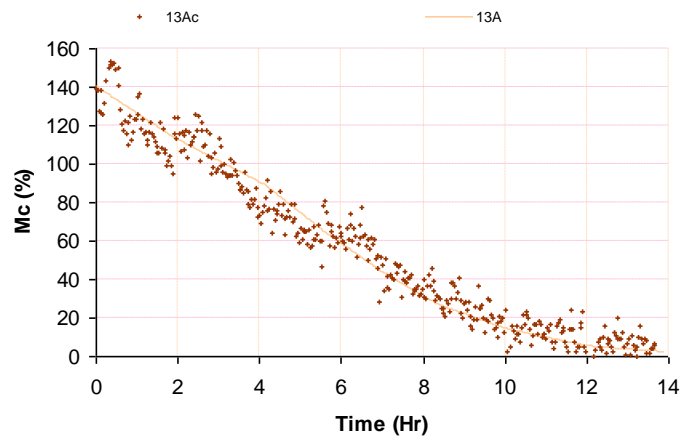


Fig. 4: Plot of computed and experimental Moisture content for sample 13A

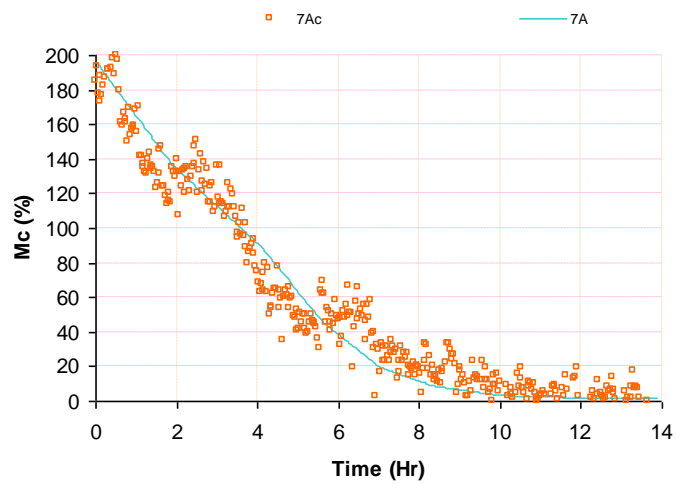


Fig. 5: Plot of computed and experimental Moisture content for sample 7A

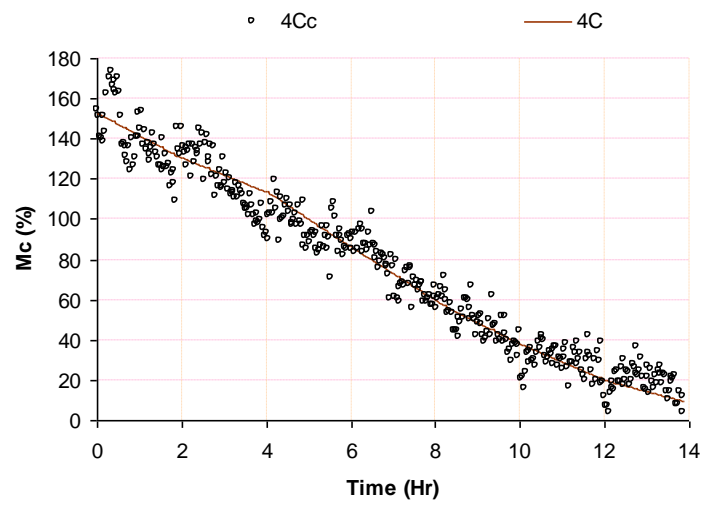


Fig. 6: Plot of computed and experimental Moisture content for sample 4C

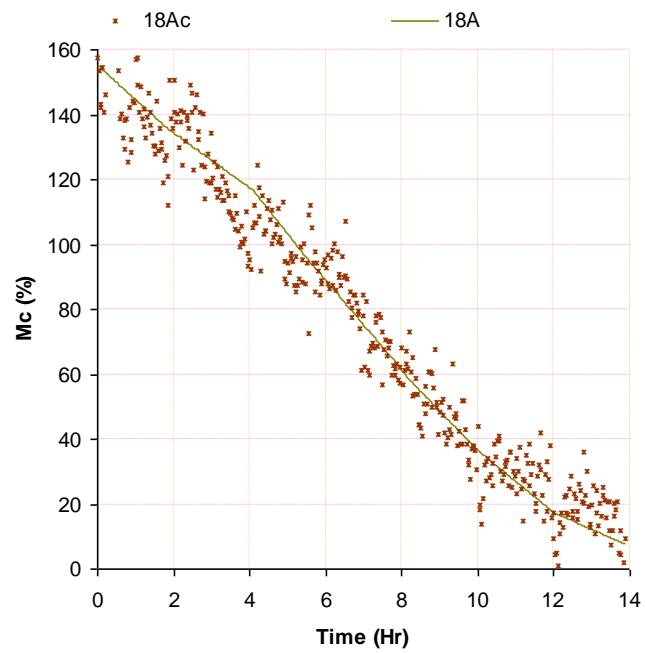


Fig. 7: Plot of computed and experimental Moisture content for sample 18A

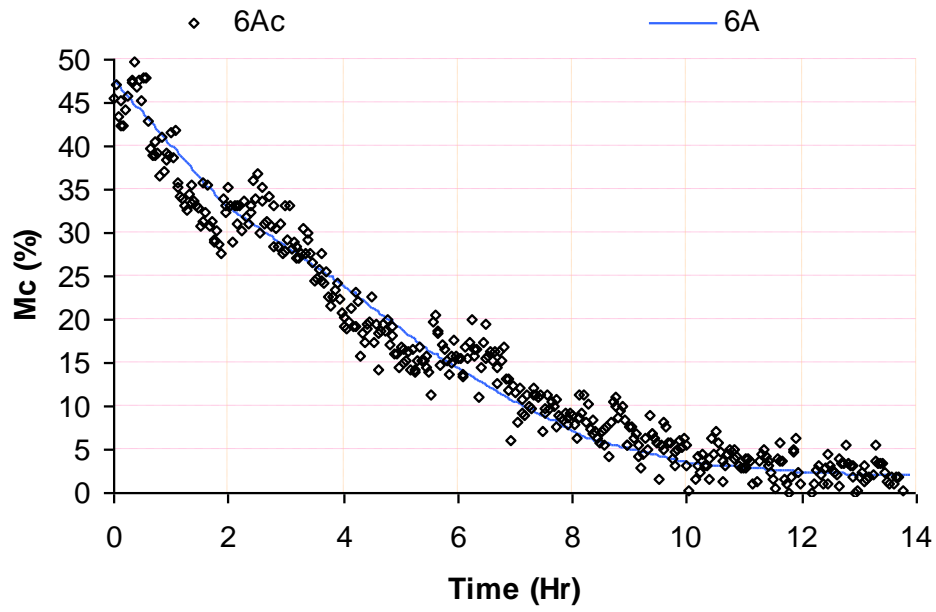


Fig. 8: Plot of computed and experimental Moisture content for sample 6A

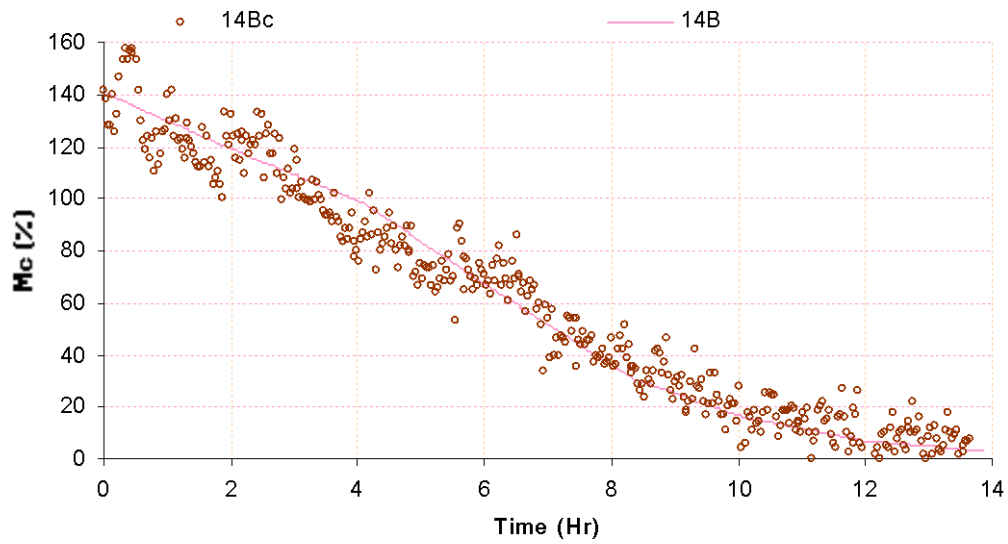


Fig. 9: Plot of computed and experimental Moisture content for sample 14B

---

**Appendix D: Regression coefficients for various samples**

	4C	5C	18A	3B	14B	12C	13A	6A	7A
Multiple R	0.9793588	0.9808673	0.9787584	0.9821162	0.9788663	0.9812253	0.9800300	0.9801952	0.9746946
R Square	0.9591436	0.9621006	0.9579679	0.9645522	0.9581793	0.9628030	0.9604589	0.9607826	0.9500295
Adjusted R Square	0.9576153	0.9606829	0.9563957	0.9632262	0.9566149	0.9614116	0.9589798	0.9593156	0.9481602
Standard Error	9.1905406	2.1950230	9.7873329	3.1854312	9.5616931	6.6575427	8.9873307	2.7485939	13.7366697
Observations	417	417	417	417	417	417	417	417	417
	<i>df</i>	<i>df</i>	<i>df</i>	<i>df</i>	<i>df</i>	<i>df</i>	<i>df</i>	<i>df</i>	<i>df</i>
Regression	15	15	15	15	15	15	15	15	15
Residual	401	401	401	401	401	401	401	401	401
Total	416	416	416	416	416	416	416	416	416
a <sub>0</sub>	112.2803309	35.4766401	112.9034610	49.5116503	122.8211108	84.9745367	119.8276529	33.5170806	196.3420207
a <sub>1</sub>	93.2838616	52.7994964	73.8107523	81.8973221	-55.3386988	113.7534678	56.1436248	92.5651520	363.7978032
a <sub>2</sub>	445.1866243	115.3375732	459.6809894	166.3933994	420.8163101	325.2723140	424.8150301	127.8950613	625.5256785
a <sub>3</sub>	-464.4859394	-109.4040345	-468.7852765	-168.8614711	-506.3055110	-359.8832921	-522.4620096	-194.6829431	-850.7827988
a <sub>4</sub>	-2215.9609217	-519.6822054	-2382.4472344	-737.1420383	-2112.8565942	-1573.7827054	-1880.5407550	-397.5147727	-1678.1376459
a <sub>5</sub>	870.0754025	180.4995561	892.8406613	301.1237545	1223.8044474	677.5657664	1177.4589459	405.2377287	1800.5358528
a <sub>6</sub>	1136.4957989	281.6337778	1209.8309172	408.8854714	1165.2856009	815.6320019	1088.2652294	264.6595364	1303.9901491
a <sub>7</sub>	964.8437995	207.8223038	1054.1000640	295.1860169	850.1104532	692.2091980	715.8277173	138.5800380	331.4908121
a <sub>8</sub>	-145.2361074	-50.5156455	-143.8703620	-75.7419948	-90.5803528	-126.2446148	-124.2794549	-60.4037313	-263.8659873
a <sub>9</sub>	1380.7358295	342.9174600	1446.0140110	498.5182094	1283.4136913	1024.9386261	1245.1919265	360.5534770	1537.3592626
a <sub>10</sub>	-355.3976558	-119.6899469	-355.9502861	-179.6155226	-274.0500260	-312.0901575	-308.5326130	-128.0771273	-540.7561472
a <sub>11</sub>	17.8288170	0.6884689	0.8622890	15.5889674	200.8698023	32.1356440	213.6544782	95.4617533	510.7871120
a <sub>12</sub>	1829.6751843	468.8226701	1958.8953528	640.6352281	1306.9413426	1338.3163967	1191.6050047	243.5866655	742.4051678
a <sub>13</sub>	-3016.3690086	-794.8981274	-3187.3974312	-1151.5783508	-2652.9649882	-2269.8799316	-2576.4004147	-713.4180727	-3045.4701367
a <sub>14</sub>	237.0331692	55.5186668	255.8006160	82.8667692	268.8066866	172.0890842	241.2661278	56.5405664	266.7350129
a <sub>15</sub>	711.9132621	186.7168622	743.2137245	276.7684033	486.0501203	569.1349661	529.6039969	206.7978036	647.5245982

---

---

## Appendix E: MKS source code

```
// MKSDlg.cpp : implementation file
#include "stdafx.h"
#include "Spiralometer.h"
#include "SpiralometerDlg.h"
#include "Comms.h"
#include <math.h>
#include <iostream.h>
#include <stdio.h>
#include <conio.h>
#include <math.h>
#include <io.h>
#include <fstream.h>
#include <fcntl.h>
#include <stdlib.h>
#include <string.h>
#include <time.h>

#include "Afxdlgs.h"

#ifdef _DEBUG
#define new DEBUG_NEW
#undef THIS_FILE
static char THIS_FILE[] = __FILE__;
#endif

#define KVs 4
#define NumStd 4

/* global variables */
//char calres[1000];
double freqlist[101];
double StartFreq, StopFreq;
int x,i,iptr,datr,calfg,CycleT,cyclecnt,cycletime,MeasTime,Numpts;
int FreqNum[101];
double P[KVs],fr,Meas[101][5];
double fstart,fstop,ph,FreqList[101];
double caldata[101][NumStd][5],phstd[NumStd],gam; /* freq,std,voltage */
double calldata[101][5][5];
double gm[6],rt[5][6],pz[KVs],px[KVs],z[KVs],xx[KVs],xn[KVs],zm,pzm,pum,um,unc;
double mpz[101][KVs],mpx[101][KVs],mz[101][KVs],mxx[101][KVs],mxn[101][KVs]; //cal coeff storage
double phase[5];
double sl[NumStd],sla[NumStd]; /* standard lengths calc and actual */

CString cs3;

/* global Definitions */
float c=200.0f;
double pi = 4*atan(1);
int nextstd;
int getcalvoltages();
int genfreqlist(),fcnt;
float standards();
int getcalcoeffs();
int denom();
int numr();
int RefCalc();
int checkcal();
void setFreq(void);
void GenFreqList(void);
```

```

////////////////////////////////////
// CAboutDlg dialog used for App About

class CAboutDlg : public CDialog
{
public:
    CAboutDlg();

// Dialog Data
   //{{AFX_DATA(CAboutDlg)
    enum { IDD = IDD_ABOUTBOX };
    }}AFX_DATA

    // ClassWizard generated virtual function overrides
   //{{AFX_VIRTUAL(CAboutDlg)
protected:
    virtual void DoDataExchange(CDataExchange* pDX); // DDX/DDV support
    }}AFX_VIRTUAL

// Implementation
protected:
   //{{AFX_MSG(CAboutDlg)
    }}AFX_MSG
    DECLARE_MESSAGE_MAP()
};

CAboutDlg::CAboutDlg() : CDialog(CAboutDlg::IDD)
{
   //{{AFX_DATA_INIT(CAboutDlg)
    }}AFX_DATA_INIT
}

void CAboutDlg::DoDataExchange(CDataExchange* pDX)
{
    CDialog::DoDataExchange(pDX);
   //{{AFX_DATA_MAP(CAboutDlg)
    }}AFX_DATA_MAP
}

BEGIN_MESSAGE_MAP(CAboutDlg, CDialog)
   //{{AFX_MSG_MAP(CAboutDlg)
    // No message handlers
    }}AFX_MSG_MAP
END_MESSAGE_MAP()

////////////////////////////////////
// CSpiralometerDlg dialog

CSpiralometerDlg::CSpiralometerDlg(CWnd* pParent /*=NULL*/)
    : CDialog(CSpiralometerDlg::IDD, pParent)
{
   //{{AFX_DATA_INIT(CSpiralometerDlg)
    // NOTE: the ClassWizard will add member initialization here
    }}AFX_DATA_INIT
    // Note that LoadIcon does not require a subsequent DestroyIcon in Win32
    m_hIcon = AfxGetApp()->LoadIcon(IDR_MAINFRAME);
}

void CSpiralometerDlg::DoDataExchange(CDataExchange* pDX)
{
    CDialog::DoDataExchange(pDX);
   //{{AFX_DATA_MAP(CSpiralometerDlg)
    // NOTE: the ClassWizard will add DDX and DDV calls here
    }}AFX_DATA_MAP
}

BEGIN_MESSAGE_MAP(CSpiralometerDlg, CDialog)
   //{{AFX_MSG_MAP(CSpiralometerDlg)
    ON_WM_SYSCOMMAND()
    ON_WM_PAINT()
    ON_WM_QUERYDRAGICON()
    ON_BN_CLICKED(IDC_BUTTON1, OnButton1)
    }}AFX_MSG_MAP

```

```

ON_BN_CLICKED(IDC_pbStop, OnpbStop)
ON_BN_CLICKED(IDOK2, OnOk2)
ON_BN_CLICKED(IDC_BUTTON2, OnButton2)
ON_BN_CLICKED(IDC_BUTTON3, OnButton3)
ON_BN_CLICKED(IDC_BUTTON4, OnButton4)
ON_BN_CLICKED(IDC_BUTTON5, OnButton5)
ON_BN_CLICKED(IDC_BUTTON6, OnButton6)
ON_BN_CLICKED(CalcCoeff, OnCalcCoeff)
ON_WM_TIMER()
ON_WM_DESTROY()
ON_BN_CLICKED(cycle, Onmkcycle)
ON_BN_CLICKED(IDC_OnTest, OnOnTest)
ON_BN_CLICKED(IDC_OnLoadCal, OnOnLoadCal)
ON_BN_CLICKED(IDC_OnSaveCal, OnOnSaveCal)
//}AFX_MSG_MAP
ON_MESSAGE(WM_COMMNOTIFY, OnCommNotify)
END_MESSAGE_MAP()
///////////////////////////////////////////////////////////////////
// CSpiralometerDlg message handlers

BOOL CSpiralometerDlg::OnInitDialog()
{
    CComboBox* pCB;

    CDialog::OnInitDialog();

    // Add "About..." menu item to system menu.

    // IDM_ABOUTBOX must be in the system command range.
    ASSERT((IDM_ABOUTBOX & 0xFFF0) == IDM_ABOUTBOX);
    ASSERT(IDM_ABOUTBOX < 0xF000);

    CMenu* pSysMenu = GetSystemMenu(FALSE);
    if (pSysMenu != NULL)
    {
        CString strAboutMenu;
        strAboutMenu.LoadString(IDS_ABOUTBOX);
        if (!strAboutMenu.IsEmpty())
        {
            pSysMenu->AppendMenu(MF_SEPARATOR);
            pSysMenu->AppendMenu(MF_STRING, IDM_ABOUTBOX, strAboutMenu);
        }
    }

    // Set the icon for this dialog. The framework does this automatically
    // when the application's main window is not a dialog
    SetIcon(m_hIcon, TRUE); // Set big icon
    SetIcon(m_hIcon, FALSE); // Set small icon

    SetMainPtr(this);
    m_hCommDev = INVALID_HANDLE_VALUE;

    m_Info.hComm = NULL;
    m_Info.Finish = true;
    m_Info.pThread = NULL;

    GetDlgItem(IDC_BUTTON1)->EnableWindow(false);
    GetDlgItem(IDC_EDIT1)->EnableWindow(false);
    GetDlgItem(IDC_EDIT2)->EnableWindow(false);

    pCB = (CComboBox*)GetDlgItem(IDC_cbStartFreq);
    pCB->AddString("2");
    pCB->AddString("3");
    pCB->AddString("4");
    pCB->AddString("5");
    pCB->AddString("6");
    pCB->AddString("7");
    pCB->SetCurSel(4);

    pCB = (CComboBox*)GetDlgItem(IDC_cbStopFreq);
    pCB->AddString("3");
    pCB->AddString("4");
    pCB->AddString("5");

```

```

pCB->AddString("6");
pCB->AddString("7");
pCB->AddString("8");
pCB->SetCurSel(4);

pCB = (CComboBox*)GetDlgItem(IDC_cbNumPoints);
pCB->AddString("1");
pCB->AddString("10");
pCB->AddString("20");
pCB->AddString("50");
pCB->AddString("100");
pCB->SetCurSel(2);

pCB = (CComboBox*)GetDlgItem(IDC_cbCycleTime);
pCB->AddString("1");
pCB->AddString("5");
pCB->AddString("10");
pCB->AddString("15");
pCB->AddString("20");
pCB->SetCurSel(2);

pCB = (CComboBox*)GetDlgItem(IDC_cbParity);
pCB->AddString("NOPARITY");
pCB->AddString("ODDPARITY");
pCB->AddString("EVENPARITY");
pCB->AddString("MARKPARITY");
pCB->AddString("SPACEPARITY");
pCB->SetCurSel(0);

return TRUE; // return TRUE unless you set the focus to a control
}

void CSpiralometerDlg::OnSysCommand(UINT nID, LPARAM lParam)
{
    if ((nID & 0xFFFF) == IDM_ABOUTBOX)
    {
        CAboutDlg dlgAbout;
        dlgAbout.DoModal();
    }
    else
    {
        CDialog::OnSysCommand(nID, lParam);
    }
}

void CSpiralometerDlg::OnPaint()
{
    if (IsIconic())
    {
        CPaintDC dc(this); // device context for painting

        SendMessage(WM_ICONERASEBKGND, (LPARAM) dc.GetSafeHdc(), 0);

        // Center icon in client rectangle
        int cxIcon = GetSystemMetrics(SM_CXICON);
        int cyIcon = GetSystemMetrics(SM_CYICON);
        CRect rect;
        GetClientRect(&rect);
        int x = (rect.Width() - cxIcon + 1) / 2;
        int y = (rect.Height() - cyIcon + 1) / 2;

        // Draw the icon
        dc.DrawIcon(x, y, m_hIcon);
    }
    else
    {
        CDialog::OnPaint();
    }
}

// The system calls this to obtain the cursor to display while the user drags
// the minimized window.

```

```

HCURSOR CSpiralometerDlg::OnQueryDragIcon()
{
    return (HCURSOR) m_hIcon;
}
//*****
//*****
LRESULT CSpiralometerDlg::OnCommNotify(WPARAM W,LPARAM L)
{
    char instr[256];
    int carcom,i,j,ivolt;
    char volt[5];
    CString cs,cs2;

    if( carcom = read_comm_string( instr, sizeof(instr)-1 ) )
    {
        //      instr should be "1111222233334444CRLF"
        if( carcom > 15 )
        {
            for( i=0; i<KVs; i++ )
            {
                for(j=0;j<4;j++)
                    volt[j] = instr[i*4+j];
                volt[4] = 0;
                ivolt = atoi(volt);
                P[i] = double(ivolt)*0.001221;
                Meas[fcnt][i] = P[i];          //store 4 voltages in array
            }

            cs.Format("F:%1d: Voltages:%6.3f %6.3f %6.3f %6.3f", fcnt,P[0],P[1],P[2],P[3] );
            if( !calflg )
            {
                RefCalc();
                cs.Format("%s gam:%6.3f ph:%6.3f Time: %d ",LPCTSTR(cs),gam,ph,MeasTime);
                if( m_bFileFlag )
                {
                    cs2.Format("%s\n",LPCTSTR(cs));
                    cf.WriteString(cs2);
                }
                GetDlgItem(IDC_EDIT2)->SetWindowText(cs);
            }
            }
            fcnt++; //next freq
            return 0;
        }

//*****
//*****

void CSpiralometerDlg::OnButton1()
{
    CString cs;
    char outstr[256], crx[2];

    crx[0] = 13;
    crx[1] = '\0';

    if( m_Info.hComm != INVALID_HANDLE_VALUE )
    {
        GetDlgItem(IDC_EDIT1)->GetWindowText(cs);
        strcpy(outstr,LPCTSTR(cs));
        if(m_bRxFlag)
            strcat(outstr,crx);

        send_comm_string( outstr, strlen( outstr ) );
    }
}

void CSpiralometerDlg::OnCancel()
{
    OnpbStop();
}

```

```

        CDialog::OnCancel();
    }

void CSpiralometerDlg::OnOK()
{
    CComboBox* pCB;
    BYTE commport,parity,bytesize,stopbits;
    DWORD baud;

    BYTE byCommPort[] = {1,2,3,4};
    DWORD dwBaud[] =
{ CBR_110,CBR_300,CBR_600,CBR_1200,CBR_2400,CBR_4800,CBR_9600,CBR_14400,CBR_19200,CBR_38400,CBR_56000,CBR_5
7600,CBR_115200,CBR_128000,CBR_256000};
    BYTE byParity[] = { NOPARITY, ODDPARITY, EVENPARITY, MARKPARITY, SPACEPARITY };
    BYTE byStopBits[] = { ONESTOPBIT, ONE5STOPBITS, TWOSTOPBITS };
    BYTE byByteSize[] = { 4, 5, 6, 7, 8 };

    BYTE byStartFreq[] = { 2, 3, 4, 5, 6, 7 };
    BYTE byStopFreq[] = { 3, 4, 5, 6, 7, 8 };
    BYTE byNumPoints[] = { 1, 10, 20, 50, 100 };
    BYTE byCycleTime[] = { 1, 5, 10, 15, 20 };

    pCB = (CComboBox*)GetDlgItem(IDC_cbStartFreq);
    StartFreq = byStartFreq[pCB->GetCurSel()];

    pCB = (CComboBox*)GetDlgItem(IDC_cbStopFreq);
    StopFreq = byStopFreq[pCB->GetCurSel()];

    pCB = (CComboBox*)GetDlgItem(IDC_cbNumPoints);
    Numpts = byNumPoints[pCB->GetCurSel()];

    pCB = (CComboBox*)GetDlgItem(IDC_cbCycleTime);
    CycleT = byCycleTime[pCB->GetCurSel()];
    m_bRxFlag = ( ( ((CButton*)GetDlgItem(IDC_CHECK1))>GetState()&3 ) == 1 );
    m_bFileFlag = ( ( ((CButton*)GetDlgItem(IDC_cbxSaveToFile))>GetState()&3 ) == 1 );

// *****
// generate frequency list
double fstep;
int xx;
fstep = (( StopFreq - StartFreq))/Numpts;

for( xx=0; xx<Numpts+1; xx++ )
{
    FreqList[xx] = (StartFreq)+((double)xx*fstep); /* GHz */
    FreqNum[xx] = abs( (int)((FreqList[xx]-2.0)*682.66) );
}

// *****
GetDlgItem(IDC_BUTTON2)->EnableWindow(false);
GetDlgItem(IDC_BUTTON3)->EnableWindow(false);
GetDlgItem(IDC_BUTTON4)->EnableWindow(false);
GetDlgItem(IDC_BUTTON5)->EnableWindow(false);
GetDlgItem(IDC_BUTTON6)->EnableWindow(false);
GetDlgItem(IDC_OnSaveCal)->EnableWindow(false);

calflg = 0;
fcnt = Numpts;
m_nTimer = SetTimer(1,1000,NULL); // timer to control speed of measurement
cycletime = 0;
datrx=0;
commport = 3;
baud = 115200;
stopbits = 1;
bytesize = 8;
parity = NOPARITY;
m_bRxFlag = true;
m_bFileFlag = true;

```

```

if( m_bFileFlag )
{
    OPENFILENAME ofn;
    char szFilter[] = "Text Files (*.txt)|0*.txt|0All Files (*.*)|0*.*|0";
    char szFileName[256];

    ofn.lStructSize = sizeof(ofn);
    ofn.hwndOwner = m_hWnd;
    ofn.hInstance = NULL;
    ofn.lpstrFilter = szFilter;
    ofn.lpstrCustomFilter = NULL;
    ofn.nFilterIndex = 0;
    szFileName[0] = '\0';
    ofn.lpstrFile = szFileName;
    ofn.lpstrDefExt = ".txt";
    ofn.nMaxFile = 256;
    ofn.lpstrFileTitle = NULL;
    ofn.nMaxFileTitle = 0;
    ofn.lpstrInitialDir = NULL;

    ofn.lpstrTitle = "Save RX Data";

    ofn.Flags = OFN_HIDEREADONLY | OFN_OVERWRITEPROMPT | OFN_PATHMUSTEXIST;
    if( GetSaveFileName(&ofn) )
    {
        CFileException e;
        if( !cf.Open( szFileName, CFile::modeCreate | CFile::modeWrite, &e ) )
            m_bFileFlag = false;
    }
    else
        m_bFileFlag = false;
}

open_comm(commport,baud,parity,bytesize,stopbits);

if( m_Info.hComm != INVALID_HANDLE_VALUE )
{
    m_Info.hWnd = m_hWnd;
    m_Info.hComm = m_hCommDev;
    m_Info.Finish = false;
    m_Info.pThread = AfxBeginThread( ThreadProc, &m_Info );

    GetDlgItem(IDC_BUTTON1)->EnableWindow(true);
    GetDlgItem(IDC_EDIT1)->EnableWindow(true);
    GetDlgItem(IDC_EDIT2)->EnableWindow(true);

    GetDlgItem(IDC_CHECK1)->EnableWindow(false);
}
}

void CSpiralometerDlg::OnpbStop()
{
    close_comm();
    CDialog::OnDestroy(); // turn off timer

    m_Info.Finish = true;
    m_Info.pThread = AfxBeginThread( ThreadProc, &m_Info );
    if( m_Info.pThread && !m_Info.IsFin )
    {
        Sleep(1000);
        if( m_Info.pThread && !m_Info.IsFin )
            TerminateThread( m_Info.pThread, 0 );
    }

    if( m_bFileFlag )
        if( cf )
            cf.Close();

    m_hCommDev = INVALID_HANDLE_VALUE;

    m_Info.hComm = NULL;
    m_Info.Finish = true;
}

```

```

    m_Info.pThread = NULL;

    GetDlgItem(IDC_BUTTON1)->EnableWindow(false);
    GetDlgItem(IDC_EDIT1)->EnableWindow(false);
    GetDlgItem(IDC_EDIT2)->EnableWindow(false);
}

/*****
// calibrate sixport using 5 standard lengths
void CSpiralometerDlg::OnOk2()
{
    char stds[25];

    // turn off Frequency setup
    GetDlgItem(IDC_cbStartFreq)->EnableWindow(false);
    GetDlgItem(IDC_cbStopFreq)->EnableWindow(false);
    GetDlgItem(IDC_cbNumPoints)->EnableWindow(false);
    GetDlgItem(CalcCoeff)->EnableWindow(false);
    GetDlgItem(IDC_BUTTON2)->EnableWindow(true);
    GetDlgItem(IDOK2)->EnableWindow(false);
    GetDlgItem(IDC_OnLoadCal)->EnableWindow(false);

    //Calculate and display calc std lengths
    calflg = 1;
    standards();

    gcvt(sl[0],4,stds);
    GetDlgItem(IDC_EDIT3)->SetWindowText(stds);
    gcvt(sl[1],4,stds);
    GetDlgItem(IDC_EDIT5)->SetWindowText(stds);
    gcvt(sl[2],4,stds);
    GetDlgItem(IDC_EDIT7)->SetWindowText(stds);
    gcvt(sl[3],4,stds);
    GetDlgItem(IDC_EDIT9)->SetWindowText(stds);
    gcvt(sl[4],4,stds);
    GetDlgItem(IDC_EDIT11)->SetWindowText(stds);
}

/*****
// get actual five standard lengths
void CSpiralometerDlg::OnButton2()
{
    char act2[256];
    CString actstd;

    GetDlgItem(IDC_EDIT4)->GetWindowText(actstd);
    strcpy(act2,LPCWSTR(actstd));
    sla[0] = atof(act2);
    calflg = 1;
    fcnt = 0; //stops frequency sweep
    GetDlgItem(IDC_EDIT4)->EnableWindow(false);
    GetDlgItem(IDC_EDIT3)->EnableWindow(false);
    GetDlgItem(IDC_BUTTON2)->EnableWindow(false);
    GetDlgItem(IDC_BUTTON3)->EnableWindow(true);
}

void CSpiralometerDlg::OnButton3()
{
    char act2[256];
    CString actstd;
    int f,y;

    GetDlgItem(IDC_EDIT6)->GetWindowText(actstd);
    strcpy(act2,LPCWSTR(actstd));
    sla[1] = atof(act2);
    calflg = 2;
    GetDlgItem(IDC_EDIT5)->EnableWindow(false);
    GetDlgItem(IDC_EDIT6)->EnableWindow(false);
    GetDlgItem(IDC_BUTTON3)->EnableWindow(false);
}

```

```

        GetDlgItem(IDC_BUTTON4)->EnableWindow(true);

        for( f=0; f<= Numpts-1; f++)
            for( y=0; y<KVs; y++)
                calldata[f][0][y] = Meas[f][y];
        fcnt = 0;
    }

void CSpiralometerDlg::OnButton4()
{
    char act2[256];
    CString actstd;
    int f,y;

    GetDlgItem(IDC_EDIT8)->GetWindowText(actstd);
    strcpy(act2,LPCTSTR(actstd));
    sla[2] = atof(act2);
    calflg = 3;
    GetDlgItem(IDC_EDIT8)->EnableWindow(false);
    GetDlgItem(IDC_EDIT7)->EnableWindow(false);
    GetDlgItem(IDC_BUTTON4)->EnableWindow(false);
    GetDlgItem(IDC_BUTTON5)->EnableWindow(true);
    for( f=0; f<= Numpts-1; f++)
        for( y=0; y<KVs; y++)
            calldata[f][1][y] = Meas[f][y];
    fcnt = 0;
}

void CSpiralometerDlg::OnButton5()
{
    char act2[256];
    CString actstd;
    int f,y;

    GetDlgItem(IDC_EDIT10)->GetWindowText(actstd);
    strcpy(act2,LPCTSTR(actstd));
    sla[3] = atof(act2);
    calflg = 4;
    GetDlgItem(IDC_EDIT10)->EnableWindow(false);
    GetDlgItem(IDC_EDIT9)->EnableWindow(false);
    GetDlgItem(IDC_BUTTON5)->EnableWindow(false);
    GetDlgItem(IDC_BUTTON6)->EnableWindow(true);
    for( f=0; f<= Numpts-1; f++)
        for( y=0; y<KVs; y++)
            calldata[f][2][y] = Meas[f][y];
    fcnt = 0;
}

void CSpiralometerDlg::OnButton6()
{
    char act2[256];
    CString actstd;
    int f,y;

    GetDlgItem(IDC_EDIT12)->GetWindowText(actstd);
    strcpy(act2,LPCTSTR(actstd));
    sla[4] = atof(act2);
    calflg = 5;
    GetDlgItem(IDC_EDIT12)->EnableWindow(false);
    GetDlgItem(IDC_EDIT11)->EnableWindow(false);
    GetDlgItem(IDC_BUTTON6)->EnableWindow(false);
    GetDlgItem(CalcCoeff)->EnableWindow(true);
    for( f=0; f<= Numpts-1; f++)
        for( y=0; y<KVs; y++)
            calldata[f][3][y] = Meas[f][y];
    fcnt =0;
}

/*+++++-----*/
//CALCULATE THE CALIBRATION COEFFICIENTS
void CSpiralometerDlg::OnCalcCoeff()

```

```

{
    int f,y;

    calflg = 0;
    for( f=0; f<= Numpts-1; f++) // RIK calldata is 1-indexed for "f", but 0-indexed for "y" ... messy, change f to zero-indexed
        for( y=0; y<KVs; y++)
            calldata[f][4][y] = Meas[f][y];

    //store actual calibration lengths in caldata array
    phstd[0]=0;
    for( y=0; y <= 4; y++)
    {
        phstd[y] = sla[y];
    }

    /*******
    getcalvoltages(); //testdata
    /*******
    getcalcoeffs();
    GetDlgItem(IDOK2)->EnableWindow(true);
    GetDlgItem(CalcCoeff)->EnableWindow(false);
    GetDlgItem(IDC_OnSaveCal)->EnableWindow(true);
    calflg = 0;
}

    /*******
    /*******
    // OnTimer : This routine uses the timer to synch and request measurements
    // every second after fcnt = 0 up to the max number of points.
    // also counts up in minutes during the kiln run to measure at predetermined times
    //
    /*******
void CSpiralometerDlg::OnTimer(UINT nIDEvent)
{

    char outstr[256];
    char tmpstr[256];
    int togo;

    if( cyclecnt > 0 )
    {
        if( cycletime == (CycleT*60) )
        {
            fcnt = 0;
            cycletime = 0;
            cyclecnt++;
        }
        cycletime++;
        togo = ((CycleT*60)-cycletime)/60;
        sprintf( tmpstr, "time to next scan %d minutes\r\n", togo );
        GetDlgItem(IDC_EDIT1)->SetWindowText(tmpstr);
    }

    if( fcnt < Numpts )
    {
        //Send Frequency to Micro
        sprintf( outstr, "Start %d\r\n", (int)FreqNum[fcnt] );

        send_comm_string( outstr, strlen( outstr ) );
        GetDlgItem(IDC_EDIT1)->SetWindowText(outstr);
        datrx = 1;
        if( cyclecnt > 0 )
        {
            MeasTime = (CycleT*cyclecnt) + (cycletime/60);
        }
    }
}

```

```

}

/*****
/*****

void CSpiralometerDlg::OnDestroy()
{
    CDialog::OnDestroy();
}

/*****
void CSpiralometerDlg::Onmkscycle()
{
    cyclecnt = 1;
}
/*****
// OnTest: Single sweep button. Performs a single measurement by setting the fcnt=0
void CSpiralometerDlg::OnOnTest()
{
    fcnt = 0;
}
/*****
//LoadCal: loads the calibration coefficients from a file

void CSpiralometerDlg::OnOnLoadCal()
{
    OPENFILENAME ofn;
    char szFilter[] = "CALIBRATION Files (*.cal)\0*.cal\0All Files (*.*)\0*.*\0\0";
    char szFileName[256];

    ofn.lStructSize = sizeof(ofn);
    ofn.hwndOwner = m_hWnd;
    ofn.hInstance = NULL;
    ofn.lpstrFilter = szFilter;
    ofn.lpstrCustomFilter = NULL;
    ofn.nFilterIndex = 0;
    szFileName[0] = '\0';
    ofn.lpstrFile = szFileName;
    ofn.lpstrDefExt = "txt";
    ofn.nMaxFile = 256;
    ofn.lpstrFileTitle = NULL;
    ofn.nMaxFileTitle = 0;
    ofn.lpstrInitialDir = NULL;

    ofn.lpstrTitle = "Load 6Port Cal Coefficients";

    ofn.Flags = OFN_HIDEREADONLY | OFN_OVERWRITEPROMPT | OFN_PATHMUSTEXIST;
    if( GetOpenFileName(&ofn) )
    {
        CFileException e;
        cf2.Open( szFileName, CFile::modeRead , &e );
    }

// read in 6port coefficients
}
/*****
// SaveCal: Saves the 6port calibration coeffs to a File
void CSpiralometerDlg::OnOnSaveCal()
{
    OPENFILENAME ofn2;
    char szFilter2[] = "CAL Files (*.cal)\0*.cal\0All Files (*.*)\0*.*\0\0";
    char szFileName2[256];
    char results [250];
    CString cs4;
    int y;

    ofn2.lStructSize = sizeof(ofn2);
    ofn2.hwndOwner = m_hWnd;
    ofn2.hInstance = NULL;
    ofn2.lpstrFilter = szFilter2;

```

```

ofn2.lpstrCustomFilter = NULL;
ofn2.nFilterIndex = 0;
szFileName2[0] = '\0';
ofn2.lpstrFile = szFileName2;
ofn2.lpstrDefExt = ".txt";
ofn2.nMaxFile = 256;
ofn2.lpstrFileTitle = NULL;
ofn2.nMaxFileTitle = 0;
ofn2.lpstrInitialDir = NULL;

ofn2.lpstrTitle = "Save 6port Calibration Coefficients";

ofn2.Flags = OFN_HIDEREADONLY | OFN_OVERWRITEPROMPT | OFN_PATHMUSTEXIST;
if( GetSaveFileName(&ofn2) )
{
    CFileException e;
    cf2.Open( szFileName2, CFile::modeCreate | CFile::modeWrite, &e );

}

cs4.Empty();
for (y=0; y < Numpts;y++)
{
    sprintf(results, "\r\n %6.3f \r\n", FreqList[y]);
    cs4 += results;

    for (iptr = 0; iptr <=2;iptr++)
    {

        sprintf(results, "%6.3f %6.3f %6.3f %6.3f %6.3f\n",
\r\n", mz[y][iptr], mpz[y][iptr], mxx[y][iptr], mpx[y][iptr], mxn[y][iptr]);
        cs4 += results;

    }

}

cf2.WriteString(cs4);

cf2.Close(); //close file */
}

/*routine to acquire voltages for standard lengths */
int getcalvoltages()
{
    //calreadadc(); /* caldata[freq],[std],[voltage] */

/* _____ temporarily read from file and setup variables*/
ifstream fin("68to80.pow");
char ch[20];
double f[2000];
int y, ymax, yy, k, ff, offset, npts;
y=1;
Numpts =13;
npts = 13;
ymax =694;

/*char results[256];

LPCTSTR cTextBody;
LPCTSTR cTextCaption;
cs3.Empty();
*/

while (y != ymax)
{
    fin.getline(ch,10);
    f[y] = atof(ch);
    y++;
}

```

```

cout << ("\n");
//y = 1;
fin.close();
for (y=0;y<201;y++) freqlist[y] = 0;
y=0 ;
while (y != npts)
//for (y=0;y < npts;y++)
{
    FreqList[y] = f[1+(y*32)];
//    cout << freqlist[y];
    cout << (" ");
    y++;
}

for (ff =0;ff <= Numpts-1;ff++)
{
    offset = (ff)*32;
/* extract data at one freq */
    k=3;
    yy = 0;
    for(yy=0;yy <=NumStd; yy++)
    {
        y=0 ;

        for(y=0;y<=NumStd;y++)
        {
            calldata[ff][yy][y] = f[(3*yy+k)+(y)+ offset];
        }

        k=k+3;
    }

/*
    for(yy=0;yy <=NumStd; yy++)
    {
        y=0 ;

        for(y=0;y<=NumStd;y++)
        {
            sprintf(results," %6.3f ",calldata[ff][yy][y]);
            cs3 += results;
        }

        cs3 += ("\r\n");

    }
    cTextBody = cs3;
    cTextCaption = "Calibration Results";
    MessageBox(NULL,cTextBody,cTextCaption,0);
    cs3.Empty();
*/
}

return (0);
}
/*
+++++
-----*/
int getcalcoeffs()
{

int stdloop,floop,pratio;
/* mod of reflection coeff used for stds */

/* char results[256];

LPCTSTR cTextBody;
LPCTSTR cTextCaption;
cs3.Empty();
*/

```

```

for (stdloop=0;stdloop <= NumStd;stdloop++)
{
    gm[stdloop]=1;
}
for(floop=0;floop <= Numpts-1;floop++)
{
    for (stdloop=0; stdloop <= NumStd; stdloop++)
    {
        for (pratio=0; pratio <=2; pratio++)
        {
            rt[pratio][stdloop]=calldata[floop][stdloop][pratio]/ calldata[floop][stdloop][3];
            /*          sprintf(results," %6.3f ",calldata[floop][stdloop][pratio]);
                       cs3 += results;
            */
        }

        //cs3 += ("\r\n");
        phase[stdloop]= -4*pi*phstd[stdloop]/(c/FreqList[floop]);
    }

    for (iptr = 0; iptr <=2;iptr++)
    {
        denom();
        numr();
        pz[iptr]= pzm;          // cal coeffs for use in cal checking
        z[iptr]=zm;
        px[iptr]=pum;
        xx[iptr]=um;
        xn[iptr] = unc;

        mpz[floop][iptr]=pz[iptr]; // Store cal coeffs into array for all frequencys
        mz[floop][iptr]=z[iptr];
        mpx[floop][iptr]=px[iptr];
        mxx[floop][iptr]=xx[iptr];
        mxn[floop][iptr]=xn[iptr];

        zm = pzm = 0;
    }

    //    cTextBody = cs3;
    //    cTextCaption = "Calibration Results";
    //    MessageBox(NULL,cTextBody,cTextCaption,0);
    checkcal();
    // cs3.Empty();
}

return(0);
}
/*+++++*/
int denom()
{
    double c2,c3,c4,c5,s2,s3,s4,s5;
    double a11,a12,a13,be1,be2,be3;
    double d1,g11,g12,d2,h11,h12;
    double arg0,arg1,arg2,zm1,zm2;

    c2 = cos(phase[1]);
    c3 = cos(phase[2]);
    c4 = cos(phase[3]);
    c5 = cos(phase[4]);
    s2 = sin(phase[1]);
    s3 = sin(phase[2]);
    s4 = sin(phase[3]);
    s5 = sin(phase[4]);

    a11= sin((phase[2]-phase[3])/2)/sin(phase[1]/2);
    a12= sin((phase[1]-phase[3])/2)/sin(phase[2]/2);
    a13= sin((phase[1]-phase[2])/2)/sin(phase[3]/2);

```

```

be1= sin((phase[2]-phase[4])/2)/sin(phase[1]/2);
be2= sin((phase[1]-phase[4])/2)/sin(phase[2]/2);
be3= sin((phase[1]-phase[2])/2)/sin(phase[4]/2);

d1 =(rt[iptr][1]-rt[iptr][0])*a11-(rt[iptr][2]-rt[iptr][0])*a12+(rt[iptr][3]-rt[iptr][0])*a13;
g11=((a11-a12+a13)*rt[iptr][0]- rt[iptr][1]*a11*c2+rt[iptr][2]*a12*c3-rt[iptr][3]*a13*c4)/d1;
g12=(rt[iptr][1]*a11*s2-rt[iptr][2]*a12*s3+rt[iptr][3]*a13*s4)/d1;

d2 =(rt[iptr][1]-rt[iptr][0])*be1-(rt[iptr][2]-rt[iptr][0])*be2+(rt[iptr][4]-rt[iptr][0])*be3;
h11=((be1-be2+be3)*rt[iptr][0]- rt[iptr][1]*be1*c2+rt[iptr][2]*be2*c3-rt[iptr][4]*be3*c5)/d2;
h12=(rt[iptr][1]*be1*s2-rt[iptr][2]*be2*s3+rt[iptr][4]*be3*s5)/d2;

pzm = atan((h11-g11)/(g12-h12));
arg0=g11*cos(pzm)+g12*sin(pzm);
arg2 = arg0*arg0;

if (arg2 >=1)
{
arg1 = sqrt(arg2-1);
zm1 = -arg0+arg1;
zm2 = -arg0 -arg1;
}
else
{
// cout << "\n Problem arg2 < 1 \n Redo power measurment";
zm1 = -arg0;
zm2 = -arg0;
}

if (fabs(zm1) < fabs(zm2)) zm = zm1;
else zm =zm2;
if (zm >= 0) return(0);
zm =-zm;
pzm =pzm+pi;

return(0);
}
/*****
int numr()
{
double c2,c3,c4,s2,s3,s4;
double c11,c12,c13,sp2,sp3,sp4,cp2,cp3,cp4,sp32,sp42;
double zm2,cpz,cpm2,cpm3,cpm4,pp,qq,den1,den2,num1,num2;
double pum[3],uar,arg0,sarg,unc1,unc2,um1,um2,umm[3],unc[3];
double bu,cu,dz;

c2 = cos(phase[1]);
c3 = cos(phase[2]);
c4 = cos(phase[3]);
s2 = sin(phase[1]);
s3 = sin(phase[2]);
s4 = sin(phase[3]);

sp2 = sin(phase[1]/2);
sp3 = sin(phase[2]/2);
sp4 = sin(phase[3]/2);
cp2 = cos(phase[1]/2);
cp3 = cos(phase[2]/2);
cp4 = cos(phase[3]/2);

sp32 = sp3/sp2;
sp42 = sp4/sp2;
zm2 = zm*zm+1;
cpz =cos(pzm);

cpm2=cos(pzm+phase[1]);
cpm3=cos(pzm+phase[2]);
cpm4=cos(pzm+phase[3]);

c11 =(rt[iptr][1]-rt[iptr][0])*zm2-2*zm*(rt[iptr][1]*cpm2-rt[iptr][0]*cpz);
c12 =(rt[iptr][2]-rt[iptr][0])*zm2-2*zm*(rt[iptr][2]*cpm3-rt[iptr][0]*cpz);
c13 =(rt[iptr][3]-rt[iptr][0])*zm2-2*zm*(rt[iptr][3]*cpm4-rt[iptr][0]*cpz);

```

```

pp = c11*sp32/c12;
qq = c11*sp42/c13;
num1 = pp*sp3-sp2;
den1 = cp2-pp*cp3;
num2 = qq*sp4-sp2;
den2 = cp2-qq*cp4;

pumn[0] = atan(num1/den1);
pumn[1] = atan(num2/den2);
pum=(pumn[0]+pumn[1])/2;

uar = c11/(4*sin(pum+phase[1]/2)*sp2);

dz = (zm*zm+1-2*zm*cos(pzm));
cu = rt[iptr][0]*dz ;
for (i=0;i<2;i++)
{
    bu = (cu+2*uar*cos(pumn[i]))/2;
    arg0 = bu*bu-uar*uar;
    if (arg0 < 0) arg0 = 0;
    sarg = sqrt(arg0);
    unc1 = bu-sarg;
    unc2 = bu+sarg;
    um1 = uar/unc1;
    um2 = uar/unc2;
    if (fabs(um1) < fabs(um2)) umm[i] = um1;
    else umm[i] = um2;
    uncc[i]=uar/umm[i];
}

unc= 0.5*(uncc[0]+uncc[1]);
um = 0.5*(umm[0]+umm[1]);
if (um > 0) return(0);
um = -um;
pum = pum+pi;
return(0);
}
/*****

int checkcal()
{
    /* this routine checks the validity of the calibration */

    double cz1,cz2,cz3,cx,cy,cw,ra,rb,rc,r1,r2;
    double sz1,sz2,sz3,sx,sy,sw,u1,u2,v1,v2,u3,v3;
    double zm12,zm22,zm32,rm1,rm2,rm3,denx,deny,denw,den,rm,ri;
    double actphase,mphase;
    int q;
    char results[256];

    LPCTSTR cTextBody;
    LPCTSTR cTextCaption;
    cs3.Empty();

    cz1 = cos(pz[0]);
    cz2 = cos(pz[1]);
    cz3 = cos(pz[2]);

    cx = cos(px[0]);
    cy = cos(px[1]);
    cw = cos(px[2]);

    sz1=sin(pz[0]);
    sz2 = sin(pz[1]);
    sz3 = sin(pz[2]);

    sx= sin(px[0]);
    sy = sin(px[1]);
    sw = sin(px[2]);

```

```

zm12 = z[0]*z[0];
zm22 = z[1]*z[1];
zm32 = z[2]*z[2];

cs3 += "gamma    calc    phase    calc";
for (i=0;i<= 4;i++)
{
    rm1 = rt[0][i]/xn[0];
    rm2 = rt[1][i]/xn[1];
    rm3 = rt[2][i]/xn[2];

    denx = rm1*zm12-(xx[0]*xx[0]);
    deny = rm2*zm22 - (xx[1]*xx[1]);
    denw = rm3*zm32 - (xx[2]*xx[2]);

    u1 =(rm1*z[0]*cz1-xx[0]*cx)/denx;
    v1 = (xx[0]*sx-rm1*z[0]*sz1)/denx;

    u2 = (rm2*z[1]*cz2-xx[1]*cy)/deny;
    v2 = (xx[1]*sy-rm2*z[1]*sz2)/deny;

    u3 = (rm3*z[2]*cz3-xx[2]*cw)/denw;
    v3 = (xx[2]*sw-rm3*z[2]*sz3)/denw;

    ra = (1-rm1)/denx;
    rb = (1-rm2)/deny;
    rc = (1-rm3)/denw;
    r1=ra-rb;
    r2=ra-rc;

    den = (u2-u1)*(v3-v1)-(u3-u1)*(v2-v1);
    rm = 0.5*(r1*(v3-v1)-r2*(v2-v1))/den;
    ri = 0.5*(r2*(u2-u1)-r1*(u3-u1))/den;

    gam = sqrt((rm*rm)+(ri*ri));
    q= 0;
    if (rm == 0)
    {
        if (ri > 0) ph = pi;
        else ph=(3*pi/2);
        if (r1 == 0) ph =0;
        q=1;
    }

    if (r1 == 0)
    {
        if (rm > 0) ph = 0;
        else ph = pi;
        q=1;
    }
    if (q == 0)
    {
        ph = atan(ri/rm);
        if (rm < 0) ph = ph+pi;
    }

    if (phase[i]*180/pi <= -0.0000001) actphase= phase[i]*180/pi+360; // make angles positive
    else actphase=phase[i]*180/pi;

    if (ph*180/pi <= -0.0001) mphase= ph*180/pi+360; // make angles positive
    else mphase=ph*180/pi;

    // Print cal results to message box
    sprintf(results, "\r\n %6.3f    %6.3f    %6.3f    %6.3f% \r\n", gm[i], gam, actphase, mphase);
    cs3 += results;
}

cTextBody = cs3;
cTextCaption = "Calibration Results";
MessageBox(NULL,cTextBody,cTextCaption,0);

return(0);

```

```

}
/*****
int RefCalc()
{
  /* this routine calculates reflection coefficient from measured voltages */

  double cz1,cz2,cz3,cx,cy,cw,ra,rb,rc,r1,r2;
  double sz1,sz2,sz3,sx,sy,sw,u1,u2,v1,v2,u3,v3;
  double zm12,zm22,zm32,rm1,rm2,rm3,denx,deny,denw,den,rm,ri;
  int q;

  cz1 = cos(mpz[fcnt][0]);
  cz2 = cos(mpz[fcnt][1]);
  cz3 = cos(mpz[fcnt][2]);

  cx = cos(mpx[fcnt][0]);
  cy = cos(mpx[fcnt][1]);
  cw = cos(mpx[fcnt][2]);

  sz1 = sin(mpz[fcnt][0]);
  sz2 = sin(mpz[fcnt][1]);
  sz3 = sin(mpz[fcnt][2]);

  sx = sin(mpx[fcnt][0]);
  sy = sin(mpx[fcnt][1]);
  sw = sin(mpx[fcnt][2]);

  zm12 = mz[fcnt][0]*mz[fcnt][0];
  zm22 = mz[fcnt][1]*mz[fcnt][1];
  zm32 = mz[fcnt][2]*mz[fcnt][2];

  rm1 = (P[0]/P[3])/mxn[fcnt][0];
  rm2 = (P[1]/P[3])/mxn[fcnt][1];
  rm3 = (P[2]/P[3])/mxn[fcnt][2];

  denx = rm1*zm12 - (mxx[fcnt][0]*mxx[fcnt][0]);
  deny = rm2*zm22 - (mxx[fcnt][1]*mxx[fcnt][1]);
  denw = rm3*zm32 - (mxx[fcnt][2]*mxx[fcnt][2]);

  u1 = (rm1*mz[fcnt][0]*cz1-mxx[fcnt][0]*cx)/denx;
  v1 = (mxx[fcnt][0]*sx-rm1*mz[fcnt][0]*sz1)/denx;

  u2 = (rm2*mz[fcnt][1]*cz2-mxx[fcnt][1]*cy)/deny;
  v2 = (mxx[fcnt][1]*sy-rm2*mz[fcnt][1]*sz2)/deny;

  u3 = (rm3*mz[fcnt][2]*cz3-mxx[fcnt][2]*cw)/denw;
  v3 = (mxx[fcnt][2]*sw-rm3*mz[fcnt][2]*sz3)/denw;

  ra = (1-rm1)/denx;
  rb = (1-rm2)/deny;
  rc = (1-rm3)/denw;
  r1 = ra - rb;
  r2 = ra - rc;

  den = (u2-u1)*(v3-v1)-(u3-u1)*(v2-v1);
  rm = 0.5*(r1*(v3-v1)-r2*(v2-v1))/den;
  ri = 0.5*(r2*(u2-u1)-r1*(u3-u1))/den;

  gam = sqrt((rm*rm)+(ri*ri));
  q = 0;

  if(rm == 0)
  {
    if (ri > 0)
      ph = pi;
    else
      ph = (3*pi/2);

    if(r1 == 0)
      ph = 0;
  }
}

```

```

        q = 1;
    }

    if(r1 == 0)
    {
        if(rm > 0)
            ph = 0;
        else
            ph = pi;

        q = 1;
    }

    if(q == 0)
    {
        ph = atan(ri/rm);
        if(rm < 0)
            ph = ph+pi;
    }
    ph = ph*180/pi;

    return(0);
}

/*
+++++
-----
routine to calculate standard lengths required for the sliding short*/
float standards()
{
    double thmin;
    int j;

    thmin = pi/8;
    sl[0] = 0;
    for(j=1; j<=4; j++)
        sl[j] = (j*c)/(2*pi*StartFreq)*(2*pi/5-(2*pi-thmin)/8);

    return(0);
}

```